62431

Study of Novel Concepts of Power Transmission Gears

P 90

Final Report for NASA Grant NAG3-918

Period Covered: 7/1/88 - 6/30/91

Principal Investigator:
Eugene I. Rivin, Professor
Department of Mechanical Engineering
Wayne State University
Detroit MI 48202

COLLEGE OF ENGINEERING

Wayne State University

TABLE OF CONTENTS

SUMMARY

After outstanding successes, intensive R&D efforts in gearing started to yield diminishing returns, thus necessitating conceptual changes. Two novel concepts in power transmission gear design are proposed which provide a potential for significant noise reduction and for improving weight-to-payload ratio due to use of advanced fiber-reinforced and ceramic materials. The report briefly describes these concepts.

Since both concepts are utilizing ultra-thin-layered rubber-metal laminates for accomodating limited travel displacements, properties of the laminates, such as their compressive strength, compressive and shear moduli have been studied. Using previously published analytical results, design changes have been introduced which resulted in development of the laminates having ultimate static compressive strength in the 80,000 - 90,000 psi range. Dynamic tests of the laminates were also performed. They indicated significantly lesser compression loads which can be accomodated by the laminates under alternating loads, in the range of 5,000 - 10,000 psi. Since failure of the laminates under the static loads was due to breakage og intermediate metal layers, and failure under the alternating loads was due to delamination ("squeezing") of rubber, it was concluded and experimentally confirmed that the static strength can be enhanced by enhancing strength of the intermediate metal layers, while enhancement of the dynamic strength can be achieved by improving bonding processes. A test system for testing thin-layered rubber-metal laminates was developed and described, which takes into consideration extremely high values of compression stiffness of the laminates, which frequently exceeds structural stiffness of conventional state-of-the-art servohydraulic testing machines.

Extensive testing and computational analysis were performed on the "first concept" gears (laminate-coated conformal gears). Requirements to laminate design have been established on the basis of computer simulation of the meshing process. Test facilities for testing under rotation and loading conditions; under limited rotation and loading condition ("vibratory testing"), and for study meshing conditions have been developed. The tests demonstrated that the laminate-coated gears have the potential to transmit loads comparable or exceeding those for metal gears. The design problems are diminishing for larger size gears. These results should be considered in conjunction with the previously published results which demonstrated very significant noise reductions associated with the laminate-coated gears.

Design and testing of the first prototype of the second conceptual design ("composite" gear with separation of sliding and rolling motions) are specifically described. The concept involves engagement between an involute gear and a composite gear in which sliding and rolling motions are kinematically separated. The contact strength is enhanced due to elimination of sliding and possibility of using ceramic materials for the contacting component. The bulk strength is enhanced due to elimination of bending deformations and a possibility of using advanced fiber-reinforced materials for the gear body. Geometrical analysis of the gear system has been performed and computational algorithm for the design synthesis developed. It was shown that although the system is only approximately a conjugate one, the approximation is very close. Influences of various design parameters on the mesh have been studied. A prototype composite gear pair has been designed, fabricated, and tested. Although accuracy of the fabricated prototype composite gear was not as high as expected, the testing demonstrated that the system is performing in accordance with the expectations and warrants further development.

CHAPTER 1. INTRODUCTION AND STATE OF THE ART

Gear transmissions play two major roles: l) maintaining precise transmission ratios between various mechanisms, as in gear-cutting machines, mechanical computing devices, etc., and 2) transmitting substantial torques and/or power between prime motors and output members of machines and mechanisms. The first group of gear applications is becoming less and less important with the advancement of mechatronics and the successful development of precision electronic motion control devices (e.g., "the electronic gear box" [1]). However, the importance of power transmission gears is not diminishing. Power transmission gears are critical in the performance of numerous machines and mechanisms. With a general trend toward more power-intensive machines, the allowable speeds and payload capacity of gears frequently determine costs, reliability and, sometimes, feasibility of power transmission systems. This explains the very large R&D efforts in many countries aimed at advancing the state of the art in power transmission gears. The very significant progress in power transmission gearing in the last 50 years (e.g., see [2, 3]) was achieved due to major R&D efforts along several directions:

a. Materials and heat treatments. State of the art gears are always made of steel. While special alloying and high metal purity standards contribute to the higher performance characteristics of gears, the greatest progress is due to the development of special heat treatments which, in combination with special bulk and/or surface alloying, provide the different required properties of the core (high bending strength) and surface (high contact durability). Due to the need to satisfy conflicting core and surface requirements, advanced new materials with superior specific strength (high strength/weight ratios) cannot be used for industrial gearing. For example, fiber-reinforced gears show substantial advantages in bending strength [4],[5], but they have very poor wear sliding-under-load resistance. The same is true for high-strength aluminum and titanium alloys, metal matrix composites, etc. On the other hand, ceramics have very high hardness and contact strength, but a poor performance in bending. For example: 20 cm diameter steel gears were used for a single action mechanism for deploying the antenna of a communication satellite, even though adding one kilogram to the payload can increase launching costs up to $25,000 [6].

b. Manufacturing and assembly accuracy. The load carrying capacity of power transmission gears deteriorates at high rpm due to intensive dynamic loads caused by deviations from the ideal geometry. These deviations include pitch errors as well as profile and helix deviations, which can be reduced by accurate machining. They also include teeth deformations under load as well as shaft misalignments caused by deformations of the housings, especially housings made of light metals (such as helicopter gearboxes). Compensating for these deformations is difficult due to their torque dependency; it requires costly teeth profile modifications, as well as derating of the gears. The same deviations also result in high noise levels, which frequently become a critical factor, both for civilian and for military applications.

Although developments in approaches a) and b) have contributed greatly to progress in gear technology in recent years, these approaches now yield diminishing returns whereas more and more costly R&D and production investments bring less and less significant improvements in performance.

c. Geometry modifications. The bulk of geometry-related research is in the domain of involute gears. Profile modifications during machining allow a beneficial redistributing of bulk (bending) stresses between the gear and the pinion; one- and two-dimensional crowning/flanking allow reduced gear sensitivity to misalignments and to changing deformations caused by changing loading, etc. (e.g., [7], [8], [9]). However, these approaches are also nearing their saturation levels, where incremental improvements require increasing investments in new, sophisticated equipment and tooling. The "reinvention" of conformal gears by Novikov in the late fifties (a slightly different embodiment had been invented by Wildhaber in 1920 [10]) raised hopes for a

dramatic breakthrough in gear technology due to the theoretically higher strength of conformal Wildhaber/Novikov (W/N) gears. However, these hopes faded after it was discovered, that high noise levels and high sensitivity to center distance deviations are very difficult to abate.

Main problems preventing a wider application of the conformal gears are their sensitivity to center distance variation; high rigidity of the "squat" teeth causing very high dynamic loads as well as vibration and noise levels even at moderate speeds; impossibility of grinding the tooth surfaces by a generating method, only by a contoured wheel which complicates use of hardened gears [11].

A generic problem for all types of power transmission gears is noise, which becomes more and more of a determining factor for assigning the machining/assembly tolerances for gears and, thus, for their costs. In some cases noisy gears require additional and very costly acoustical treatments, even when gears are produced to a high degree of accuracy (e.g., in submarines and "low noise" helicopters). Numerous effective techniques for noise abatement, such as plastic or metal-polymer gears, gears with rims insulated from the hubs, (e.g. [12]), etc., are usually associated with substantial derating.

Although the power transmission efficiency of state of the art gears is quite high (up to and even exceeding 0.99), in cases when multi-stage or planetary gear trains are used, their overall efficiency can be as low as 0.85-0.90. Such values are typical, for example, in vehicles, and cause secondary weight and power consumption penalties (e.g., associated with the need to use larger engines and supporting structures, etc.). Although energy losses are generated not only in gears but also in other components of the transmission (bearings, lubrication systems, etc.), up to 80% of the losses are due to the gear mesh itself [13]. Reduction of the losses in conventional gears requires more stringent tolerances and thus is associated with high costs.

Summarizing, the following major problems should be addressed to upgrade the state of the art of power transmission gearing in response to design needs in high-technology mechanical design:

- Radical increase in payload capacity.

- Radical reduction in noise levels of heavy duty high-speed gear transmissions.

- Development of low weight power transmissions.

- Cost containment for high grade gears.

- Reduction of energy losses.

1.1 NOVEL CONCEPTS IN POWER TRANSMISSION GEAR DESIGN

As noted above, after about 50 years of continuous improvements in gear state of the art, a "saturation" period is now approaching when larger expenses on R&D bring diminishing returns in improved performance. Usually, this is a time for conceptual changes in the technology. Recently we proposed development of two novel concepts in power transmission gear designs. Both concepts are based on the principles of separation between rolling and sliding processes during engagement between the meshing teeth. Such separation results in elimination of the need for a tooth surface to endure high contact loads together with sliding.

The first concept [14], [15] involves elimination of physical sliding between the meshing tooth profiles, and accommodation of inevitable geometric sliding by internal shear in thin-layered metal-elastomer laminates attached to the profile(s), Fig.1.1. Recent research results, partly described in [16], have shown that, due in part to volumetric incompressibility of elastomeric

(rubber-like) materials, the thin-layered laminates have a relatively high compression modulus (up to 2,500 MPa), and very high compressive strength (up to and exceeding 200-300 MPa). At the same time, their shear modulus is very low (for soft elastomers, optimal for the applications under discussion, G = 0.5-0.7 MPa). Another important property of the laminates is a virtual independence of their resistance to shear deformation from compressive forces (as opposed to frictional joints). Depending on the rubber blend a relative shear of 50-75% is tolerated for rubber parts under repeated shear deformation (e.g., [17]).

The unique characteristics of thin-layered metal-elastomer laminates are utilized in several engineering applications, including such critical applications as limited-travel bearings in helicopter rotor hubs [18], torsionally-rigid misalignment compensating couplings [19], etc. The application of laminates to power transmission gears is made possible by the fact that the total sliding travel between the meshing profiles during one cycle of engagement is limited.

An important issue is the contact (surface) strength of the laminate-coated gears. While state of the art materials/heat treatments allow contact pressures up to 1,300 MPa (e.g., [20]), the laminates allow only 200-300 MPa [16]. However, actual contact stresses on surfaces of the laminate-coated gears are greatly reduced due to a lesser compression modulus of the laminates and thus to distribution of the load across a larger area of contact. The advantages of the laminate-coated gears in effective bending strength are enhanced, for a given center distance and transmission ratio, with increasing tooth size (thus, reducing teeth number). There are two reasons for this: 1) with increasing tooth size, the overall thickness of elastomer in the laminate should be increased, but not the thickness of the face metal layer; 2) for the larger teeth the number of laminate segments can be increased, thus effectively reducing the total thickness of the coating . A steep reduction in the numbers of teeth can be naturally achieved in conformal (W/N) gears, in which Z = 3-5 can be easily designed [21]. The laminate coating, due to its local compliance, alleviates the basic deficiencies of W/N gears -sensitivity to center distance variations and high dynamic load/noise generation. Because of it, additional bending and surface strength enhancements inherent in W/N gears (e.g., see [22]) can be utilized. This would further advance the art of gear design. It was shown in [23] that noise of the coated W/N gears is reduced by 15-20dB.

Due to the beneficial effects of the laminate coating on both surface and bending strength of gears, and also due to separation between the components of the gear responsible for accommodating bending and contact loading, laminate-coated gears can utilize cores made of light but strong materials. These can be aluminum or titanium alloys, or composite fiber-reinforced materials, as in [4], [5].

An advantage of W/N gears for application of this concept is the constancy of curvature radii of the circular cross section in conformal tooth profiles, Fig.1.2. As a result, accommodation of the sliding path by the laminate coating involves only pure shear deformation in the laminate. On the other hand, the curvature radius of the involute profile is constantly changing, increasing towards the tooth addendum. Thus, shear deformation during accommodation of sliding is accompanied by the changing curvature of the laminate, that is, by some bending and thus by compression in the laminate. Although the degree of the curvature change is alleviated due to the segmenting of the coating, even minor compression significantly increases the deformation resistance of the laminates due to the huge differences between their compression and shear moduli.

If both profiles of the teeth of at least one of the engaging gears have the elastomeric coating, then the mesh can be preloaded. With such an arrangement the backlash is eliminated, but sliding resistance between the teeth (and energy losses) are not increasing since the shear modulus of a thin-layered metal-elastomer laminate does not depend on the compression load [16]. Some increase in losses would occur in bearings due to additional radial forces on the shafts of the

preloaded gears, but this is only a small fraction of the losses incurred in conventional preloaded anti-backlash gears, such as in [15]. The independence of shear modulus from compressive loads also results in the improved efficiency of the laminate-coated gears.

Since losses in the laminates do not depend on the compressive loading, efficiency of such gears at high payloads is expected to be better than for conventional gears.

The second concept is applicable to involute gears.It suggests resolution of the combined rolling-sliding motion between the engaging involute teeth into pure sliding and pure rolling [24]. A so-called "composite gear" is meshing with an involute gear. Pure rolling occurs between the involute profile of one tooth and a specially synthesized profile of a special "crescent" which, in turn, slides along the circular cylindrical surface of the tooth core of the counterpart "composite" tooth.

To achieve this effect, each tooth of at least one of the gears (12a in Fig.1.3) is composed of: tooth core 14 with a circular convex profile 20, crescent 18 with an internal concave circular profile matching convex profile 20 of core 14, and external profile constructed in such a way that when it is meshing in a rolling motion with an involute tooth 15, a conjugate action ensues. Thus, the gear pair 12a-12b is equivalent to a pair of involute gears. It was shown [25] that external profile of 18 can be synthesized by a simple geometric/computational procedure to be approximately conjugate with an involute gear.

Any known type of bearing can be used to accommodate sliding between tooth core 14 and crescent 18, such as a conventional lubricated or a hydrostatic bearing, rolling bodies, springs, metal-elastomer laminates, etc. The latter two techniques seem to be preferable, since they combine accommodation of the required limited motion with automatic return of crescent 18 to its initial position and with keeping it in a proper configuration. Although other design means can be used to achieve the same results, internal friction connections seem to be the most effective means. They also result in a superior efficiency.

It is very important to note that the crescent is subjected to compression force only, Fig.1.4a, contrary to conventional involute gears in which teeth are subjected to bending loading with a significant tensile stress in the fillet area, Fig.1.4b. Since the compression load is applied in a purely rolling mode, without sliding,the crescent can accomodate much higher loads even if it is made of the conventional gear materials. It is shown in [26] that the allowable contact stress in case of simultaneous rolling and sliding action between the contacting bodies is only about 50% of the allowable stress for a pure rolling contact for the same reference number of stress cycles. In addition, since there are no tensile stresses in the crescent, it can be fabricated from materials having superior strength in compression and contact endurance (e.g., ceramics). The tooth core (and the gear body) can be made of a light material which has high bulk strength (e.g., fiber reinforced composites) since the loads are applied to the tooth core in a distributed mode.

1.2 GOALS OF THE PROJECT

This project had as its goals a detailed study of engagement processes in both novel conceptual designs of power transmission gears, a study of static and dynamic characteristics of thin-layered rubber-metal laminates and ways to improve their performance; design of an actual gear pair for a performance testing.

CHAPTER 2. THIN - LAYERED RUBBER - METAL LAMINATES

2.1 STATIC CHARACTERISTICS

Elastomeric (rubber-like) materials are practically incompressible, their degree of compressibility being dependent on small deviations of Poisson's ratio ν from the ideal value of $\nu = 0.5$. Thus, compression under a force P_z of a cylindrical rubber element 1 in Fig.2.1a, which is bonded to metal end plates 2, 3, can occur only due to bulging of element 1 on its free surfaces. If an intermediate metal layer 4 is placed in the middle of and bonded to the rubber element 1 as in Fig.2.1b, thus dividing it into two layers 1' and 1", then the bulging is restricted and compression deformation with the same P_z is reduced. While the compression stiffness for a given total height of the rubber element can be varied in a broad range by means of selecting a number of metal interleaves, the shear stiffness in the direction of horizontal force P_x remains constant since shear deformation is not associated with a volume change. Thus, the best properties of the rubber-metal laminates for applications as limited travel bearings can be expected for very thin rubber layers, when stiffness in the compression direction can be made very high without increasing their shear stiffness.

Actual properties of ultra-thin layered rubber-metal laminates are influenced by deviations of n from 0.5; by effects of adhesive layers; deformations in metal interleaves; nonlinearity. A detailed study of properties of ultra-thin layered rubber-metal laminates is described in [16]. The material has a remarkable strength. It was shown in [16] that the compressive strength of laminates is as high as 200-300 MPa (30-45,000 psi), and that their failures always started in the metal interleaves, not in the rubber. It was shown analytically, that the maximum stress in the metal interleaves of a round laminate is

$$\sigma = p_z/2[h_r/h_m(1-\nu) + \nu + (h_r/h_m + \nu h_r/h_m - \nu + 2)/\phi], \qquad (2.1)$$

where: h_r - thickness of rubber layer; h_m - thickness of metal layer; $\phi = 1 - 2I_1(aR)/[aR)I_0(aR)]$; $\alpha = 12G/Kh_r^2$; G, K -shear modulus, volumetric compressibility modulus of rubber; R - external radius of the laminate; I_o, I_1 - modifified Bessel functions.

In order to use laminate on the concept gears under investigation, static properties of the laminates such as compression modulus, ultimate compression stress, shear modulus, relationship between stress and strain should be known. For ultrathin-layerd laminates with strain larger than 1%, the compression stiffness is nonlinear, no close-form solutions [besides expressions for stresses, like (2.1)] for this case are known; finite element analysis is difficult due to significant influence of the bonding (glue) layers. In this project,experimental studies were performed to further evaluate mechanical properties of the laminates.

2.1.1 Test System

Fig.2.2 shows the test set-up for load-deformation tests. In this Figure: INSTRON is a electrohydraulic testing machine (Instron mod, 1351) which can provide 0-20,000 lb static and dynamic load in the frequency range 0-100 Hz; LVDT is a linear variable differential transformer which was used to measure static and dynamic displacements in the range 0.001-0.25 in. INSTRON "stroke" readout shows the total deformation of the sample and the actuator system, and the machine frame. In conventional cases, deformation of the actuator system and frame could be neglected and the readout is adequately representing deformation of the specimen. However,

deformations of a ultrathin-layered laminates are very small and deformations of the actuator system and frame could not be neglected [16]; LOAD CELL is a part of the testing machine; it measures the load applied to the laminate; Nicolet mod 4094 digital oscilloscope was used to observe, record and transmit to a PC the test data on both load and deformation.

2.1.2 Experimental Results

Important static characteristics of the laminates include compression stiffness, compression modulus, ultimate compression stress and strain, shear stiffness and modulus. All of these parameters have to be considered when a laminate is applied to the gear teeth as a load-carrying component.

According to reference [16] , the following formulas were used to calculate the compression modulus E_c and the shear modulus G from the load- deformation experiment results:

$$E_c = \Delta\sigma_z h_{ri}/\Delta z, \tag{2.2}$$

where:

$\Delta\sigma_z$ is increment of compression stress;

h_{ri} is total thickness of rubber, which varies during loading process;

Δz is increment of the compression deformation;

$$G = \Delta\sigma_x h_r \Delta x \tag{2.3}$$

where:

$\Delta\sigma_x$ is increment of the shear stress;

Δx is increment of the shear deformation.

2.1.2.1 Compression Modulus and Ultimate Compression Stress

At first, the compression load-deformation tests were performed. Test specimens were chosen using different rubber materials such as neopren rubber, natural rubber, and latex rubber, different thicknesses of rubber layers, and different surface areas. From test results shown in Tables 2.1, 2, 3, Figs.2.3 a,b,c,d the following conclusions could be obtained.

(1) Compression Modulus and Ultimate Compression Stress

Table 2.1 and Fig.2.3a show the results of compression load-deformation tests for six different samples A, B, C, D, E, F which have the same design (two layers of rubber and three layers of steel, the thickness of each layer of steel sheet is 0.002 inch, were bonded together by the Loctite Black Label glue), same square area (About 0.1 sq.in). Rubber materials of samples are different and their thicknesses varied from 0.01 inch to 0.05 inch. The rubber of specimens B, C, and D is natural rubber with Shore durometer 30, 40, 40, respectively; A was made of Neoprene rubber; and E, F - from latex rubber. All specimens demonstrated very high ratios of compression stiffness to shear stiffness (up to 1000-2600 times) and very high ultimate compression stresses. For the sample C, in which thickness of rubber layers is 0.01 in. (the thinnest), compression modulus (E=158,000 psi) is about 0.2% of that for steel and ultimate compression stress (S=54,000 psi) is close to one third of that for steel. Also, Table 2.3 indicates that for sample G5, in which thickness of the intermediate steel layer is increased from 0.002 inch to 0.004 inch, the surface area of the laminate is increased from 0.1 to 0.16 sq.in and there are four

layers of rubber, the maximum compression modulus is E=481,600 psi which is close to 1.5% of the Young's modulus for steel and the ultimate compression stress is S=117,000 which approaches ultimate stress for steel. These results are encouraging for application of the laminates as load-carrying components attached to the gear teeth.

(2) Ultimate Compression Strain

The ultimate compression strains for samples A, B, C, D are about 0.3 and for E and F are about 0.55, as shown in Fig.2.4. Generally, the maxmimum allowable compression strain for natural rubber is 0.35 and higher strains are allowable for latex rubber. The thinner is the rubber layer, the higher the stiffness of the laminate.

(3) Effect of Intermediate Metal Layer on Compression Modulus

Thickness of the intermediate metal layers has remarkable effect on static properties of the laminates. In Table 2.2, two samples D and D7 have the same structure except for different thicknesses of the intermediate steel layer: the 0.002inch thickness for D and 0.002*2=0.004 in. for D7. The test results in Table 2.2 show that the compression modulus of D7 is 4 times that of D and the ultimate compression stress is 2 times of that of D. The same conclusion can be obtained from Table 2.3. Samples G3, G4, G5, have the same four layers of rubber and the same surface area 0.16 sq.in , but different thicknesses of intermediate and top metal layers. G3 has the thicknesses of intermediate steel layers 0.002 in., G4 and G5 - 0.002*2=0.004in.. The thickness of top steel layers for G3 and G4 is 0.002*5=0.010 in., for G5 0.002*10=0.02 in.. The compression modulus of G4 is 2 times that of G3 and compression ultimate stress - 2.5 times of G3. The compression modulus of G5 is only 1.1 times that of G4. These test results are corresponding well with formula (2.1) from Biderman [27].

(4) Effect of Shape Factor on Compression Modulus

The compression modulus of laminates is correlated with the shape factor S [28] which is the ratio of surface areas of one loaded surface and the load-free surface. For our square sample, the formula for calculating S is as follows:

$$S = a^2/4at = a/4t, \qquad (2.4)$$

where a is side length of square, and t is thickness of one rubber layer.

In this formula, there are two parameters - thickness of one layer of rubber and surface area of laminate, which effect the shape factor. The effect of thickness of a rubber layer is shown in Table 2.1 and Fig.2.3(a). Samples C and D have the same structure except for the thickness of rubber layers; namely, the thickness of the rubber layers for C is half of that for sample D and the shape factor S of C is 8.4 and the shape factor S of D is 4.3. As a result, the compression modulus and ultimate compression stress of the sample C are twice these for D. Similarly, the thickness of the rubber layers of the sample E is 60% of that of F, shape factor $S_E = 2.7$ and $S_F = 1.5$, resulting in compression modulus and compression ultimate stress of the sample E being 120% of that of F. Thus, the thinner the thickness of each layer of rubber, the higher the compression stiffness and the ultimate compression stress.

The effect of surface area of laminates can be observed in Figs.2.3(b) and (c). Two samples have the same structure (three layers of rubber 0.015inch thick, thickness of a steel layer is 0.012inch) but different area. For the ratio of their areas 1.5 (the ratio of the shape factors 1.2) the maximum compression modulus and ultimate stress are increasing 1.5 times and 1.75 times

respectively. It should be noted that there is no apparent effect of the laminate area in the small strain range (linearity range of stress-strain relationship) as shown in Fig.2.3(b), (c).

(5) Effect of Rubber Materials on Compression Modulus

The rubber materials also affect the static properties of laminates. Specimens E and F have shape factors, respectively, 2.7 and 1.5, which are smaller than the 4.7 for B and 4.3 for D. Although they have the same surface areas and other structural perameters, the compression moduli and ultimate compression stresses of the specimens with latex rubber are almost twice of those for B and are equal to ones for D. This is because the latex rubber is a very pure rubber and its Poisson's ratio is almost equal to 0.5.

2.1.2.2 Shear Modulus of Laminates

The shearing load-deformation test system is shown in Fig.2.5 in which compression loading surfaces are round to simulate the tooth profiles. All test results are shown in Fig.2.6, 7, 8, 9, 10. Fig.2.6 shows shear modulus vs. shear stress for six samples which are the same samples whose perameters were described above. Three conclusions can be fomulated:

(1) Shear Modulus G Is Equal to 1/3 of Young's Modulus

According to elasticity theory

$$G = E/2(1-\nu) = E/2(1-0.5) = 3. \qquad (2.5)$$

In Fig.2.6, shear moduli for six samples with the rubber durometers 30-45 are about 50-80 psi, which means that Young's moduli of rubber are about 150-240 psi. The moduli of natural rubber with durometers 30-45 are 130-261 psi from Table 2.4 and these moduli are close to ones from the above test results.

(2) Compression Load Variation Does Not Effect the Value of Shear Modulus

The shear modulus of laminates under different specific compression loads 400 psi, 1000 psi, 5000 psi, 10000 psi varies only about 15% as shown in Figs.2.7, 8, 9 for samples D, E, F, respectively. This is another important property of laminates for our application. As the compression stress increases during the meshing process, the shear stiffness of the laminate attached to the tooth remains constant. This is very useful when shear deformation of the laminate is used instead of sliding motion between the tooth profiles.

(3) Non-uniform Compression Load Does Not Effect the Value of Shear Modulus

When a laminate is subjected to a non-uniform distribution of the compression load, variation of the shear stress is not significant as shown in Fig.2.10 for specimens located in different positions in the test set-up in Fig.2.5. The test sample G1 consists of four layers of rubber 0.015*4 and intermediate steel layers 0.002 in thick, the top and bottom steel are 0.02 in thick. Compression preload is 12,000 psi. These test results confirm that two gears would remain in mesh, although the tangential force is acting on different locations of the laminate. The shear stress always is low and it is easy to have shear deformation instead of sliding motion between the tooth profiles.

2.1.2.3 Modified Formula for Estimating Compression Modulus E_c

Compression modulus E_c of laminates is a more convenient parameter than compression stiffness because it excludes influences of the surface area and the number of layers. Compression modulus E_c of a laminate can be expressed [28] as

$$E_c = E_o(1 + 2KS^2), \tag{2.6}$$

where E_c is Young's (elastic) modulus for rubber, and K is a numerical factor. Both E_o and K can be obtained from Table 2.4 [28].

Formula (2.6) is based upon the classical small strain elasticity theory and assumes stress to be proportional to strain. Up to 10% compression strain, this assumption does not lead to excessive errors. However, strains up to 15%-30% are used in our application situation in which the laminate is used as a load-carrying component on the profiles of the gear teeth. Therefore, three factors should be considered.

The first factor a is a coefficient considering the non-linearity of Young's modulus E_o when the strain in the laminate increases gradualy, as shown in Fig.2.11. Thus the effective Young's modulus is

$$E_o \text{ '} = \alpha E_o. \tag{2.7}$$

The second factor is change of thickness of rubber t' with increasing compression load,

$$t' = t(1-\varepsilon). \tag{2.8}$$

The third factor β is used to modify the thickness of rubber due to a chemical reaction at the adhesion surface between rubber and metal, which results in the rubber at the adhesive surface losting its elastic property:

$$t'' = \beta t' = \beta(1-\varepsilon)t \tag{2.9}$$

$$S' = \alpha/4t'' = \alpha/4t\beta(1-\varepsilon) = S/\beta(1-\varepsilon). \tag{2.10}$$

Considering above three factors, the modified formula for estimating the compression modulus of laminate becomes

$$E_c = \alpha E\{1+2K[S/(1-\varepsilon)\beta]^2\}, \tag{2.11}$$

where E is chosen from Table 2.4, a is chosen from Fig.2.11, and b is thickness coefficient which equals 1 for latex rubber, and 0.65 for other rubber blends, as concluded from our experimental results.

For six specimens, the calculated compression moduli E_{cal} were calculated according to this modified formula (2.10) and the experimental compression moduli E_{ex} were obtained by the formula (2.2) as shown in Tables 2.5, 6, 7. The ratios E_{ex} /E_{cal} are about 0.5-1.7, which means that the calculated results are reasonably close to the test results. Therefore this modified formula could be used for obtaining crude estimates of compression moduli of ultrathin layered laminates

2.2 DYNAMIC PROPERTIES OF LAMINATES

It was discovered during testing of the elastomer-coated gears, that when the shapes of the laminate pieces match the shape of the profile of the laminate coated gear whose diametral pitch is 5, the gear could be subjected to a high static torque, up to 1250 lb-in.. However when the gear was subjected to the high dynamic torque, the rubber in the laminateis was gradually spreading untill the laminate failed as it is shown in Table 3.6. In order to understand the problem, properties of flat laminate pieces under dynamic loading have been studied. The following four groups of specimens were chosen to test the dynamic properties.

The first group of laminates consisted of rubber sheets 0.010 and 0.015 in. with natural rubber durometer 40, 0.030 and 0.050 in. with latex rubber durometer 40, and blue tempered steel sheets 0.002 in with the laminates having been fabricated in our lab. Dynamic test results for this group are listed in Table 2.8. The second and third groups of specimens were made by CR Industries Co. with thickness of one layer of rubber 0.015 in. and a steel sheet 0.012 in.. Their test results are shown in Tables 2.9,10. The second group of specimens have soft rubber (durometer 40) and the third group was made with hard rubber (durometer 75). The samples of the fourth group have very thin rubber 0.00125 in. and brass sheet interleaves 0.025in thick and their test results are shown in Table 2.11. Surface areas of the laminate specimens are 0.03-0.09 sq.in, applied compression stress 5,000-20,000 psi and total thickness of rubber about 0.045-0.100 in. The test system is the same as described in 2.1 above. The dynamic compression load includes 55% static preload and 45% alternating load as shown in Fig.2.12. According to the test results shown in Tables 2.8-11, the following conclusions could be observed.

2.2.1 Laminates with Hard Rubber Have the Best Dynamic Properties

Comparing the tests results of four specimens in four groups : No.1 in Table 2.8, No.2 in Table 2.9, No.3 in Table 2.10 and No.2 in Table 2.11 with the same surface areas about 0.035 sq.in, same total thickness of rubber about 0.045 in, and subjected to the same compression stress 10,000 psi, the laminate with three layers of a harder rubber in group three demonstrated the best dynamic performance; it was in good condition after 45,000 cycles (2.5 hours). The laminate made in our lab in group one failed after 1440 load cycles, the laminate with three layers of soft rubber in group two came close to failure in a twisting mode due to buckling after 1,200 cycles and the laminates with very thin rubber layers and brass interleaves were damaged due to rubber tearing after 3,000 cycles.

2.2.2 Relationship between Dynamic Stress and Static Ultimate Stress

The experimental results indicate that the allowable dynamic stresses are lower than 1/4 of static uitimate stresses. The Table 2.12 shows that the static ultimate stress of a laminate with three layers of soft rubber is 25,000 psi, one with three layers of hard rubber 42,500 psi and one with very thin rubber layers 0.00125in.and brass sheets is 22,800 psi. In dynamic tests, the sample with three layers of soft rubber failed under 5,000 psi lasting 13,500 cycles, the laminate with very thin rubber failed under 10,000 psi and 3,000 cycles, and the best specimen with the hard rubber was in good shape after 45,000 cycles under applied 10,000 psi stress. The specimens No.3,4, or 5,6 in Table 2.9 show that the laminate was in good condition under 5,000 psi dynamic compression load (about 1/5 of static ultimate stress) at the first half hour, then as loading cycles were accumulating, rubber in the laminate started to spread gradually until completely failed due to rubber tearing after 13,500 cycles (45 minutes). Specimens No.1,2,3,4 in Table 2.9 also indicate that the higher dynamic compression load, the less loading cycles to failure. Therefore when rubber-metal laminated parts are being designed, both dynamic load and fatigue life should be considered.

2.2.3 Effect of Surface Area of Laminates on Dynamic Properties

Surface area of laminated specimens effects their static and dynamic properties. For the static properties, a larger area increases the shape factor and thus increases the compression stiffness and ultimate stress. On the other hand, if an area is relatively small, i.e. the ratio of the area to the total thickness of the laminate is small, under compression load an unstability of the laminate develops. It is pronounced as relative shifting between the layers of the laminate (also called staggering). The shifting is intensifying until the laminate approaches to buckling condition and then completely fails due to rubber tearing.

According to structure of samples and approximate formulas in reference [28] the buckling stresses for the samples were calculated and listed in Table 2.12. Table 2.12 also lists characteristics of five laminated pieces having the same surface area about 0.035 sq.in. For a laminate with three layers of soft rubber the static ultimate stress determined from the tests is close to the calculated buckling stresses as shown in Table 2.12: the ultimate stress is 25,000 psi and the calculated buckling stress is 27,000 psi; for the four soft-rubber-layer specimen the ultimate stress 18,500 psi corresponds with the calculated buckling stress 21,000 psi; for the specimen with five soft-layers the ultimate stress is 8,400 psi while the calculated buckling stress is 18,000 psi. For the samples with soft rubber No.2,3 in Table 2.12, although dynamic compression stress 10,000 psi is smaller than the experimental ultimate static stresses 18,500 and 25,000 psi, the samples failed quickly after 1,000 cycles because their "start-of-shifting" stresses are 4,620 psi for 3 layers element with soft rubber, 3,820 psi for 4 layers of soft rubber. The samples No.3,4 in Table 2.9 also indicate that when the dynamic stress 5,000 psi (about 1/5 of static ultimate stress) is larger than the start-of-shifting stress 4620 psi, the failure also happened after 13,500 loading cycles (45 minutes). Therefore, according to the experimental results, if the area of laminate is small, e.g. a ratio of the area to the total thickness of laminate is smaller than 2, a buckling force must be considered in the design process.

2.2.4 Elastic Stability and Buckling Stress of Small Area Laminates

For a laminate with a small surface area, the ratio of the area to the total thickness of the laminate is also a very important factor which has a direct effect on its load-carrying capacity. The following buckling force is calculated using formulas in reference [28] which were derived for laminates made from thicker (several millimeters thick) rubber layers. The critical buckling force P is determined from the equation

$$P^2 + k'P - 4\pi^2 T'k'/L^2 = 0 \qquad (2.12)$$

where:

$T' = Tt_T$; $T = E(1 + 2KS^2)I/t$; $k' = AE/3T$;

P - critical buckling force; T' - bending stiffness of a column of unit height; k' - shear stiffness of a column of unit height; T - bending stiffness; E - Young's modulus of rubber from Table 2.4; t_T - total thickness of a column unit consisting of a rubber block and a rigid separating plate; t - rubber thickness; A - cross sectional area; B - numerical constant; k - numerical factor from Table 2.4; S - shape factor which is a ratio of one loaded surface to the force-free surface; L - height of the column; I - cross sectional moment of inertia.

Constant parameters for the tested specimens are as follows:

$a = 0.2$ in; $A = 0.04$ sq.in; $I = a^4/12 = 1.3*10^{-4}$ in^4; $t = 0.015$ in; $t_T = 0.0275$ in; $S = a/4t = 3.3$

for specimens made of softer rubber with durometer 40: E= 218 psi; k= 0.85 ;

for specimens made of harder rubber with durometer 75: E=1,363 psi; k= 0.52;

for specimens with three rubber layers: $L_3 = 0.015*3+0.0125*4 = 0.095$ in;

for specimens with four rubber layers : $L_4 = 0.015*4+0.0125*5 = 0.1225$in;

for specimens with five rubber layers : $L_5 = 0.015*5+0.0125*6 = 0.15$ in;

$k'_{soft} = AE/3t = 0.04*218/3*0.015 = 193$;

$k'_{hard} = 0.04*1,363/3*0.015 = 1,212$;

$T'_{soft} = E(1+2kS^2)It_T/t = 218(1+2*0.85*11)1.3*10^{-4}*0.027/0.015 = 1.02$;

$T'_{hard} = 1,363(1+2*0.52*11)1.3*10^{-4}*0.027/0.015 = 4.18$.

Accordingly, the values of the critical buckling force are:

1) For three layers soft rubber specimen:

$P^2 + 193P - 4\pi^2*193*1.02/0.0952 = 0$; P = 1,030 lb ($\sigma$ = 27,000 psi);

2) For four layers soft rubber specimen: P = 823 lb (σ = 21,000 psi)

3) For five layers soft rubber specimen: P = 690 lb; (σ = 18,000 psi)

4) For three layers hard rubber specimen: P = 5,350 lb; (s = 133,750 psi).

Above calculation results show that the laminate with hard rubber has a much higher allowable buckling stress than all the soft rubber specimens (133,750 psi), which correlates well with its satiafactory performance under the alternating compression stress 10,000 psi for 45,000 cycles.

2.2.5 Influence of Rubber Material

For the larger area laminates the buckling stress is high, so there is no instability problem under high compression loads. In such cases the rubber material is becoming an important factor influencing dynamic properties of the laminates. The following three samples which have the same surface area 0.070 sq.in were subjected to the same dynamic compression stresses 10,000 psi. The sample with natural rubber sheets glued to metal interleaves and total thickness of rubber 0.045 in (No.2 in Table 2.8) was only subjected to 1,920 loading cycles after which the rubber permanently spread out for 0.016in from the free side of the laminate; the sample with glued latex rubber sheets and total thickness of rubber 0.060in (No.5 in Table 2.8) was intact after 18,000 cycles, then rubber gradually spread and failed at 27,000 cycles; the sample bonded and cured at a high temperature (made by CR Industry Co.) with a synthetic rubber of durometer 75 and total thickness of rubber 0.075in. (No.8,9 in Table 2.10) was in good shape after 54,000 cycles at 10,000 psi, and then after being subjected to 15,000 psi lasting 54,000 cycles rubber spread for 0.016in. permanently. Thus, the laminate with the blend hard rubber has been shown to be the best one. However, a better bonding quality also contributed to the better performance of this specimen.

2.2.6 Heat Buildup in Laminates under Dynamic Load

For the laminates which failed in the "rubber spreading" mode under the alternating loading, temperature increases during the loading process have been studied. A thermocouple was used to measure the temperature rise during dynamic compression test of a flat laminate at INSTRON test machine. Some measurement results are listed in Table 2.13 which shows the temperature raising about 8°F after three hours. The temperature remained almost constant after the first half hour. This is a very good property of laminates applying for machine design applications.

The equation for heat conductivity in a solid body containing an internal heat source is as follows [29]:

$$k\nabla^2 T + \dot{Q} = \frac{k}{\alpha}\frac{\partial T}{\partial t}$$

where: k - thermal conductivity; T - absolute temperature of the sample; $\dot{Q}$ - rate of internal heat generation; α - thermal diffusivity; t - time.

Therefore, the amount of heat generated is governed by two factors -- the inherent hysteresis of the elastomeric material and the degree of strain. The rate of heat generation $\dot{Q}$ is related to the strain rate. The other important process is the transport of heat generated inside the sample to the sample surface. The rate of heat transport is governed by the thermal conductivity of the internal structure and surface condition corresponding to term $k\nabla^2 T$ in the heat transfer equation. According to the measured results the temperature increase of the laminate with hard rubber is the same as for one with soft rubber. Although the hard rubber has a higher heat generation capacity, its strain is smaller than the strain in the soft rubber. The temperature remained constant after dynamic loading for half an hour because there is a good surrounding environment for the specimen surface (see Fig.3.6), namely, two big steel disks contact the top and bottom of laminate sample which can transport heat quickly.

CHAPTER 3 ENHANCEMENT OF LOAD-CARRYING CAPACITY OF LAMINATE COATED CONFORMAL GEARS

In the laminate coated gears [23] physical sliding between the meshing profiles is eliminated and bending and contact loading of the teeth are separated. Geometrical sliding is accommodated by internal shear deformation in specially designed rubber metal laminates, thus materials with high bulk strength but poor contact properties (aluminum, fiber-reinforced composites, etc.) could be used for heavy duty gears. Fig.1.1 shows this concept of gear design. From the tests described in Chapter 2, it can be concluded that specially designed laminates have very high compression load capacity and very high ratio of compression-to-shear stiffness which can satisfy requirements of the gear meshing. The obvious advantages of these gears are high expected dynamic load capacity and fatigue life which are the things for engineers to consider. In the previous sdudy [23] the maximun torque of the laminate-coated gear (module m=5mm, face width F=65mm) was 300 lb-1n. during several minutes of rotation. Our purpose was to improve the load capacity and fatique life to satisfy real industrial application requirements.

The test data in reference [23] shows that the sound pressure level for the laminate coated gears is reduced 10-20 dB as compared with the traditional gears. The largest noise reduction (15-20 dB) has been achieved for the conformal (Symmark) gears, while a lower reduction (10-15 dB) was demonstrated for involute gears due to variation of curvature radii of involute profile causing distortional compression deformation of the laminates. Therefore, Symmark gears were chosen as the test gears. Symmark gear is a conformal gear belonging to the Wildhaber-Novikov gear family whose tooth profiles are shaped as circular arcs in the transverse plane. In the Novikov gear, the mating gears have teeth with concave and convex surfaces, with the circular arcs of the pinion and the gear nearly conforming. Thus the tooth shapes conform, or envelope one another. Symmark gear has symmetrical arc profiles with its center at the intermeshing pitch point in the transverse cross section. The addenda of both pinion and gear teeth have convex profiles, and the dedenda have concave profiles as shown in Fig.3.1. Available in the Laboratory Symmark gears used in the previous tests [23] have the following parameters: tooth number of the pinion and gear $N_1 = N_2 = 12$; module m = 5 mm; face width F = 65 mm; center distance C= 64 mm. The laminate pieces were attached to the tooth surface of the pinion. All tests were performed with the gears mounted in the gear pump housing as shown in Figs.3.2 a,b,c. Two symmetric housings were assembled on the SCHENCK-PEGASUS servohydraulic four-square torsional test system. This system has variable rotational speed within the range 200 - 2000 rpm and can apply static and dynamic torque within 0 - 5000 lb-in with six dynamic functions in 0 - 100 Hz frequency range. Two housings were used in order to satisfy the assembling requirement of SCHENCK-PEGASUS test machine which has the same rotation directions of input and output shafts.

The key problem for improvement the load capacity of the laminate coated gears is development of an optimal laminate design, since it is the critical load-carrying component of the gear. The laminate is subjected to high contact loads during the meshing process, so it has to possess an adequate compression strength while its shape matches closely to the tooth profile of the Symmark gear. Shear deformation of the laminates is used to replace a sliding motion between tooth profiles during the meshing process, so the laminate has to have a large enough range of allowable shear deformation in order to accommodate the required sliding distance. In the following, calculations and analysis are described for the principal requirements: rated strength of the test gears; maximun sliding distance between the tooth profiles; an approximate geometric analogue of the tooth profile.

Several kinds of laminated elements have been designed and the prototype gears were fabricated using these elements; then the tests were performed to determine the best configuration. The tests were composed of two parts: rotational tests and vibration fatigue tests. The latter allowed to improve the test efficiency largely because only a few teeth paticipated in the test in one time.

to improve the test efficiency largely because only a few teeth paticipated in the test in one time. The best results achieved are: the static torque applied to the laminate coated gear has reached 1,600 lb-in, and the dynamic torque - 1,250 lb-in with 600 loading cycles and 1 Hz frequency.

3.1 STRENGTH CALCULATION OF SYMMARK GEARS

The laminated elements attached to the tooth are mainly subjected to contact loading during the meshing process. Therefore they must have high compression stiffness and high allowable compression stress. Thus in designing the special laminated elements, the first step is to determine the maximum contact stress on tooth profiles of Symmark gears for a given transmitted load. The bending stresses were also determined.

3.1.1 Bending Stress

One of advantages of the conformal gears is that they can accomodate three to five times higher contact loading as compared with involute gears without detrimental pitting or wear on the tooth profiles because conformal contact between a convex and concave surface of conformal gears results in a relative large contact elliptical area, which reduces the contact stress. On the other hand, the bending stress in the conformal gear teeth is close to bending stresses in the involute gear with the same dimensions and applied loads. Therefore, the load capacity of the test gears depends on their allowable bending stress. The bending stress of the test gear is calculated as in [22], using the same approach as for involute gears.

$$S_b = W_t K_a P_d K_b K_m / K_v F_E J \text{ psi}, \qquad (3.1)$$

where: S_b is bending stress number, psi; W_t - transmitted tangential load, lb; $K_a = 1.25$, bending application factor ; $K_b = 1.00$, rim thickness factor for bending strength; $K_m = 2.50$, bending load distribution factor; $K_v = 0.80$, bending dynamic factor; $P_d = 5$, transverse operating diametral pitch; $F = 2.28$ in., effective face width; J - bending geometry factor.

Assuming the applied torque to be 1,250 lb-in, the transmitted tangential load W_t is

$$W_t = T/R_p = 1{,}250/1.25 = 1{,}000 \text{ lb};$$

$$J = J' Q_{TR} Q_{TT} Q_A Q_H,$$

where $J' = 0.27$, basic geometry factor; $Q_{TR} = 0.84$, tool radius adjustment factor; $Q_{TT} = 1.00$, tooth thickness adjustment factor; $Q_A = 1.00$, addendum adjustment factor; $Q_H = 1.40$, helix-angle adjustment factor.

Thus,

$$J = 0.27 * 0.84 * 1.0 * 1.0 * 1.4 = 0.3175$$

$$S_b = 1{,}000*1.25*5*1.0*2.5/0.8*2.28*0.3175 = 26{,}980 \text{ psi}.$$

The calculated bending stress S_b must be within safe operating limits as defined by

$$S_b \leq \frac{S_{at} K_L}{K_T K_R}$$

where: $S_{at} = 41{,}000$ psi, allowable bending stress number for steel; $K_L = 1.0$, life factor for number of load cycles 10^7; $K_T = 1.0$, temperature factor; $K_R = 1.5$, reliability factor.

Thus

$S_b = 26{,}980 < 27{,}300$ psi.

Therefore, the assumption of the maximum torque T = 1,250 lb-in is acceptable.

3.1.2 Contact Stress

For the rated torque = 1,250 lb-in, the contact stress of the laminate coated conformal gear was calculated according to [20]. The calculation result indicates that the contact stress of the laminate coated gear is very small. This proves again the advantage of the new gears. The data were used to design the laminates.

$$S_c = (W_N E_c / 5.72 \rho_N L_N)^{0.5}, \tag{3.2}$$

where: S_c - contact stress, psi; W_N - normal contact load as shown in Fig.3.3 (equal to 1,258 lb as calculated below; E_c - compression modulus of the laminate, psi; ρ_N - lengthwise radius of the curvature (calculated below); L_N - line of contact in the normal cross section (calculated below).

According to the assumed maximun contact stress 16,800 psi, the compression modulus of laminate E_c is 100,000 psi from Fig.2.3b. The assumed maximun contact stress 16,800 psi came from the following estimation: the contact area of the laminated elements during meshing process is about 0.12 sq.in (=1/4 of face width * arc radius of tooth profile=15mm*5mm=0.6in.*0.2in.), thus the estimated average contact stress is 10,500 psi (W_N/0.12/=1,258 lb/0.12 sq.in). However, since the contact area of the tooth profile of the Symmark gear is helical cylindrical surface, the contact stresses are not distributed uniformly; thus the assumed maximum contact stress is 16,800 psi=10,500*1.6 psi, or 1.6 times higher than the estimated average contact stress.

$$W_N = W_t / m'_F \cos\psi \cos\phi; \tag{3.3}$$

where: W_t is tangential load at the pitch diameter, lb; m'_F - integral portion of m_F, here m'_F = 1.0; $\psi = 20.36^o$ - helical angle; $\phi = 32^o$ - pressure angle in transverse plane;

$$\rho_N = 0.5d \frac{(1 + \tan\psi \cos\phi)^{1.5}}{(\tan\psi)^2 \sin\phi} \frac{M_c}{M_c + 1}, \tag{3.4}$$

where : d = 2.5 in is pitch diameter; $m_G = R_2/R_1 = 12/12 = 1.0$ - reduction ratio;

$$L_N = L(\sin\phi / \sin\phi_N), \tag{3.5}$$

where: L is height of contact area, in; ϕ_N - pressure angle in normal plane;

$$L = 2\sin(\phi - \delta)\rho_1, \tag{3.6}$$

where: ρ_1 is profile radius of curvature of the pinion, $\rho_1 = m = 5/25.4 = 0.197$ in; δ - clearance angle required by the hobbing operation, which is chosen as 5^o from the reference [20].

According to above formulas and the constants, the calculating process runs as follows:

$L = 2\sin(32^o - 5^o)*0.197 = 0.1787$ in;

$\phi_N = \tan\text{-}1(\tan 32^o \cos 20.36^o) = 30.36^o$;

$L_N = 0.1787(\sin 32^o / \sin 30.36^o) = 0.1874$;

$\rho_N = 0.5*2.52\{(1 + \tan 20.36^o * \cos 32^o)^{1.5}/(\tan 20.36^o)^2 \sin 32^o\}*1/2 = 13.01$ in;

$W_t = T/d = 1{,}250/1.25 = 1{,}000$ lb;

$W_N = W_t/\cos 32^o \cos 20.36^o = 1{,}258$ in-lb;

$S_{c\text{-steel}} = (1{,}258*3*10^7/5.72*13.01*0.1874)^{0.5} = 52{,}000$ psi;

$S_{c\text{-lam}} = (1{,}258*10^5/5.72*13.01*0.1874)^{0.5} = 3{,}020$ psi.

From these calculations, it was found that if $E = 3*10^7$psi (steel), the contact stress of the conventional conformal gears is 52,000 psi which is about 32% of the contact stress for the similar size involute gears. It means that our calculations are right because, in general case, the contact stresses of the conformal gears are equal about 1/3 of the contact stresses in the involute gears. The contact stress in the laminate-coated gear is $S_{c\text{-lam}} = 3{,}020$ psi; this should be considered as an average contact stress. Although there is a difference between the calculated contact stress 3,020 psi and the estimated contact stress 10,500 psi, it is clear that the contact stress of the laminate-coated gear is much lower than that of the involute gears and these contact stress values could be a reference for designing the laminated elements.

3.2 CALCULATION OF THE SLIDING DISTANCE

Besides accomodating of high contact loads in order to transmit the torque, another main task of the laminate is to perform shear deformation in order to accomodate sliding motion during the meshing process. Thus the design parameters for the laminate pieces are the shear stiffness and the range of shear deformation. In Chapter 2 it was shown that the laminates have low shear stiffness. The range of shear deformation of the laminates should not exceed 75% of the total thickness of rubber. Below, the necessary sliding distance to be accommodated by the shear deformation of the laminate is calculated, according to the reference [30], to determine the total thickness of rubber in the laminates.

The sliding velocity between the mating involute teeth is constantly changing. However, for the conformal teeth, contact always occurs at a constant distance from the pitch point as shown in Fig.3.4, and sliding velocity is constant and unidirectional (for one particular direction of the gear rotation). In the helical direction the mating teeth with helical curvature R'_H and R''_H will roll together while in the transverse plane there will be a relative sliding velocity approximately equal to $(\omega_1 + \omega_2)r_N$, as shown in Fig.3.5. It represents a circular ring of radius R'_H with the circular cross section radius r_N, rolling along a stationary concave track with radius R''_H. The body of the ring is also rotating about the peripheral axis with a velocity $(\omega_1 + \omega_2)$. The sliding distance was calculated as following:

(1) Sliding Velocity :

$V_S = (\omega_1 + \omega_2)r_N = \omega_1(1 + \omega_1/\omega_2)r_N$;

(2) Rotation Time t_1 through the Face Width F

$1/\omega_1$ sec/rad = $t_1/(2\pi/N_1$ rad); $t_1 = 2\pi/N_1\omega_1$;

(3) Rotation Time $t_{1\text{-}b}$ through the Length of an Elliptical Contact Area

$t_{1\text{-}b} = t_1(b/F) = 2\pi b/N_1\omega_1 F$;

(4) Sliding Distance

$S = V_S t_{1\text{-}b} = \omega_1(1 + \omega_2/\omega_1)r_N(2\pi b/N_1\omega_1 B) = \{(1 + \omega_2/\omega_1)2\pi r_N b\}/N_1 B$;

Given: $\omega_1 = \omega_2$; r_N = 5 mm = 0.197 in; b = 6 mm = 0.236 in; N_1 = 12; B = 2.228 in. Then:

S = (1 + 1/1)2π*5*6/12*58 = 0.63 mm = 0.025 in.

(5) Shear Strain

If the total thickness of rubber is 0.045 in = 0.015 in * 3 layers, then shear strain of the rubber ε is

ε = 0.025/0.045 56%;

if the total thickness of rubber is 0.060 in = 0.015 in * 4 layers, then shear strain of the rubber is :

ε = 0.025/0.060 = 42%.

3.3 ANALYSIS OF PROFILE SURFACE OF CONFORMAL GEAR

Accuracy of the surface shape of the tooth profile is a very important factor in the mesh process, thus the shape of the laminate has to match very well with the profile of the Symmark gear which is the surface of a complex helical cylinder. In order to simplify the manufacturing process of laminate pieces of the prototype gear, the laminate pieces were cut obliquely from a laminate tube. How much error does this cause for the laminate match with the tooth profile? The following analysis and calculation is to prove that it is acceptable, although the error should be compensated by the local compliance of the laminate.

3.3.1 Formulas for Calculating Curved Surfaces of Conformal (Novikov) Gear

Since any transverse section of the surface of a Novikov gear is an arc and also a Novikov gear is a helical gear, the profile surface of this gear can be imaged as a part of a helical cylindrical surface with radius r whose central axis wraps on the pitch cylindrical surface with radius R_p along the angle β shown in Fig.3.6. Thus, to get the equation of the curved surface we only need to write down the equation of the helical cylindrical surface.

r and trace of whose center points is a helical line (the helical angle is β which is always on the surface of the pitch cylinder of radius R_p). From Fig.3.7, we get that when $z = 0$, the center point of circle O' is at (a, b, 0) , and

$$a^2 + b^2 = R_p^2;$$

$$\langle xOO' = \alpha_o = \tan^{-1}(b/a).$$

When $z = z_1$, the center point of circle O" is at (x_1, y_1, z_1), and

$$x_1^2 + y_1^2 = R_p^2 = a^2 + b^2;$$

$$\langle x'O_1O'' = \alpha_o + \alpha.$$

Now, we need to find α. From Fig.3.8, we can see that when a point P moves from P to P' along the helical line, it rotates an angle $\alpha = 2\pi$ and arc $= 2\pi\sqrt{a^2+b^2}$ in the plane of the circle and moves in z direction

$$z_{2\pi} = 2\pi(\sqrt{a^2+b^2}/\tan\beta).$$

Thus, when a point P moves from O' to O" in Fig.3.7 (or moves from P to P" in Fig.3.8), it moves z_1 in z-direction and rotates for angle α in the circle plane O" which could be expressed as follows:

$$\alpha/z_1 = 2\pi/z_{2\pi} = 2\pi\tan\beta/(2\pi\sqrt{a^2+b^2});$$

$$\alpha = (\tan\beta/\sqrt{a^2+b^2})z_1. \qquad (3.7)$$

Then we can get coordinates of x_1 and y_1 represented by z_1,

$$x_1 = \sqrt{a^2+b^2}\cos(\alpha_o + \alpha) = \sqrt{a^2+b^2}\cos\{(\tan\beta/\sqrt{a^2+b^2})\, z_1 + \tan^{-1}b/a\}; \qquad (3.8)$$

$$y_1 = \sqrt{a^2+b^2}\sin(\alpha + \alpha_o) = \sqrt{a^2+b^2}\sin\{(\tan\beta/\sqrt{a^2+b^2})z_1 + \tan^{-1}b/a\} \qquad (3.9)$$

Thus the equation of the helical cylindrial surface is

$$(x - x_1)^2 + (y - y_1)^2 = r^2; \qquad (3.10)$$

$$\{x - \sqrt{a^2+b^2}\cos[(\tan\beta/\sqrt{a^2+b^2})z_1 + \tan^{-1}b/a]\}^2 + \{y - \sqrt{a^2+b^2}\sin[(\tan\beta/\sqrt{a^2+b^2})z_1 + \tan^{-1}b/a]\}^2 = r^2 \qquad (3.10')$$

In order to get a curve A_1- A_2 on the tooth profile which is parallel to central axis O'O" shown in Fig.3.9, a cylindrical surface of radius R_1 is used to dissect the helical cylinder surface of radius r and the common intersectional curve of these two curved surfaces is curve A_1A_2. From Fig.3.9, we also can get equation of the cylindrical surface of radius R_1 as follows:

$$x^2 + y^2 = R_1^2, \qquad (3.11)$$

$$x^2 + y^2 = R_1^2, \tag{3.11}$$

where

$$R_1^2 = (a - r\sin\theta)^2 + (b - r\cos\theta)^2. \tag{3.12}$$

Therefore, when a series of values $z = z_1$ is given, coordinates (x, y) of the points on the curve A_1A_2 can be calculated from the equations (3.10') and (3.12).

3.3.2 Formulas for Calculating Oblique Cylinder Surface

In order to get an oblique cylinder surface which is used to approximately match the helical cylinder surface, let't imagine a cylinder, which at first rotates an angle α_1 around X axis from the frame XYZ to X'Y'Z'and then rotates an angle β_2 around Y' axis from the frame X'Y'Z' to X"Y"Z", Fig.3.10.

Any normal cross section of the oblique cylinder which is perpendicular to Z" axis is a circle. From Fig.3.11, when $Z = Z_1$, coordinates of this circle center is

$$\{a + (Z_1/\cos\alpha_1)\tan\beta_2,\ b + Z_1\tan\alpha_1,\ Z_1\},$$

thus the equation of the oblique cylindrial surface with fixed Z_1 is

$$\{X" - [a + Z_1\tan\beta_2/\cos\alpha_1]\}^2 + \{Y" - (b + Z_1\tan\alpha_1)\}^2 = r_1^2, \tag{3.13}$$

where $r_1 = r\cos\alpha_1$.

Now the relationship between X"Y"Z" and XYZ can be described as follows:

$$\begin{pmatrix} X' \\ Y' \\ Z' \end{pmatrix} = \begin{pmatrix} 1 & 0 & 0 \\ 0 & \cos\alpha_1 & -\sin\alpha_1 \\ 0 & \sin\alpha_1 & \cos\alpha_1 \end{pmatrix} \begin{pmatrix} X \\ Y \\ Z \end{pmatrix}$$

$$\begin{pmatrix} X" \\ Y" \\ Z" \end{pmatrix} = \begin{pmatrix} \cos\beta" & 0 & \sin\beta" \\ 0 & 1 & 0 \\ -\sin\beta" & 0 & \cos\beta" \end{pmatrix} \begin{pmatrix} X" \\ Y" \\ Z" \end{pmatrix} \tag{3.14}$$

Then,

$$\begin{pmatrix} X" \\ Y" \\ Z" \end{pmatrix} = \begin{pmatrix} \cos\beta" & \sin\beta"\sin\alpha' & \sin\beta"\cos\alpha' \\ 0 & \cos\alpha' & -\sin\alpha' \\ -\sin\beta" & \cos\beta"\sin\alpha' & \cos\beta"\cos\alpha' \end{pmatrix} \begin{pmatrix} X \\ Y \\ Z \end{pmatrix} \tag{3.15}$$

$$X'' = X\cos\beta'' + Y\sin\beta''\sin\alpha' + Z\sin\beta''\cos\alpha' \quad (3.16)$$

$$Y'' = Y\cos\alpha' - Z\sin\alpha' \quad (3.17)$$

Substituting (3.16), (3.17) into (3.13), an equation of oblique cylindrical surface becomes

$$\{X\cos\beta'' + Y\sin\alpha'\sin\beta'' + Z_1\cos\alpha'\sin\beta'' - [a + (\tan\beta''/\cos\alpha')Z_1]\}^2 +$$

$$\{Y\cos\alpha' - Z_1\sin\alpha' - (b + Z_1\tan\alpha')\}^2 = r_1^2. \quad (3.18)$$

As it was mentioned above, in order to get a curve $A'_1A'_2$ to approximately match the curve A_1A_2, a cylindrical surface of radius R_1 is used to intersect the oblique cylindrical surface of radius r, and the common curve of these two curved surfaces is the curve $A'_1A'_2$. Therefore, when a series of values $Z = Z_1$ is given, the coordinates (X_1, Y_1) of the points on the curve $A'_1A'_2$ can be calculated from equations (3.18) and (3.12).

Using the simultaneous equations (3.10'), (3.12) and (3.18),(3.12), the values (x_1, y_1) and (X_1, Y_1) can be obtained by computer calculations. The constants for the prototype Symmark gear are as follows:

a = 1.1969 inch ; b =0.4094 inch; $\beta = 20.64^o$; r = 0.2756 inch.

Then rotation angles of the oblique cylinder α', β' are optimized and a curve $A'_1A'_2$ which is approximately identical to A_1A_2 is obtained . Table 3.1 shows that when

$\theta = 8.2^o$; $Z_1 = 0, 1, 2, \ldots, 5$ mm, and $\alpha' = 8.5^o$; $\beta'' = -1^o$; (see Fig.3.9)

then

$error_x = (x - X)_{max} = 29.402 - 29\ 389 = 0.013$ mm;

$error_y = (y - Y)_{max} = 3.072 - 4.188 = -0.116$ mm.

Table 3.2 shows that when

$\theta = 40^o$; $Z_1 = 0, 1, \ldots, 5$ mm; $\alpha' = 8.5^o$; $\beta'' = -1^o$; (see Fig.3.9)

then

$error_x = (x - X)_{max} = 25.588 - 25.534 = 0.054$ mm;

$error_y = (y - Y)_{max} = 6.131 - 6.353 = -0.22$ mm.

Thus, the pieces of laminates cut obliquely from a laminate tube can approximately match the profile of the prototype Symmark gear and the error can be compensated by the local compliance of the laminates.

3.4 DESIGN OF SPECIAL LAMINATE PIECES

The above calculations have shown that the contact stress on the laminate is less then 10,000 psi and its shear deformation is 0.025 in under 1250 lb-in torque. The static test results in Tables 2.1, 2.2, 2.3 also indicate that the ultimate compression stresses of the laminates are higher than 20,000 psi. According to the above described calculations, the test results, and also to the measured amount of clearance between the gear teeth, as well as in order to reduce fabrication difficulties, parameters of the laminates were specified as follows:

rubber material - natural rubber;

thickness of one rubber layer - 0.015 in;

number of rubber layers - 3-4;

total thickness of rubber - 0.045-0.060 in (shear strain 56%-42%);

thickness of one intermediate steel layer - 0.002 in.

Geometric dimensions of the test gear are such that the length of arc of the profile is 0.15-0.20 in., thus the required width of the laminate is about 0.15-0.20 in. To obtain an adequqte flexibility of the laminate piece to match the tooth profile there was established a relationship between the thickness of the top steel layer and the length of the laminate. For a top steel layer thickness less than 0.004 inch, longer flat laminates (length about 0.5 inch) were chosen since they had adequate flexibility to match the tooth profile; for the top steel layer thickness 0.01-0.02 inch, the laminate pieces 0.15-0.2 inch long were cut from the laminate tube in order to match the tooth profile.

3.5 TEST ARRANGEMENT AND RESULTS

The test process had two stages:

1) rotation test (rotational speed 200 rev/min) and

2) vibration fatigue test

3.5.1 Rotation Tests

For these tests, all laminates were made in our lab with 0.015 inch thickness of rubber layers and 0.002 inch thickness of intermediate steel plates. The torque capacity tests were performed for different structure and thickness of the top steel layer; various numbers of rubber layers; various width of laminates; various positions of laminate attachment on the tooth profile. The test results are shown in Table 3.3.

At first, the laminates had four layers of rubber, the thickness of rubber sheet was 0.015 inch with area 0.45*0.2 sq.inch and the top steel thickness 0.002*8=0.016 inch; the top steel layer was made thicker to avoid indentation of the laminate under high contact stresses. The applied torque was 50, 100, 150, 200 lb-in. After rotating for 1,300 cycles the top steel layer was failing due to bending. The cause of failure was the fact that the laminate pieces were too wide, thus the bottom side of the laminates already exceeded the circular curved area of the working segment of the tooth profile. During the meshing process, the shear deformation of the laminate caused the

bottom of the laminate to touch fillet of the tooth, and then the top steel layer was broken due to its low flexibility.

In the next step, the laminate width was changed from 0.2 to 0.14 inch and applied torques were increased to 200, 250, 300, 350, 400 lb-in, while the total number of rotation cycles was increased to 4,000. The laminates were failing due to bending of the top steel layer and, also, some layers of steel and rubber were unglued; a fast bonding cyanoacrilate metal-to-rubber glue was used. Since the thicker top steel layer did not have adequate flexibility, the thinner top steel layer with thickness 0,002*3=0.006 inch and area 0.5*0.2 sq.inch was chosen for the next series of tests. As #3 of Table 3.3 shows, the maximum applied torque reached 500 lb-in and the total number of rotation cycles reached 5,500 (for 0-500 lb-in torque). After the width of laminate was further reduced to 0.16 inch, the maximum applied torque was increased to 700 lb-in (for 1,200 rotation cycles), with the total number of rotation cycles 5,600 as indicated in #4 of Table 3.3. After correcting position deviations of the laminates on the tooth profile to values smaller than 0.02in, further improvements were achieved (the maximum torque 850 lb-in for 300 rotating cycles, with the total number of rotating cycles 6,500). All laminates were failing by bending or breakage of the steel layer, as well as by some rubber spread.

3.5.2 Vibratory Tests

In order to improve efficiency of the experimental studies during the initial development stage, vibratory fatigue tests were introduced instead of the rotation tests. In the rotation tests, a lot of time was spent to prepare the prototype gear for which fabrication and attachment of 6*12=72 pieces of laminate by hand was required. To keep the same load conditions for the vibratory test as for the rotation test (shear deformation of the laminates during the meshing process should be same as for therotation tests), the required alternate rotation angle was established to be about 5^{o}:

the prototype gear has 12 teeth; since six pieces of laminate were applied to each tooth, then each laminate piece rotates in one rotating cycle for $360^{o}/12*6 = 5^{o}$.

The alternating rotation angle measurement system is shown in Fig.3.12. It transfers a rotational motion to a translational motion which is then measured by LVDT. One end of a thick wire is wound onto a coupling mounted on the gear shaft and another end is connected to a spring. When the gear shaft rotates, a block fixed on the wire moves up-and-down and pushes a LVDT. Then through a LVDT conditioner, the displacement signals of the LVDT can be displayed (or stored) on Nicolet 4094 oscilloscope. Finally, a rotation angle is calculated by converting the measured displacement of the LVDT. Vibration frequency was selected to be 1 Hz. The total dynamic torque includes 30-40 % static preload plus 60-70% alternating torque. The values of the static and alternating torque components were displayed on the front panel (controller) of the test machine.

The prototype gear (Symmark gear having symmetrical arcs) with laminates attached either to the addendum or to the dedendum part of the tooth profile were tested. Table 3.4 includes 8 sets of the test result. It shows that there are two sets of the test results. Regardless of where the laminates were attached - on addendum or on dedendum part - the maximum dynamic torque reached 1000 lb-in with more than 1000 cycles, and the laminates were always failing by separation of the top steel layer. In other sets of tests having lower maximum torques (700-800 lb-in), the failures were due to ungluing or tearing off of the rubber layers.

From analysis of these test results, it was suggested that the main failure reason was the inadequate adhesive strength of the glue. In the next step, the prototype gear with the laminates cut from the laminate tubes fabricated by CR Industries Co. (using high temperature bonding) were tested. The test results are shown in Table 3.5. In one set of tests the maximum torque reached

1250 lb-in, while in other tests it was in the range of 700-800 lb-in. All laminates had failed by rubber failure, not due to bonding disintegration. It means that the adhesive strength in this case was higher than strength of the rubber itself.

According to the strength calculations of the prototype gear, the average contact stress is lower than 10,000 psi and thus is much lower than the maximun allowable compression stress 20,000 psi for the laminates as described in Chapter 2. Therefore, it was concluded, that the reason for failure of the laminates on the tooth profile is not the strength of the laminate itself. It is possible that the effective shape of the tooth profiles deteriorated after the laminates were attached to them.

3.6 IMPROVING THE LAMINATE-COATED TOOTH PROFILE

It was already known that in the direction of the tooth width the laminate cut from an oblique cylinder can match the helical cylindrical tooth profile if the length of the laminate is about 0.2 inch. After the unsuccessful series of tests, a study was performed to find out if the tooth profile of the laminate-coated gear matches the tooth profile of the counterpart Symmark gear in the direction of transverse cross section.

A transparent frame shown in Fig.3.13 was made in order to observe the meshing process of the laminate coated gear. We found that two tooth profiles did not touch conformally along a circular surface, but only touched at the edge of the laminate. Then a computer graphical simulation shown in Fig.3.14 was performed. Obviously, the uniform thickness laminate shown with dashed line could not fit the tooth profile shown with solid line. A maximum error is about 0.035 inch. This is why the thinner top steel layer (thickness 0.006 in.) could withstand 800 lb-in torque(see Table 3.3, No.5) during the rotating test. It happened because it is flexible enough to match the engaging tooth profile. However, its bending strength was not high enough for such high contact stresses. It seems that the laminates made by CR Industries Co. failed in a rubber tearing mode because the deteriorated tooth profile distorted the rubber of the laminate during the meshing process.

In accordance with this analysis, the laminate pieces cut from the tube made by CR Industries Co., were grounded along the arc in order to reach the thickness profile corresponding to the shape obtained from the computer graghics simulation. This led to a significant improvement in performance. Several test results have shown the following: the maximum torque increased to 1,300 lb-in lasting 650 vibration cycles with the total number of cycles 1,300 for the applied torques 700 to 1300 lb-in; the number of the rotation cycles was more than 1,000 with 8^{o} and 1 Hz frequency under 1,000 lb-in. torque; , the number of rotation cycles is 1800 with 6 degree and 1 Hz Under 800 lb-in torque. All laminates were failing in such a mode that the top steel layer gradually shifted down and the rubber was gradually spreading, but no pronounced rubber failure was observed. In addition, rotation cycles reached 10,000-12,000 (half hour) with rotation angle 1^{o} and 8-10 Hz under 800-1,000 lb-in torque. In such a regime the laminates have shown only a minor spreading. These results are shown in Table 3.6 from which it can be seen that the laminates could be subjected to 1600 lb-in static torque. The ensuing stress

$$s = 1600/(1.25*0.12) = 10,700 \text{ psi}$$

is corresponding with the properties of laminates as described in Chapter 2.2. But when the gear dynamic test (under load and rotation) was performed, the laminates failed in a rubber spreading mode. This led to a study of dynamic properties of laminates as described in Chapter 2.3.

CHAPTER 4 COMPOSITE GEAR

4.1 MESHING CONDITIONS OF COMPOSITE GEAR SYSTEM AND GENERATION OF TEETH PROFILES

See Appendix 1 "Study of Meshing Condition of A Novel Gear System"

4.2 DESIGN OF THE COMPOSITE GEAR

According to the concepts of the composite gear system described in Chapter 1 and in the Appendix, a pair of gears was designed which included an involute gear meshing with a composite gear. The set was fabricated for testing on the Schenck-Pegasus servohydraulic torsional test system (see Fig.3.2) using gear pump cases as gear housings. Design dimensions of the gears should allow them to be fitted in these housings.

4.2.1 Design Parameters of Prototype Composite Gears

Considering the given center distance of the gear pump case 2.52 inch and for easy fabrication (minimun tooth number), basic parameters of prototype gears are as follows: teeth numbers of both the involute the composite gears $N_1 = N_2 = 10$, diametral pitch $P_d = 4$, face width $B = 1.25$ inch. Others parameters are:

a) Pressure Angle α

The formula which considers the minimum teeth number without undercut for an involute gear is

$$N_{min} = 2h^*_a/(\sin\alpha)^2 = 2*1/(\sin 31^o)^2 = 8 < 10, \qquad (4.1)$$

where $h^*_a = 1$ is addendum factor . Thus pressure angle $\alpha = 31^o$ satisfies the requirment of minimum tooth number for the involute gear.

b) Operating pressure angle α'

The given center distance of the housing is C'=2.52 inch and the center distance for the prototype gears is C=2.5 inch,

$$c = (N_1 + N_2)/2P_d = (10 + 10)/2*4 = 2.5.$$

Thus :

$$\alpha' = \cos^{-1}[(C/C')\cos\alpha] = \cos^{-1}[(2.5/2.52)\cos 31^o] = 31.7371^o.$$

c) Check of Contact Ratio E

$$E = 1/2\pi\{N_1(\tan\alpha_{a1} - \tan\alpha') + N_2(\tan\alpha_{a2} - \tan\alpha')\},$$

where:

α_{a1}, α_{a2} are addendum angles of gear 1 and gear 2;

$\alpha_{a1} = \alpha_{a2} = \cos^{-1}(r_{b1}/r_{a1}) = \cos^{-1}(1.07146/1.5) = 44.4136^{o}$,

where:

pitch radius $r_{p1} = N_1/2P_d = 10/2*4 = 1.25$ in;

base radius $r_{b1} = r_{p1}\cos\alpha = 1.25\cos31^{o} = 1.07146$ in;

addendum radius $r_{a1} = r_{p1} + 1/P_d = 1.25 + 0.25 = 1.5$;

$E = 1/\pi\{10(\tan44.4136^{o} - \tan31.7371^{o})\} = 1.15$.

4.2.2 Structural Design of the Prototype Composite Gear

The basic design concept of composite gears involves only pure rolling motion between the contacting tooth profiles, and torsional deformations of laminate bushings replace the sliding motion between the tooth profiles during the meshing process. A pair includes a composite gear and a involute gear. The structural design of the prototype composite gear is shown in Fig.4.1. Each tooth of the composite gear consists of a tooth segment 1, a pair of laminate bushings 2 and pins 3 inside the bushings which connect them with the tooth segments. The laminate bushings 2 have two functions. They serve as bearings and also as torsional springs with high radial stiffness. Each tooth segment is mounted on two pins whose other ends are press fit into the laminate bushings. The outside sleeves of the laminate bushings are fixed in the gear face plates 4. During a meshing process, there is a pure rolling motion between the surfaces of the tooth segment of the composite gear and the tooth profile of the involute gear, meanwhile the tooth segment rotates about 10^{o}. The rotation is supported by torsional deformation of the laminate bushings (i.e. by shear deformation of the rubber).

4.2.3 Strength Calculations

a) Bending Stresses [20]

Bending of an involute gear tooth is equivalent to bending of a cantilever beam. However, it is not necessary to check the bending stresses for the composite gear since its tooth segment can rotate around the bushing pins and thus is experiencing pure compression, see Fig.1.4 in Ch.1. Thus, the bending stress is checked only for the involute gear [20],

$$S_t = (W_t*k_a/k_v)P_d/B(k_s*k_m/J) \text{ psi.} \qquad (4.2)$$

Here: S_t is bending stress, psi; W_t --- transmitted tangential load, lb; k_a --- application factor = 1.15; k_s --- size factor =1; k_m --- load distribution factor =1.4; k_v --- dynamic factor = 0.8; J --- geometry factor = 0.30.

$$S_t < S_{at}*k_L/k_Tk_R, \qquad (4.3)$$

where: S_{at} --- allowable bending strength =36,000 psi (steel HB =250); k_L --- life factor =1; k_T --- temperature factor = 1; k_R --- reliability factor = 1.25.

Thus,

$S_t = 36,000*1\ /1\#.\ 1.25 = 28,000$ psi,

and

$W_t = (S_t k_v/k_a)B/P_d(J/k_s k_m) = (28{,}800*0.8/1.15)1.25/4(0.30/1*1.4) = 1{,}300$ lb.

Therefore (see Fig.4.2) the resultant (compression) tooth load is:

$W = W_t/\cos\alpha = 1{,}300/\cos 31^o = 1{,}500$ lb.

Radial tooth load is:

$W_d = W_t \tan\alpha = 1{,}300\tan 31^o = 780$ lb,

and the torque is

$T = W_t r_p = 1{,}300*1.25 = 1{,}625$ lb-in

b) Contact Stress of Composite Gears [20]

The contact stress S_c is

$$S_c = C_p(W_t C_a C_s C_m C_f/C_v dFI)^{1/2}, \tag{4.4}$$

and the transmitted tangential load W_t is

$$W_t = S_c^2 C_v dFI/C_p^2 C_a C_s C_m C_f. \tag{4.5}$$

Value of S_c in equation (4.5) is

$$S_c < S_{at}(C_L C_H/C_T C_R), \tag{4.6}$$

where: S_{ac} --- allowable contract stress=122 ksi for HB = 277 or RC = 28 (tooth hardness of the test involute gear); C_L --- life factor =1 for N=107; C_H --- hardness ratio factor = 1.09 for surface finish = 32 μin; C_T --- temperature factor = 1; C_R --- reliability factor = 1.25. Thus

$S_c < 122*1*1.09/1*1.25 = 106{,}400$ psi.

Other parameters in equation (4.4) are: W_t --- transmitted tangential load; C_p --- elastic coefficient = 2,300 for steel; C_a-- application factor = 1.15; C_s --- size factor = 1.0; C_l --- load distribution factor= 1.6; C_f --- surface condition factor = 1; C_v --- dynamic factor = 0.8 for V_t = 1300 ft/min; d --- pitch diameter = 2.5 in; F --- face width of the gears = 1.25 in; I --- geometry factor = 0.092. Thus,.

$W_t = S_c^2 0.8*2.5*1.25*0.1104/2{,}300^2*1.15*1*1.6*1 = 2.36*10^{-8}S_c^2$,

and the allowable maximun torque T is

$T = W_t(d/2) = 1.25W_t = 2.95*10^{-8}S_c^2$.

Therefore, for the prototype involute gear

$T = 2.95*10^{-8}*106{,}400^2 = 335$lb-in.

The relatively low torque value is due to the fact that the prototype gear was fabricated from a mild (not heat treated) steel. It should be noted that the allowable contact stresses for the composite gear can be expected to be about two times higher than that for the involute gear. It was shown in [26] that the allowable contact stresses for a pure rolling motion are two to three times higher than the allowable contact stresses for a combination of rolling and sliding motions. Thus the allowable contact stress for the composite gear can be assumed to be $S_{c\text{-}comp} = 2S_c$, and the maximun allowable torque for composite gears would be

$$T_{comp} = 3.54*10^{-8}S^2_{c\text{-}comp} = 3.54*10^{-8}(2*106{,}400)^2 = 1{,}337 \text{ lb-in.}$$

c) The Shaft Diameter of Gears d [20]

$$d = \{(32/\pi)n[M/S_e + (\sqrt{3}/2)(T/S_u)]\}^{1/3}, \qquad (4.7)$$

where (for the shaft material steel 1040): n --- design factor = 1.6; M --- bending moment = $F_r(L/4)$ = 1,500(2.8/4) = 1,050 lb-in; T --- torque = 1,625 lb-in; S_e --- bending endurance strength = 16,000 psi; S_u --- ultimate strength = 103,000 psi. Thus,

$$d = \{(32/\pi)1.6[1{,}050/16{,}000 + (\sqrt{3}/2)(1{,}625/103{,}000)]\}^{1/3} = 1.09 \text{ in.}$$

d) Pin Diameter of the Tooth Segment d_1 in the Composite Gear

The pin is subjected to a shear load which is equal to half compression load (W/2) applied to the gear,

$$\tau_a < W/2(\pi d^2/4), \qquad (4.8)$$

where τ_a is allowable shear stress = $0.6S_u/2 = 0.6*103{,}000/2 = 30{,}900$psi. Thus

$$d_1 = 2\sqrt{\frac{W}{\pi\tau_a}} = 2\sqrt{\frac{1{,}500}{2\pi*30{,}900}} = 0.176 \text{ in.}$$

e) Design of Laminated Bushing for the Composite Gear

All dimensions of the bushing are determined by the following three criteria:

* The inside diameter of the bushing should be equal to the above calculated pin diameter;

* Value of the maximum shear deformation of rubber should be smaller than the total thickness of rubber.

* Restrictions of structural space in the housing should be considered.

The laminated bushing, Fig.4.3, consists of an outer and inner steel sleeves with the thickness 0.02 in. each, five layers of rubber made of rubber sheet 0.015 in., and four interleave layers of steel 0.002 in. thick. The main dimensions of the bushing are: inside diameter d_{in} = 0.1875 in.; outside diameter d_{out} = 0.46 in.; width B = 0.44 in.; total thickness of rubber h = 0.075 in.(=0.015*5 in.).

The maximun shear deformation of rubber in the laminated bushing during a meshing process is determined as follows:

the maximun rotation angle of the tooth segment $12^o = 0.21$rad;

the smallest radius of a rubber layer $r_1 = 0.5*(0.1875+0.02*2) = 0.114$ in.;

the largest radius of a rubber layer $r_2 = 0.5*(0.46-0.02*2) = 0.21$ in.

Accordingly, the length of rotation arc is $l_1 = r_1\alpha = 0.114*0.21 = 0.024$ in.
$l_2 = r_2\alpha = 0.21*0.21 = 0.044$ in.;

the shear strain $\varepsilon_1 = l_1/h = 0.024/0.075 = 32\ \%$;
$\varepsilon_2 = l_2/h = 0.044/0.075 = 59\ \%$.

Therefore, the shear deformation of the laminate bushing is in the allowable range.

Compression loading of the laminate bushing is

$$\sigma_{com} = F_{com}/A = 1500 \text{ lb}/0.369 \text{ sq.in} = 4{,}058 \text{ psi},$$

where F_{com} is compresion force; A - projection of the rubber layer surface area of the bushing,

$$A = 2r_2B = 2*0.42*0.44 = 0.369 \text{ sq.in};$$

factor 2 considers two bushing supporting one tooth segment.

According to the previous test results in Chapter 2, the above compression stress satisfies the strength requirements of the laminate.

4.3 APPROXIMATION OF EXTERNAL SURFACE OF THE TOOTH SEGMENT BY CIRCULAR ARCS

It can be seen from Table 4.1, that variation of the curvature radius of the profile surface with the center O' is (0.6971 - 0.6753) / 0.6753 = 3.2%. Therefore, it can be concluded that if an optimum center O_p were chosen, the radius variation would become minimal and a circular profile of the segment would approximate the computed profile, and manufacturing of the tooth segment would be simplified. A method of three point approximation on the arc was used for finding the optimum center O_p. After the optimization procedure had been performed, it was found that the best three points are points of addendum (x_1, y_1), pitch circle (x_2, y_2) and dedendum (x_3, y_3) which were used to form the circular surface. The calculation from a set of simultaneous equations is as follows:

$$(x_1 - x)^2 + (y_1 - y)^2 = (x_2 - x)^2 + (y_2 - y)^2$$
$$(x_1 - x)^2 + (y_1 - y)^2 = (x_3 - x)^2 + (y_3 - y)^2 \qquad (4.9)$$

Simplifying these equations, obtain

$$(x_2 - x_1)x + (y_2 - y_1)y = [(x_2^2 - x_1^2) + (y_2^2 - y_1^2)]/2$$
$$(x_3 - x_1)x + (y_3 - y_1)y = [(x_3^2 - x_1^2) + (y_3^2 - y_1^2)]/2 \qquad (4.9')$$

By solving these simultaneous equations, the optimum center is found to be O_p(0.10594, 0.036165). The difference between accurate curvature radii and the constant radius associated with the optimum center is 0.5850 - 0.5829 = 0.021 in, or the relative deviation (0.5850-0.5829)/0.5829 = 0.36%. Since the error is very small and can be easily compensated by local compliance of the laminated bushing, the circular surface of the tooth segment was adopted in the design as shown in Fig.4.4.

4.4 TESTING OF LAMINATED BUSHINGS

The laminated bushing is an important component of the composite gear. According to previous test results, the design parameters, such as compression stress and stiffness as well as shear stiffness, could satisfy the strength requerement. However, to consider the differences between laminated plate and laminated bushing, the tests were performed in the following three aspects.

4.4.1 Torsional stiffness of Laminated Bushing

As mentioned above, the shear stiffness of laminates plate is very small. The laminated bushings made in our lab have a spiral structure, e.g. a rubber strip and a steel strip were bonded and wound around the steel sleeve. In order to obtain a low shear stiffness, each laminated bushing was slit thus generating a narrow gap. Two designs of the laminated bushings: with a gap and without the gap were tested for their shear stiffness, compression stiffness and fatigue life. The test results indicate that there are no significant differences for these two structures. Thus the laminated bushings without the gap were used in the composite gear. The torsional stiffness of the laminated bushing is very small, about 0.08-0.1 lb-in/^{o}, as shown in Fig.4.5

4.4.2 Compression Stress and Compression Modulus

The tests were performed on INSTRON test mashine. Under the compression load 1,080 lb the compression stress is 5,000 psi (design requirement is 4,058 psi) with the compression strain 21% and compression modulus is 47,600 psi as shown in Table 4.2. The tests were repeated several times and the repeatibility of the results was good.

4.4.3 Fatigue Life

The fatigue tests of the laminated bushings simulated their real load condition in the meshing process of composite gears, e.g. the relative rotation angle of inside and outside rings of the laminate bushing was 15^o with a compression preload (compression strain 20%). The test set up is shown in Fig.4.6. After 12 hours test with the total number of loading cycles $4*10^5$ (5.5 hours with loading frequency 5Hz and 4 hours with frequency 18 Hz), the laminated bushing was intact. Fig.4.7 indicates that the torsional stiffness of the laminated bushing has not changed after the fatigue tests. The temperatute rise of the laminated bushing during the tests was 5-7^{o}F as shown in Fig.4.8

4.5 TESTS OF COMPOSITE GEARS

Tooth segments were fabricated by wire EDM and then measured using a Coordinate Measuring Machine at the GM Technical Center. Schematic of the tooth segment indicating the measured dimensions is shown in Fig. 4.9; the final drawing dimensions and measured dimensions for two segments are listed in Table 4.3. Although there were discovered significant deviations, a decision had been made to go ahead with the tests due to time constraints.

Rotational tests of the composite gear pair were performed on SCHENCK-PEGASUS torsional machine described in Chapter 3. The tests started at low speed (200rpm) with the gradually increasing speed up to 1,600 rpm and running at torques up to 300 lb-in. Then, the testing was performed in stages.

At the first stage, the gears had been run at 300 rpm & 200 lb-in; 300 rpm & 300 lb-in; 400 rpm & 200 lb-in; 400 rpm & 300 lb-in, for one half hour at each regime. Temperature increase was from 4°F at the first regime to about 10°F at the heaviest regime. At the second stage the running regimes were 400 rpm & 300 lb-in; 500 rpm & 200 lb-in; 500 rpm & 300 lb-in, all one half hour long; at the third stage - 600 rpm & 200 lb-in and 600 rpm & 300 lb-in; at the fourth stage - from 700 rpm & 200 lb-in up to 800 rpm & 400 lb-in (nine laps by 1/2 hour). After each stage, minor repairs were performed, related to imperfections of glue lines in the bushings and to inaccuracies of the teeth profiles together with soft surfaces of the teeth. At the final fifth stage of testingthe runs were performed at 1,000 rpm & 300 lb-in (2.9 HP); 1,000 rpm & 400 lb-in (4.6 HP); 1,200 rpm & 300 lb-in (4.1 HP); and 1,200 rpm & 400 lb-in (7.2 HP), all 1/2 hour long. Temperature increases of the gears were measured to be 47°F for the 4.1 HP regime and 81oF for the 7.2 HP regime. No desintegration of the bushings was observed, although the surface of the teeth segments deteriorated significantly.

It was considered a satisfactory first test since the segments were fabricated with large deviations of basic dimensions from the specified values and were not hardened. This was interpreted as an indicator of a significant compensating ability of the rubber-metal laminated bushings and of low sensitivity of the system to manufacturing errors.

CONCLUSIONS

1. Thin-layered rubber-metal laminates can accomodate very high static compressive forces, limited by strength of intermediate metal layers. It was demonstrated that specific compression forces up to 80 - 90,000 psi can be accomodated.

2. Dynamic compression forces are limited by strength of bonding between the rubber and metal layers. High strength bonding agents have to be used for the laminates which are employed in power transmission components.

3. Test facilities for testing of thin-layered rubber-metal laminates as well as novel gear concepts have been developed.

4. Conformal gears with laminate coating of the profiles have been tested; it was demonstrated that the gears have a potential for transmitting at least the same torque as steel gears.

5. Geometrical analysis has shown that meshing conditions of the composite gear system correspond to an approximate conjugate engagement. Optimization has been performed allowing to achieve a very good approximation to the conjugate system.

6. Testing of the first prototype of the compoisite gear system has demonstrated that it is a viable system. Next prototype should use hard contacting surfaces and utilize professionally bonded laminated bearings.

REFERENCES

1. Dinsdale, J., Jones, P.F., "The Electronic Gearbox - Computer Software Replaces Mechanical Couplings" CIRP Annals, 1987, pp. 247-249.

2. Winter, H., "Evolution of Gear Calculaiton Methods," Proceed. of the 2nd World Congress on Gearing, Vol. 1, pp. 3-19, Paris, 1985.

3. Dudley, D.W., "The Evolution of the Gear Art," pp.90.

4. Koniuk, E.A., Andreev, S.V., Fiktash, M.D., "Strength Analysis for Teeth of Gears Reinforced with Continuous Fibers," Mekhanika Kompositnikh Materialov (Mechanics of Composite Materials), 1982, No. 5, pp. 937-939 (In Russian)

5. Ikegami, K., Takada, M., "Strength of Fiber Reinforced Plastic Gears of Monocoque Structures", ASME Paper 84-DET-72, ASME, 1984.

6. Prince, M., "Large Spacecraft Active Deployment Hinges," AIAA Paper 83-0909-CP, AIAA, 1983.

7. Weck, M. Konig, W., (eds) "Zahnradung Getribeuntersuchungen [Studies of Gears and Transmissions]", Proceedings of the 24th Workshop, WZL - Techn, University of Aachen, 1983 (in German).

8. Dudley, D.W., "Handbook of Practical Gear Design", pp. 667.

9. Litvin, F.L., Zhang, J., Chaing, W.-S., Coy, J. J., Handschuh, R.F., "Crowned Spur Gears: Optimal Geometry and Generation", AGMA Technical Paper 87FTM7, AGMA , 1987.

10. Wildhaber, E., "Helical Gearing," U.S. patent 1,601,750.

11. Smith, J.D., "Gears and Their Vibration," Marcel Decker, 1983, 170 pp.

12. Berestnev, O.V., "Self-Aligning Gears," Nauka i Technika Publishing House, Minsk, 1983, 312 pp (in Russian).

13. Anderson, N.E., Lowenthal, S.M., "Spur - Gear - System Efficiency at Part and Full Load," NASA Technical Paper 1622, 1980.

14. Rivin, E.I., " Gears Having Resilient Coatings", US Patent4,184,380.

15. Rivin, E.I., "Mechanical Design of Robots," McGraw-Hill, N.Y., 1988, 320 pp

16. Rivin, E.I., "Properties and Prospective Applications of Ultra-Thin-Layered Rubber-Metal Laminates for Limited Travel Bearings," Tribology International, 1983, Vol. 16, No.l, pp. 17-26

17. Harris C., Crede, C. (Eds), "Shock and Vibration Handbook," McGraw-Hill, N.Y., i976

18. Schmidt, W.E., "Design, Testing and Performance of Elastometric Bearings," Lord Corporation, Publication LL2129.

19. Rivin, E.I., "Design and Application Criteria for Connecting Couplings," ASME J. of Mechanisms, Transmissions, and Automation in Design, 1986, Vol. 108, pp. 96-105.

20. Joseph E. Shigley, Charlers R. Mischke, "Standard Handbook of Machine Desigh", McGraw-Hill Book Company, 1986, 1,932pp

21. Ishibashi, A., Yoshino, H., Hirai, H., "Design, Manufacture, and Load Carrying Capacity of Novikov Gears with 3-5 Pinion Teeth for High Gear Ratios," Bulletin of JSME, 1985, Vol. 28, No. 238, pp. 701-706.

22. Chironis, N., "Design of Novikov Gears," in Gear Design and Application, McGraw-Hill, 1967.

23. Rivin, E.I., Wu, R.-N., "A Novel Concept of Power Transmission Gear Design," SAE Technical Paper 871646, SAE, 1987.

24. Rivin, E. I., "Conjugate Gear System", US Patent 4,944,196.

25. Dong, B., "Study of Meshing Condition of a Novel Gear System", AGMA Technical Paper 89FTMS1, AGMA, 1989.

26. Denning, R.E., Rice, S.L., "Surface Fatigue Research with the Geared Roller Test Machine", SAE Automotive Engineering Congress, January 14-16, 1963

27. Biderman, V.L., Martyanova, G.V., "Stressed Condition of Metal Armature during Compression of Thin-Layered Rubber-Metal Elastic Elements", in Raschety na prochnost [Strength Computations], # 26, Mashinostroenie, Moscow, 1985, pp.52-56 (in Russian)

28. P.K.Freakley and A.R.Payne, " Theory and Practice of Engineering with Rubber", Applied Science Publishers LTD, London, 1978.

29. Reed, T.F. " Heat Buildup of Dynamically Loaded Engineered Elastomeric Components-1", Elastomerics, Nov.1989.

30. Allan, T., " Some Aspects of the Design and Performance of Wildhaber-Novikov Gearing", Instn .Mech. Engrs, Vol. 179, Pt .1, No. 30, 1964-65.

Table-2.1 Test results for six laminates samples

No.	Term	#A	#B	#C	#D	#E	#F
1	Shaper Factor	6.5	4.7	8.4	4.3	2.7	1.75
2	Thickness of One Layer of Rubber (in)	0.013	0.017	0.010	0.020	0.030	0.050
3	Durometer	45	30	40	40	40	40
4	Damping	High	Low	Low	Low	Low	Low
5	Rubber	Blended	Natural	Natural	Natural	Latex	Latex
6	$E_{c-\sigma-10,000}$(psi)	100,100	39,200	95,000	75,000	50,000	43,000
7	$\epsilon_{\sigma-10,000}$	15%	29%	17%	23%	38%	45%
8	E_{c-max}(psi)	133,800	39,200	158,000	76,800	89,300	65,200
9	σ_{max}(psi)	15,600	10,000	45,000	11,800	27,400	22,430
10	ϵ_{max}	18%	29%	32%	25%	45%	51%
11	Shear Modulus G (psi)	N/A	52	65	65	55	53
12	Ratio of E/G	N/A	7503	2430	1180	1620	1230

$E_{c-\sigma-10,000}$ --- compression modulus for stress 10,000 psi

$\epsilon_{\sigma-10,000}$ --- compression strain for stress 10,000 psi

Table-2.2 Comparison of two samples with different thickness layers of metal

Laminate Sample	#D	#D7
Thickness of Top Steel Layer	0.002 in	0.002 in
Thickness of Intermediate Steel Layer	0.002 in	0.002*2=0.004 in
Thickness of Rubber Layer	0.020 in	0.020 in
Thickness of Total Rubber	0.02*2=0.04 in	0.02*2=0.04 in
$\sigma_{x\text{-}max}$	11,800 psi	30,000 psi
$E_{c\text{-}max}$	76,800 psi	320,000 psi

Table-2.3 Comparison of three samples with different thickness of metal layers

Laminate Sample	G3	G4	G5
Thickness of Top Steel Layer (in)	0.002*5=0.010 in	0.002*5=0.010 in	0.002*10=0.020 in
Thickness of Intermediate Steel Layer (in)	0.002 in	0.002*2=0.004 in	0.002*2=0.004 in
Thickness of Rubber Layer	0.015 in	0.015 in	0.015 in
Thickness of Total Rubber	0.060 in	0.060 iny	0.060 in
Area of Sample (in^2)	0.160	0.160	0.160
Contact Area (in^2)	0.053	0.053	0.053
σ_{z-max} psi	41,200	107,200	117,300
E_{c-max} PSI	230,300	448,100	481,600
ϵ_{max}	47%	46%	51%

Table-2.4 Hardness and elastic moduli* (from Lindley, 1970)

Hardness IRHD ± 2	*Young's modulus* E_0 MN m^{-2}	*Shear modulus* G MN m^{-2}	k	*Bulk modulus* E_∞ MN m^{-2}
30	0.92	0.30	0.93	1 000
35	1.18	0.37	0.89	1 000
40	1.50	0.45	0.85	1 000
45	1.80	0.54	0.80	1 000
50	2.20	0.64	0.73	1 030
55	3.25	0.81	0.64	1 090
60	4.45	1.06	0.57	1 150
65	5.85	1.37	0.54	1 210
70	7.35	1.73	0.53	1 270
75	9.40	2.22	0.52	1 330

*** Based on experiments on natural rubber spring vulcanisates containing (above 48 IRHD) SRF black as filler. Note that hardness is subject to an uncertainty of about ± 2 deg.**

Table-2.5 Comparison of compression moduli E-ex and E-cal for specimens A4 and B4

A4

No.	STRESS	STRAIN	a	E-ex	E-cal	E-ex/E-cal
1	830	0.033	1.03	24320	48250	0.50
2	1870	0.069	1.07	26010	54057	0.48
3	4000	0.1	1.1	57570	59450	0.97
4	6970	0.127	1.14	86430	65466	1.32
5	10910	0.156	1.17	100110	71867	1.39
6	15550	0.18	1.2	133800	78072	1.71
7	25590	0.249	1.29	101520	100004	1.02
8	30200	0.281	1.32	77790	111615	0.70

B4

No.	STRESS	STRAIN	a	E-ex	E-cal	E-ex/E-cal
1	490	0.046	1.05	10160	14685	0.69
2	1070	0.09	1.09	11440	16740	0.68
3	1890	0.138	1.15	13400	19666	0.68
4	3220	0.187	1.2	19020	23050	0.83
5	5890	0.24	1.29	31130	28331	1.10
6	9990	0.296	1.4	39170	35802	1.09
7	14460	0.353	1.45	35720	43868	0.81
8	19900	0.417	1.62	32060	60313	0.53

Table-2.6 Comparison of compression moduli E-ex and E-cal for specimen C4 and D4

C4

No.	STRESS	STRAIN	a	E-ex	E-cal	E-ex/E-cal
1	1330	0.052	1.05	24250	72564	0.33
2	3370	0.092	1.1	43900	82843	0.53
3	6340	0.13	1.15	61740	94317	0.65
4	11210	0.167	1.19	95340	106437	0.90
5	17330	0.199	1.24	127610	119925	1.06
6	24560	0.233	1.27	130640	133933	0.98
7	31160	0.258	1.3	150250	146471	1.03
8	45120	0.316	1.35	157910	178942	0.88
9	52040	0.345	1.42	106907	205228	0.52
10	54430	0.355	1.45	100970	216102	0.47

D4

No.	STRESS	STRAIN	a	E-ex	E-cal	E-ex/E-cal
1	490	0.035	1.03	12959	18164	0.71
2	1080	0.074	1.07	13977	20472	0.68
3	1740	0.109	1.1	15558	22713	0.68
4	2890	0.152	1.17	20207	26644	0.76
5	4750	0.187	1.2	36638	29708	1.23
6	8000	0.221	1.26	60539	33951	1.78
7	11810	0.25	1.29	76758	37477	2.05
8	16230	0.287	1.35	63881	43365	1.47
9	21240	0.331	1.42	54313	51769	1.05
10	26700	0.372	1.47	55949	60775	0.92
11	31800	0.406	1.48	52330	68396	0.76

Table-2.7 Comparison of compression moduli E-ex and E-cal for specimens E4 and F4

E4

No.	STRESS	STRAIN	a	E-ex	E-cal	E-ex/E-cal
1	210	0.047	1.05	4258	4382	0.97
2	440	0.095	1.1	4113	5602	0.73
3	670	0.14	1.16	3978	7187	0.55
4	960	0.185	1.22	4517	9308	0.49
5	1380	0.233	1.27	5470	12277	0.45
6	2090	0.278	1.34	8737	16417	0.53
7	3600	0.324	1.42	16021	22545	0.71
8	7140	0.365	1.46	37063	29682	1.25
9	13590	0.404	1.5	62591	39201	1.60
10	22740	0.44	1.62	84831	54219	1.56
11	27430	0.456	1.66	89298	62343	1.43

F4

No.	STRESS	STRAIN	a	E-ex	E-cal	E-ex/E-calE
1	130	0.053	1.05	2323	1937	1.20
2	240	0.104	1.1	1830	2472	0.74
3	390	0.156	1.17	2181	3271	0.67
4	590	0.211	1.26	2422	4527	0.53
5	870	0.263	1.3	3131	6047	0.52
6	1300	0.316	1.42	4090	8795	0.47
7	2100	0.366	1.46	6938	12138	0.57
8	4230	0.417	1.55	15437	17887	0.86
9	10730	0.464	1.66	43216	26668	1.62
10	22430	0.511	1.85	65247	42723	1.53
11	27430	0.539	2	40255	58357	0.69

Table-2.8 Dynamic test results for laminates made from rubber sheets by room temperature gluing.

No	No. of Rubber Layers	Total Thickness of Rubber	Area in^2	Compre. stress psi	No. of cycles	Freq Hz	Temp Raise °F	Result
1	3-natural	0.045	0.032	12,000	1,600	6		failed, rubber spread and glue took off
2	3-natural	0.045	0.097	10,000	1,950	1		OK, rubber spread 0.016 in
3	5-natural	0.050	0.09	10,000	800	1		OK, rubber spread 0.015 in
4	2-latex	0.060	0.07	10,000	18,000	5	6	OK
5	2-latex	0.060	0.07	10,000	27,000	5	8	failed, rubber spread 0.02 in, glue took off
6	2-latex	0.100	0.07	10,000	4,500	5	5.3	failed, rubber speard 0.02 in, glue took off

Note: A thickness of one layer of steel sheet is 0.002 in.

Table-2.9 Dynamic Test for Laminates with Soft Rubber Made by CR Industries Co.

No.	No. of Rubber Layers	Area in^2	Compression Stress psi	No. of Sycles	Freq. Hz	Temp. Raise °F	Result Laminate	Result Rubber
1	3	0.034	20,000	600	1		twist and close to fail	slight spread
2	3	0.034	10,000	1,200	1		twist and close to fail	spead
3	3	0.039	5,000	9,000	5	2	OK	slight spread
4	3	0.039	5,000	13,500	5	3.4	failed	tore
5	3	0.060	5,000	9,000	5	5	OK	slight spread
6	3	0.060	5,000	13,500	5	6	failed	tore
7	4	0.032	10,000	600	1		twist and close to fail	slight spread

Note:

1. The durometer of soft rubber is 40.
2. A thermometer is used to meassure the temprature raising.

Table-2.10 Dynamic test for laminates H75 rubber made by CR Industries Co.

No.	No. of Rubber Layers	Area in^2	Compression Stress psi	No. of cycles	Freq. Hz	Temp. Raise °F	Result
1	3	0.032	10,000	1,200	1		OK
2	3	0.035	10,000	9,000	5	5.6	OK
3	3	0.035	10,000	45,000	5	6.4	OK slightly spread
4	3	0.035	15,000	9,000	5	6.2	OK
5	3	0.035	15,000	45,000	5	7.8	OK spread 0.01 in.
6	3	0.070	15,000	9,000	5	6.2	OK
7	3	0.070	15,000	45,000	5	6.4	OK spread 0.008 in.
8	3	0.070	20,000	45,000	5	6.4	OK spread 0.016
9	5	0.070	10,000	9,000	5	5.0	OK
10	5	0.070	10,000	54,000	5	9.0	OK slightly spread
11	5	0.070	15,000	54,000	5	6.2	OK spread 0.016
12	5	0.070	20,000	54,000	5	7.6	OK spread 0.024

Table-2.11 Dynamic Test Results for Laminates with Brass Interleaves

No.	No. of Rubber Layers	Total Thickness of Rubber	Area in^2	Compre stress psi	No. of Cycles	Freq Hz	Temp Raise °F	Result
1	34	0.0425	0.034	10,000	1,200	1		OK, rubber spread slightly
2	34	0.0425	0.040	10,000	3,000	5	2	failed, rubber tore
3	34	0.0425	0.077	10,000	9,000	5	3	failed, rubber torea

Note: The thickness of brass sheet is 0.0025 in.
The thickness of one layer of rubber is 0.00125 in.
The total thickness of laminate is 0.13 in.

Table-2.12 Comparison of compression properties of laminates

No.	Rubber	Total Thickness of Rubber	Stress for Begining of Shifting	Ultimate Stress,psi	Calculated Buckling Stress,psi.	Dynamic Test Stress psi.	Cycles	Result
1	5-soft	0.075in.	2900	8,400	18,000			
2	4-soft	0.060in.	3900	18,500	21,000	10,000	600	twist
3	3-soft	0.045in.	4600	25,000	27,000	10,000	1,200	twist
						5,000	13,500	failed rubber tore
4	3-hard	0.045in.	32,600	42,500	133,750	10,000	45,000	OK
						15,000	45,000	OK, rubber spread 0.02in

Note:

1. The area of each specimen is about 0.035 sq.in.

2. The stress for shifting indicates the stress when the twist between laminate layers is begining to be observed.

Table-2.13 Temperature (F°) increase of laminates in dynamic compression tests

Rubber Area,sqin. σ,psi.	3-soft *0.039 *5,000	3-soft 0.056 5,000	3-hard 0.035 10,000	3-hard 0.035 15,000	3-hard 0.070 15,000	3-hard 0.070 20,000	5-hard 0.070 10,000	5-hard 0.070 15,000	5-hard 0.070 20,000
Time,min									
0	86	89	91.4	91.8	91.6	90.4	88	93.4	89.8
5	86.4	89.8	93	92.8	92.4		89.2	94.2	91.2
10	87.2	91.4	94.2	94.4	94.6	92.4	90.8	95.2	92
20	88	93.2	96.2	96.8	97	94.6	91.6	95.8	92.6
30		94	97	98	97.8	96.8	92.8	96.8	
60			97.6					97	93.2
90				99.6					
120									
150			97.8	99.6	98	97.2			
180							97.2	99.6	97.4

Note:

1. σ- Compression stress on rubber.

2. The 3-soft means that laminate has layers of rubber with durometer H40, 3-hard-about H75.

3. For all specimens thickness of one layer of rubber is 0.015 in., thickness of steel is 0.012 in.

Table-3.1 Comparing coordinates (x,y) with (X,Y) at $\theta=8.2^{O}$ $\alpha=8.5^{0}$, $\beta=-1^{O}$

Z_1 (mm)	x (mm)	X (mm)	x-X(mm)	y (mm)	Y (mm)	y-Y (mm)
1	29.402	29.389	0.013	3.072	3.188	-0.116
2	29.364	29.354	0.010	3.412	3.494	-0.082
3	29.277	29.275	0.002	4.093	4.108	-0.015
4	29.228	29.230	-0.002	4.432	4.416	0.016
5	29.174	29.181	-0.007	4.771	4.726	0.045

Table-3.2 Comparing coordinates (x,y) with (X,Y) at $\theta=40^{O}$ $\alpha=8.5^{O}$, $\beta=-1^{O}$

Z_1	x (mm)	X (mm)	x-X(mm)	y (mm)	Y (mm)	y-Y(mm)
1	25.854	25.864	-0.045	4.938	4.837	0.001
2	25.786	25.793	-0.007	5.237	5.202	0.037
3	25.723	25.715	0.008	5.536	5.575	-0.039
4	25.658	25.629	0.029	5.834	5.958	-0.124
5	25.588	25.534	0.054	6.131	6.353	-0.222

Table-3.3 Rotation tests of the laminate coated gear

No.	Torque lb-inch	Rotation Cycles	Dimensions of Laminate in. Thickness rubber Top Steel Width*length	Failure Mode
1	50-200	1300	0.015*4 0.020 0.20*0.40	top steel bent
2	200-400	6000	0.015*4 0.020 0.14*0.40	top steel bent, glue failed
3	100-500	4200	0.015*3 0.004 0.20*0.50	top steel bent, 1 layer of rubber spread out
4	300-700	5600	0.015*3 0.006 0.20*0.50	half of top steel layer bent, glue failed
5	200-800	5300	same as No.4, more accurate position of laminate.	same as above

Table-3.4 Coated gear vibration test

No.	Dynamic Torque lb-in	Span Cycles	Dimensions of Laminates Top Steel Thickness	Width*length	Failure Mode
1	700- 800	500	0.020	0.014*0.4	top steel took off
2	600- 800	650	same as above		same
3	600- 800	300	same as above		same
4	700-1100	1350	0.002*8-0.016	0.020*0.4	top steel took off rubber spread
5	800	350	0.020	0.15*0.4	glue failed
6	700- 800	400	same	same	same
7	700- 800	450	same	same	same
8	800-1000	1000	same	0.20*0.3	same

Note:

1. Specimens no.1-4 have four layers of rubber 0.015*4=0.060 in thickness; no. 5-8 have three layers of rubber 0.015*3=0.045 in thickness.

2. Only no. 8 specimen has laminates attached to addendum.

Table-3.5 Coated gear vibration test laminates(CR Industries Co.)

No.	Dynamic Torque lb-in	Span Cycles	Structure of Laminate Top steel Width*Length	Failure Situation
1	700-800	400	0.015 in 0.18*0.35	Rubber tore at bottom
2	700-1200	1250	same	same
3	700-750	400	same	same
4	650-700	300	same	same
5	650-750	450	same	same
6	650-750	750	same	same
7	650-720	450	same	same

Note:

1. Laminates were cut from tube made by CR Industries Co. (four layers of rubber 0.015*4=0.060 in.,three layers of steel 0.005*3 in., top steel layer 0.015 in.)

2. Specimens nos. 1-4 are made of #931 blend rubber, no. 5-7 from natural rubber.

3. All laminates were attached to addendum

4. Test frequency is 1 Hz, angle 6-8 degrees.

Table-3.6 Coated gear laminates vibration test with modified thickness

No.	Torque lb-in Static	Dynamic	Total	Span Cycles	Frequency Hz	Span Angle	Failure Situation
1	220- 420	430-880	650-1300	900	1	8°	rubber under top steel tore
2	300	700	1000	1400	1	8.5°	top steel sliped
3	300	700	1000	1200	1	9.5°	rubber under top steel tore
4	800-1600	0	800-1600	0	0	0	OK
5	350	750	1100	500	1	10°	top steel shafted 0.008 in, rubber spread alittle
6	280	520	800	1800	1	6°	top steel shafted 0.01 in, rubber spread a little
7	600	400	1000	12,000	10	0.5°	OK (rubber gradually spread a little)
8	550	450	1000	10,000	6	1.5°	OK (rubber gradually spead a little)

Note:

1. Laminates were cut from tube made by CR Industries Co. (rubber #931, thickness of one urbber layer 0.015 in, thickness of one intermidate steel layer 0.005 in, thickness of top steel 0.015 in

2. Specimens no. 1-3 have four layers of rubber, no. 4-8 three layers of rubber.

3. All laminates were attached to dedendum.

Table-4.1 Curvature Radii of Tooth segment

CENTER O'	OPTIMUM CENTER
ADDENDUM PART	ADDENDUM PART
0.6887 0.6879 0.6870 0.6862 0.6853 0.6844 0.6835 0.6826 0.6818 0.6809 0.6801 0.6793 0.6786 0.6779 0.6773 0.6767 0.6762 0.6759 0.6756 0.6754 0.6753 0.6753	0.5855 0.5853 0.5852 0.5850 0.5848 0.5846 0.5845 0.5843 0.5841 0.5840 0.5838 0.5837 0.5837 0.5836 0.5836 0.5837 0.5838 0.5840 0.5843 0.5846 0.5851 0.5856
DEDENDUM PART	DEDENDUM PART
0.6904 0.6911 0.6918 0.6925 0.6932 0.6938 0.6943 0.6949 0.6953 0.6957 0.6961 0.6964 0.6967 0.6969 0.6971 0.6972 0.6973 0.6974 0.6974 0.6973 0.6972 0.6971 0.6969	0.5857 0.5858 0.5859 0.5860 0.5860 0.5860 0.5860 0.5860 0.5860 0.5859 0.5859 0.5858 0.5858 0.5857 0.5856 0.5855 0.5855 0.5854 0.5854 0.5854 0.5854 0.5855 0.5856

Table-4.2 Properties of Laminate Bushing

Num	Bload-LB	Dpress-IN	STRESL	STRAINL	E1.LB/IN2
31	0.628E+02	0.146E-02	0.161E+03	0.180E-01	0.179E+05
2	0.122E+03	0.356E-02	0.474E+03	0.385E-01	0.148E+05
3	0.183E+03	0.550E-02	0.784E+03	0.590E-01	0.154E+05
4	0.266E+03	0.736E-02	0.115E+04	0.795E-01	0.208E+05
5	0.359E+03	0.972E-02	0.161E+04	0.107E+00	0.171E+05
6	0.445E+03	0.114E-01	0.207E+04	0.124E+00	0.274E+05
7	0.556E+03	0.133E-01	0.257E+04	0.145E+00	0.262E+05
8	0.698E+03	0.153E-01	0.322E+04	0.167E+00	0.335E+05
9	0.875E+03	0.173E-01	0.404E+04	0.190E+00	0.409E+05
10	0.108E+04	0.192E-01	0.502E+04	0.211E+00	0.476E+05
	LOAD (LB)	DEFORMATION (IN)	STRESS (PSI)	STRAIN	COMPRESSION MODULUS (PSI)

Table 4.3 Dimensional Inspection of Tooth Segments

Dimension	R	L_{max}	L_{bot}	L_{top}	ϕ
Spec.	$0.585^{+0.0004}$	0.6970	0.6964	0.6747	$0.1875^{+0.005}$
Seg.1	0.5687	0.6944	0.6624	0.6747	0.1877
Seg.2	0.5575	0.6954	0.6948	0.6753	0.1887

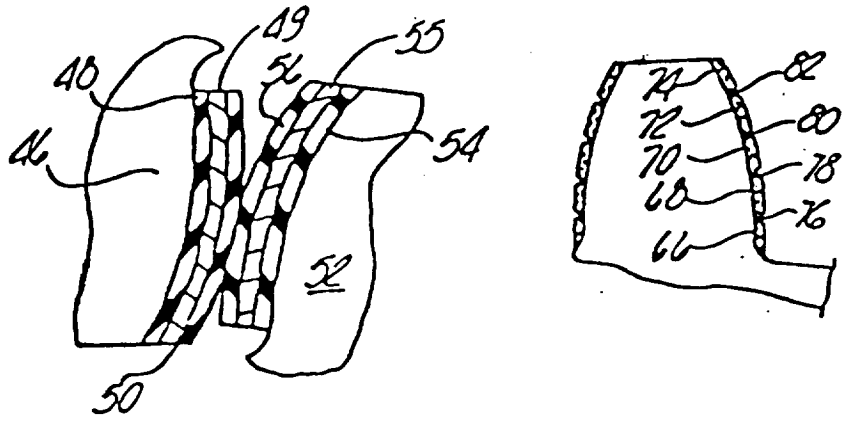

Fig 1.1 Rubber-metal laminate-coated gears

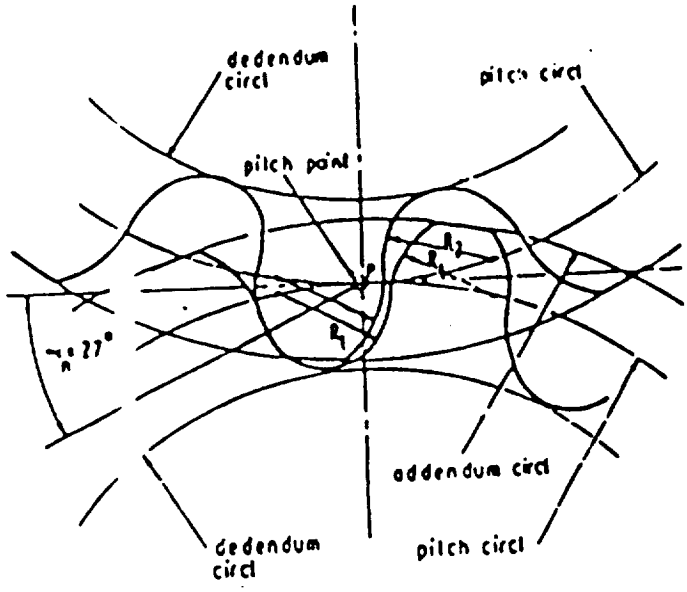

Fig. 1.2 Schematic of the conformal gear mesh

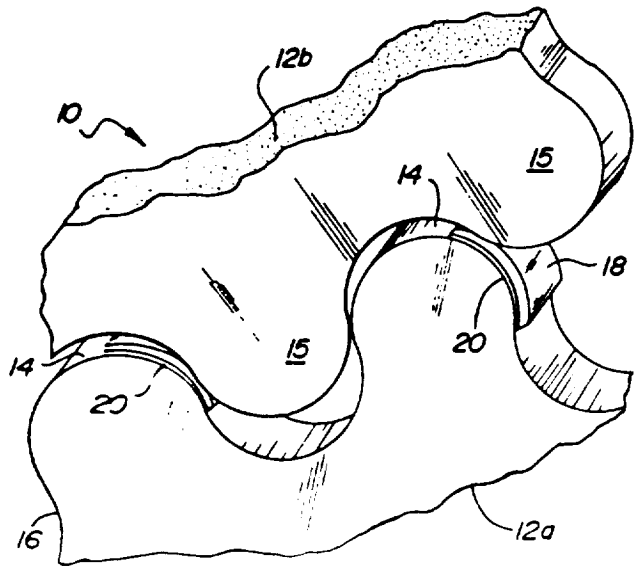

Fig. 1.3 Gears with separation of sliding & rolling (composit gears)

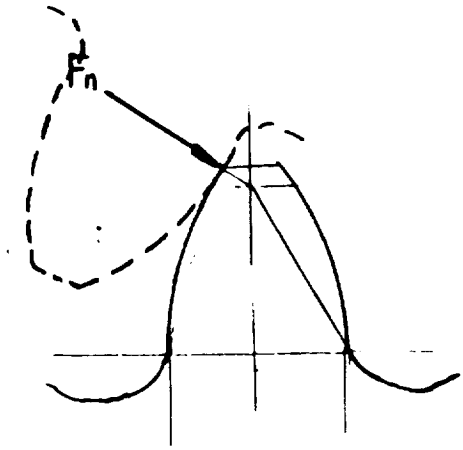

a. Involute gears

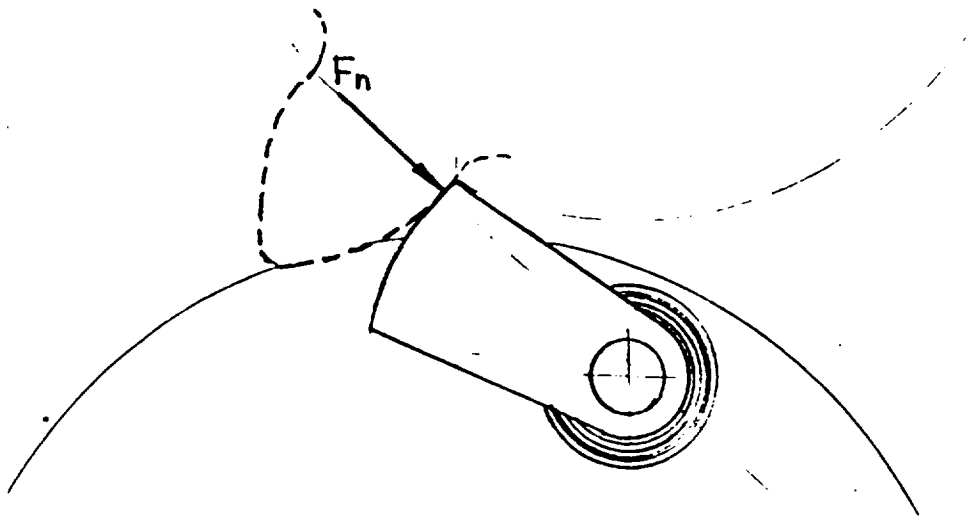

b. Composite gears

Fig 1.4 Payload accomodation in gears

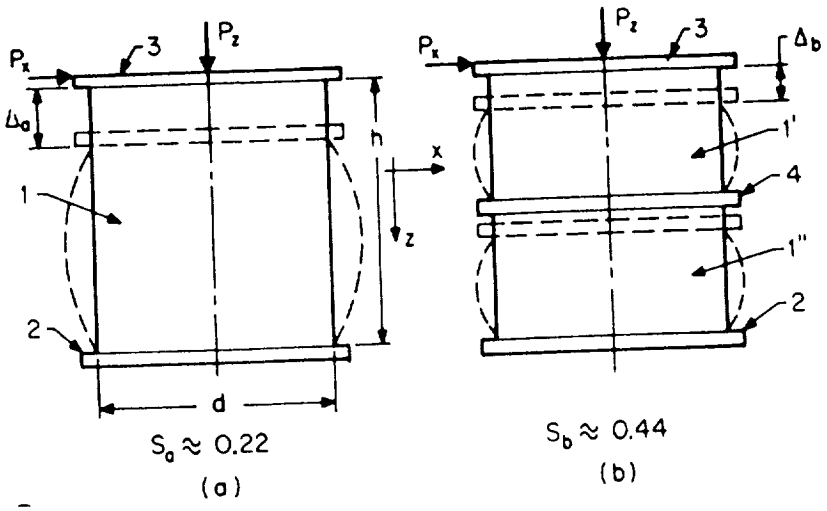

Fig. 2.1 Shape factor influence on compression deformation of bonded rubber element.

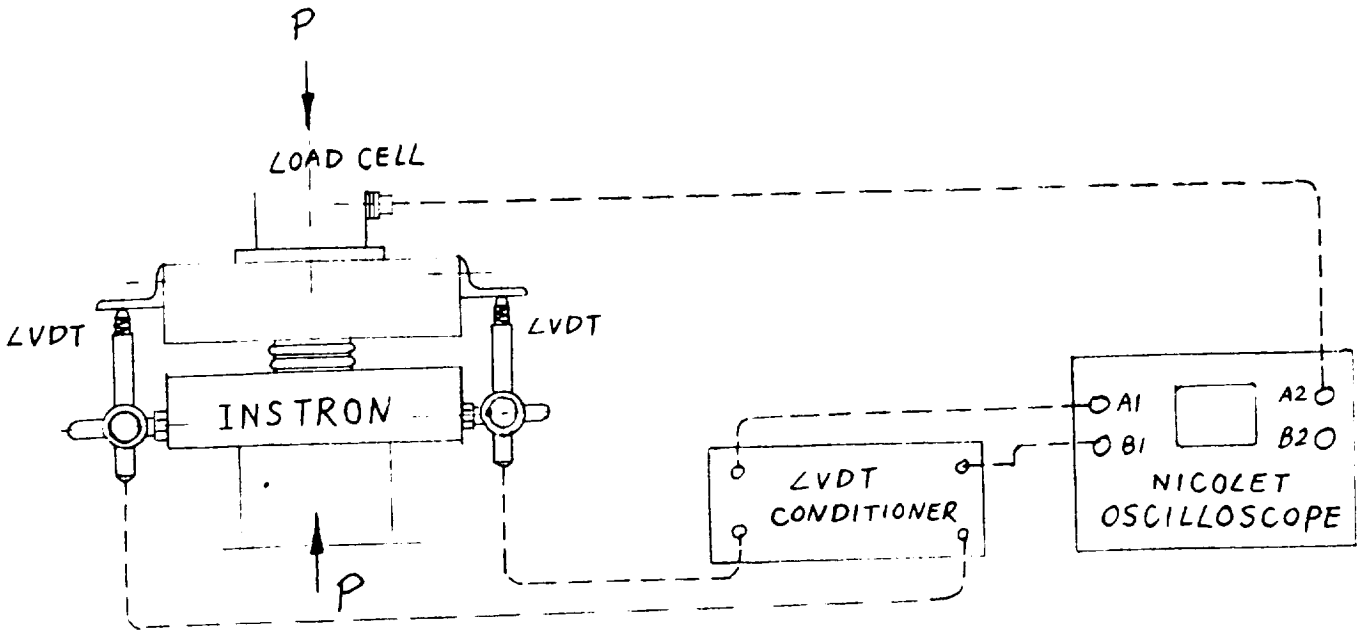

Fig. 2.2 Test set-up for compression testing of laminates

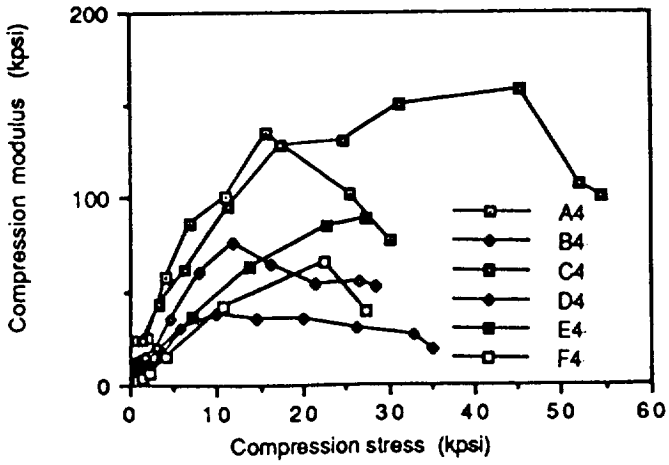

a. Modulus of six specimens

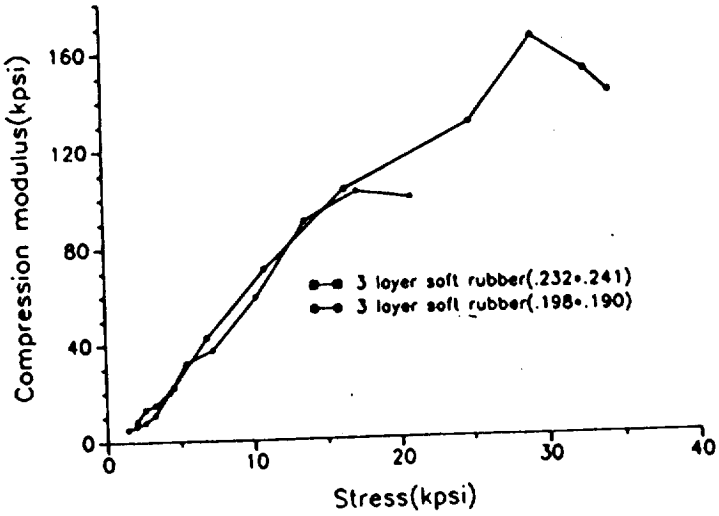

b. Soft rubber specimens of different surface areas

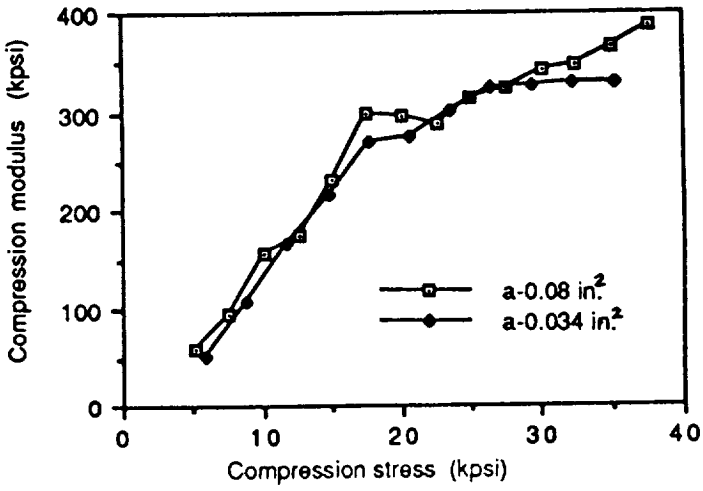

c. Hard rubber specimens of different surface areas

Fig. 2.3 Compression modulus for thin-layered rubber-metal laminates

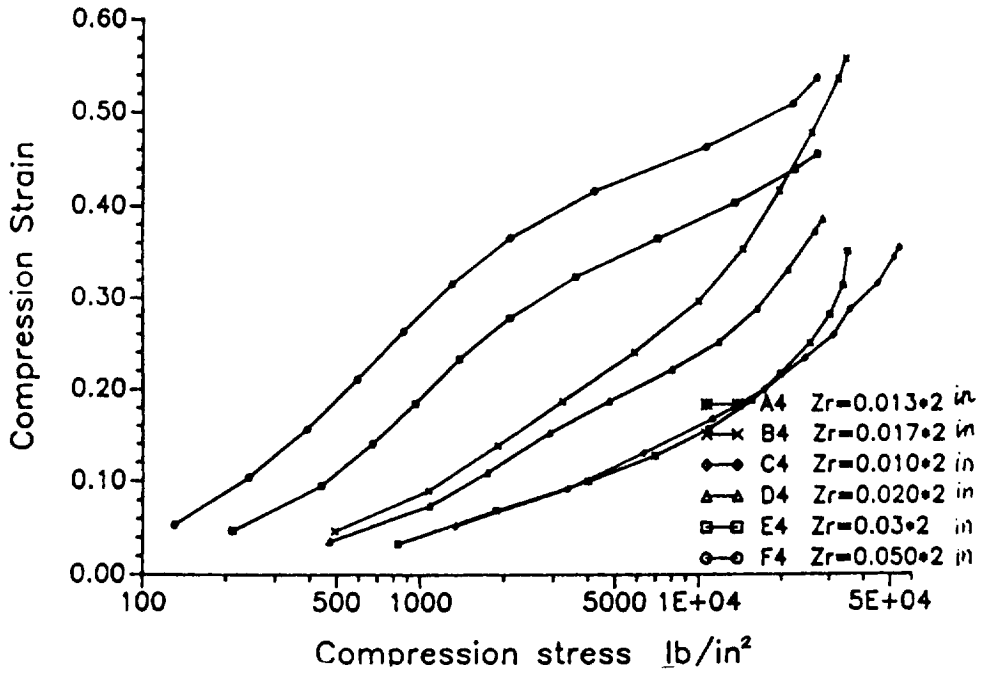

Fig. 2.4 Compression Strain vs. Stress for six laminates specimen (A=0.25*0.25 sqin.) (Zr is thickness of rubber)

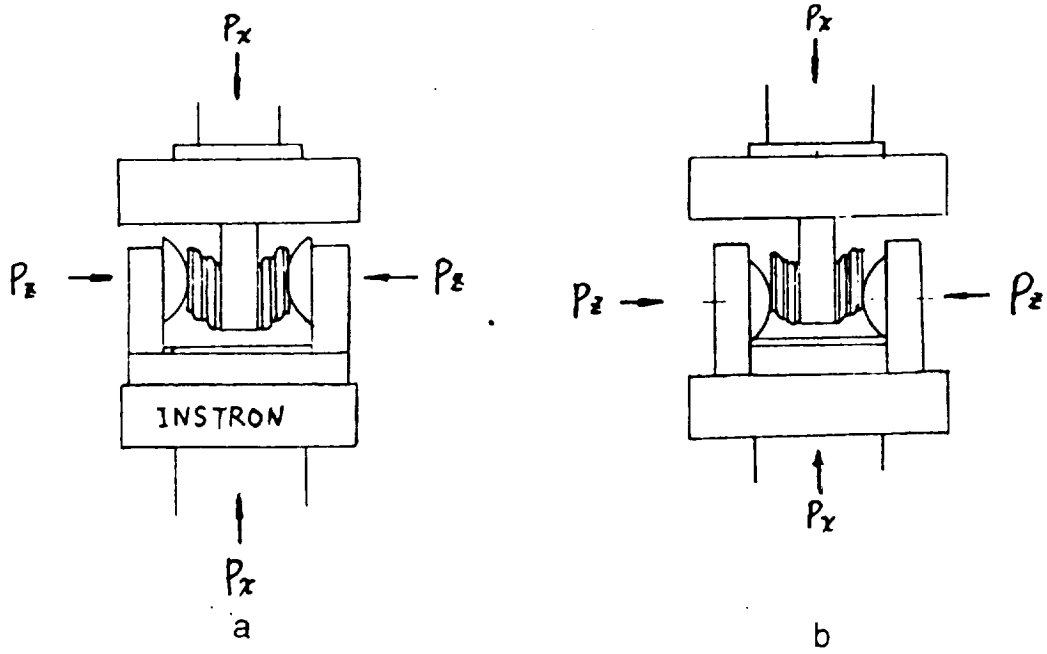

Fig. 2.5 Test set-up for shear testing of laminates with precompression

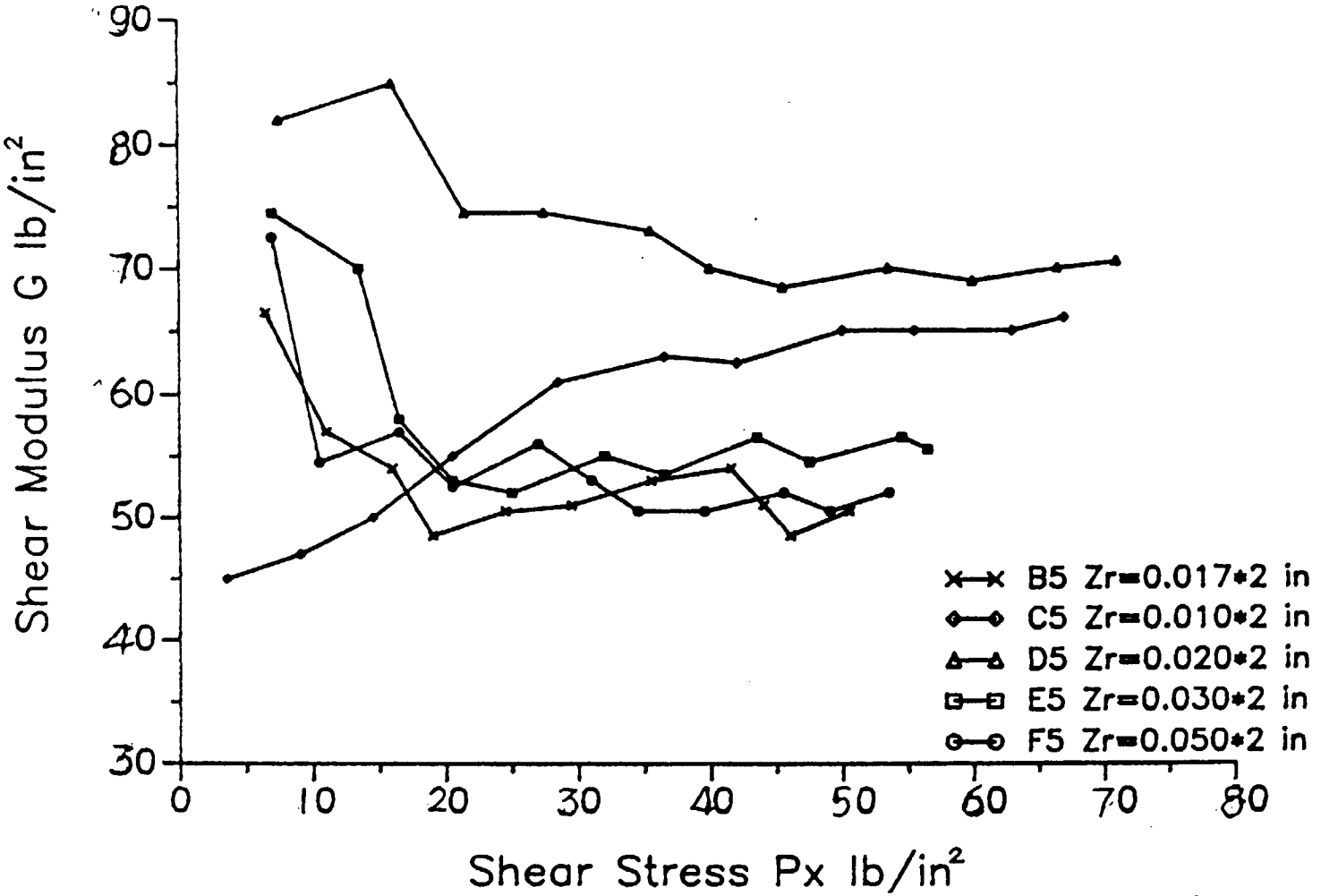

Fig. 2.6 Shear Moulus G vs.Shear Stress Px for six laminates (A=0.25*0.25 sqin.) under same compression stress Pz=5000 lb/sqin.

(Zr is thickness of rubber)

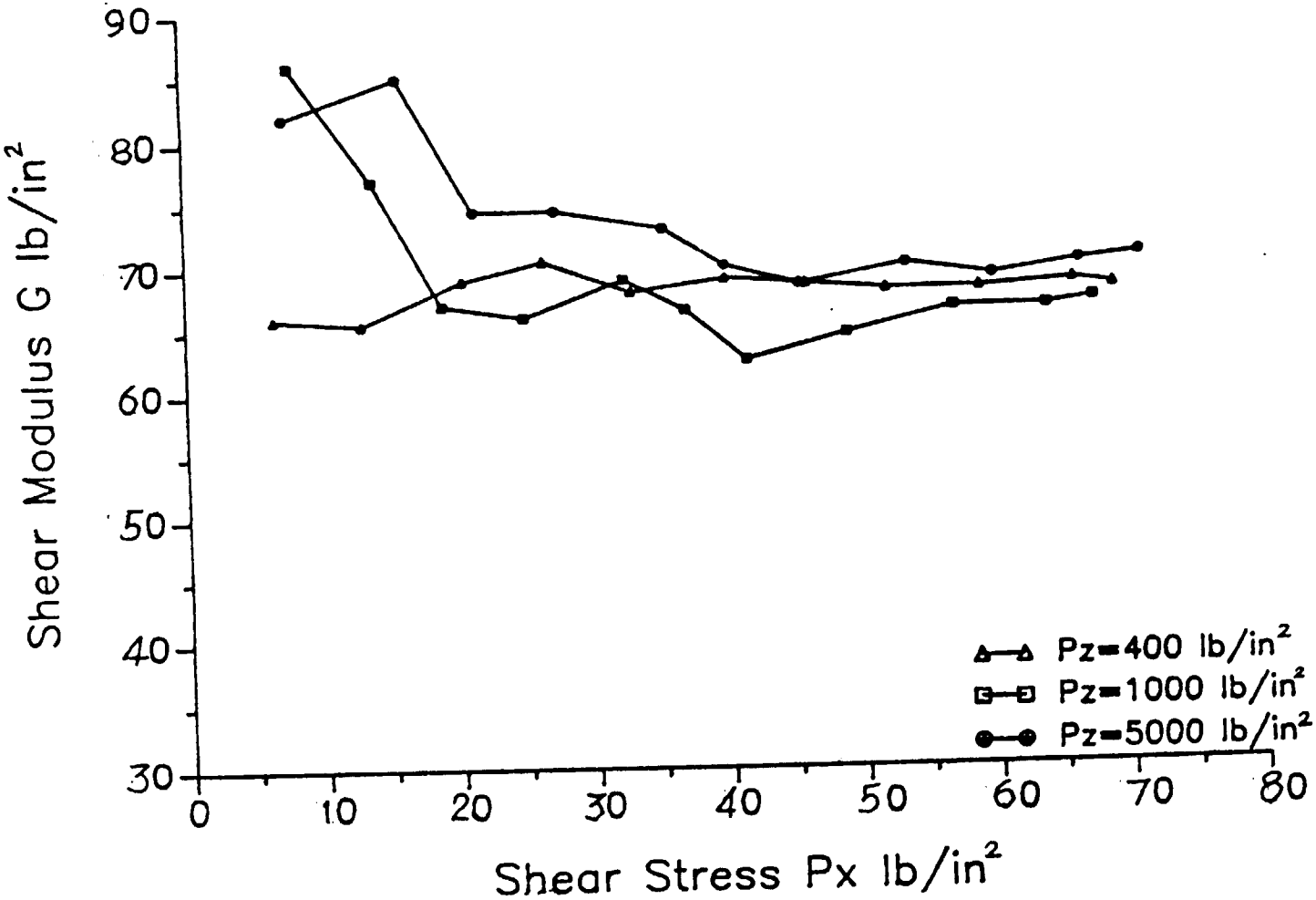

Fig. 2.7 Shear Modulus G vs. Shear Stress Px of specimen D5
(A=0.25*0.25 sqin, thickness of rubber Zr=0.020*2.0 in.)

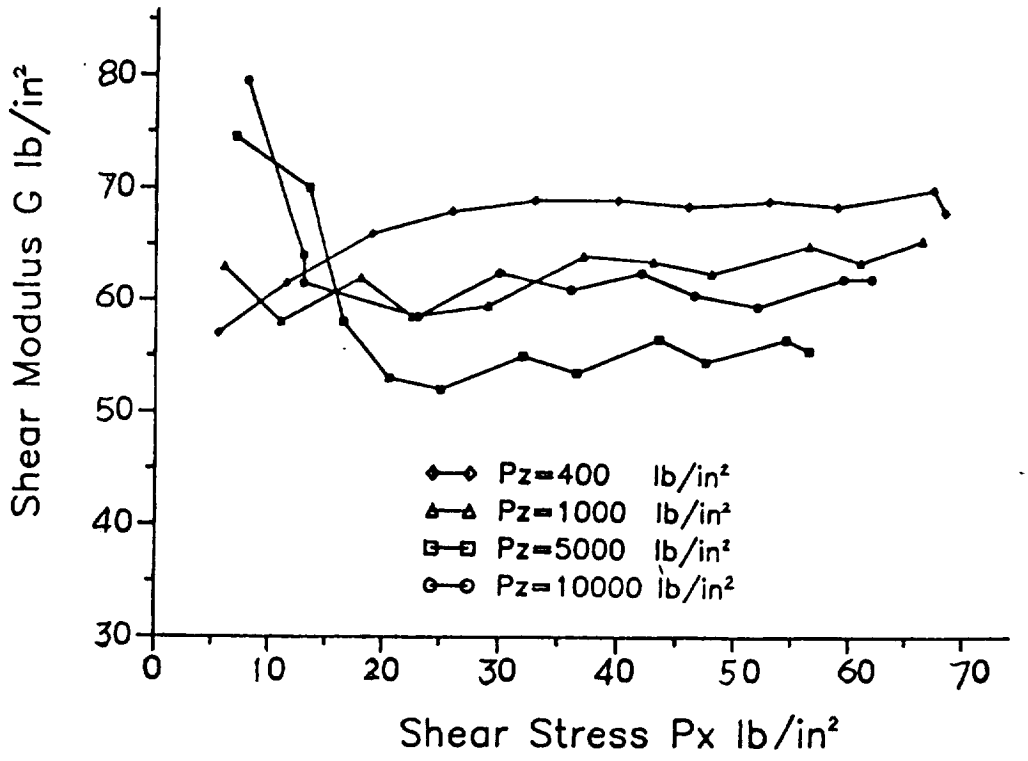

Fig. 2.8 Shear Modulus G vs. Shear Stress Px of specimen E5(A=0.25*0.25 sqin, thickness of rubber Zr=0.030*2 in)

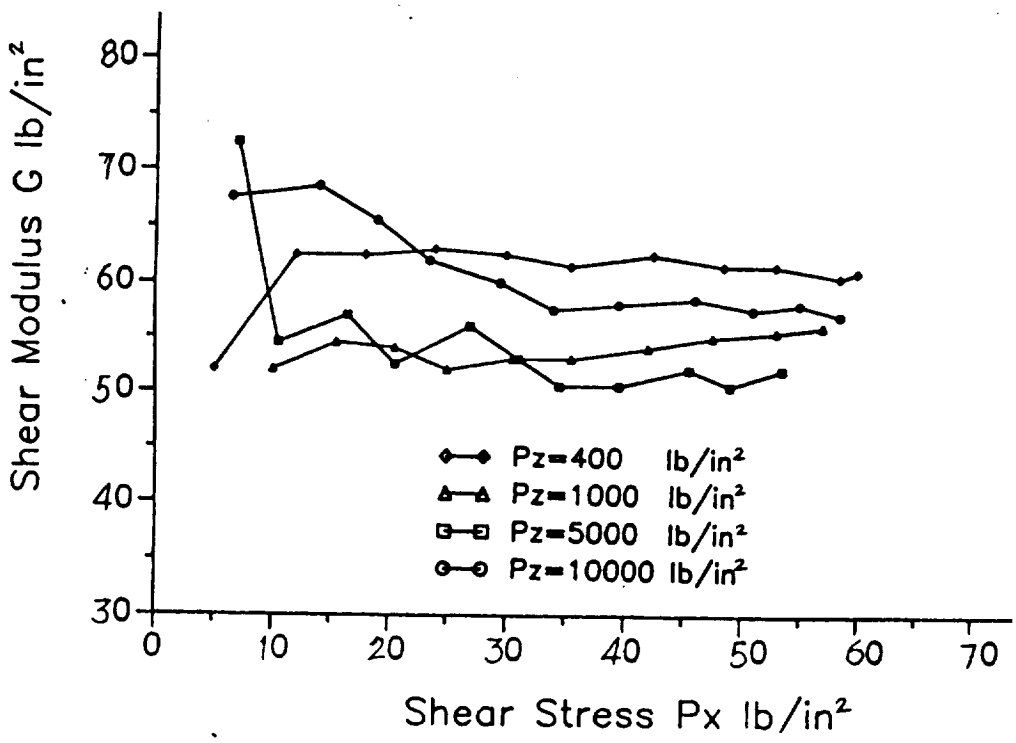

Fig. 2.9 Shear Modulus G vs. Shear Stress Px of specimen F5 (A=0.25*0.25 sqin, thickness of rubber Zr=0.050*2 in)

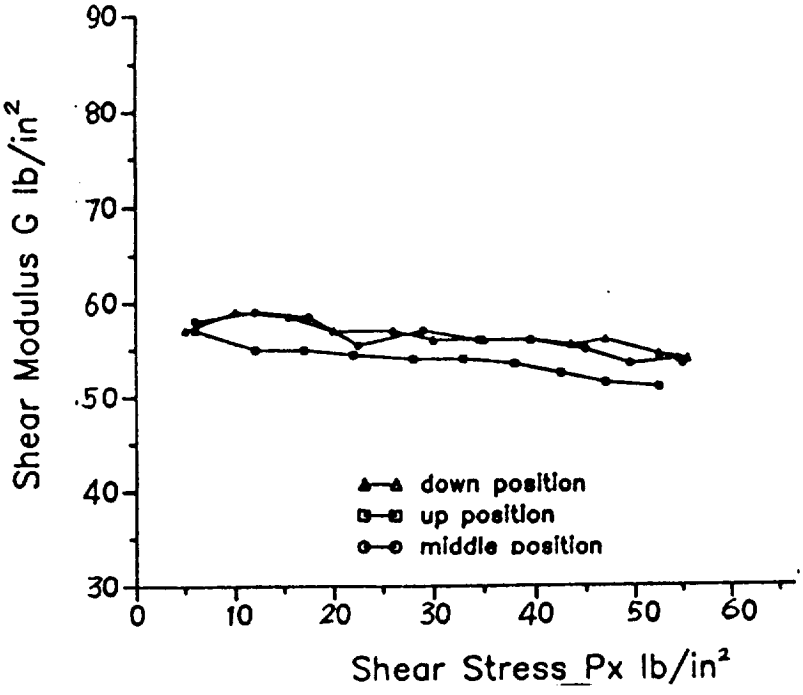

Fig. 2.10 Shear Modulus G vs. Shear Stress Px of specimen G1 (A=0.50*0.75 sqin,thickness of rubber Zr=0.015*4 in) at Pz=12,000 lb/sqin.)

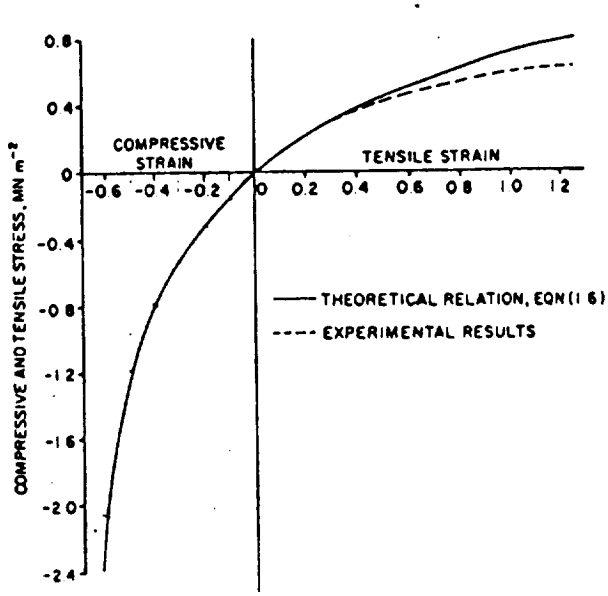

Fig. 2.11 Complete uniaxial extension and compression curve (Freakley & Payne)

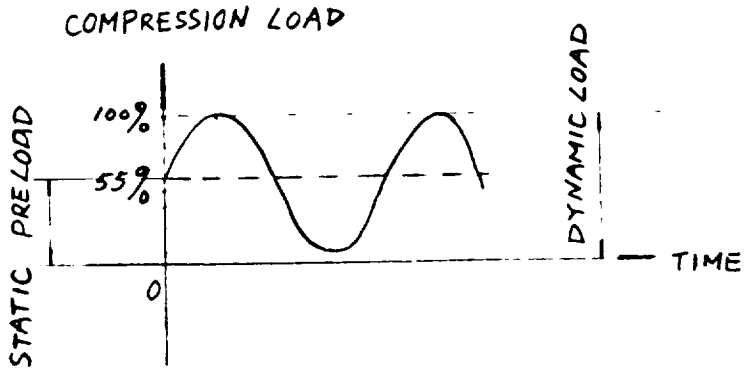

Fig. 2.12 Time history of laminate loading during dynamic tests

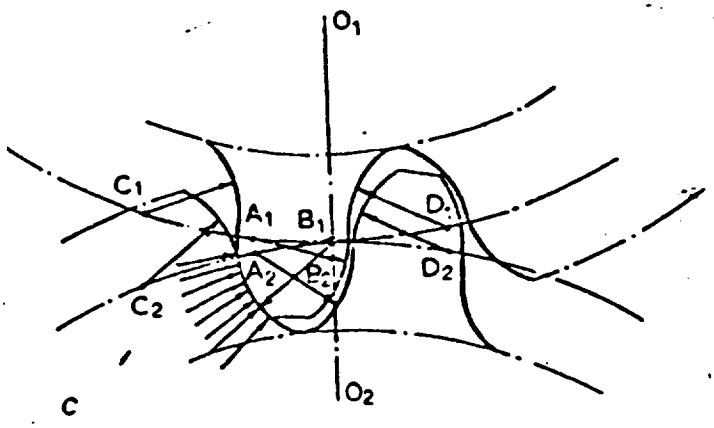

Fig. 3.1 Symmark gears

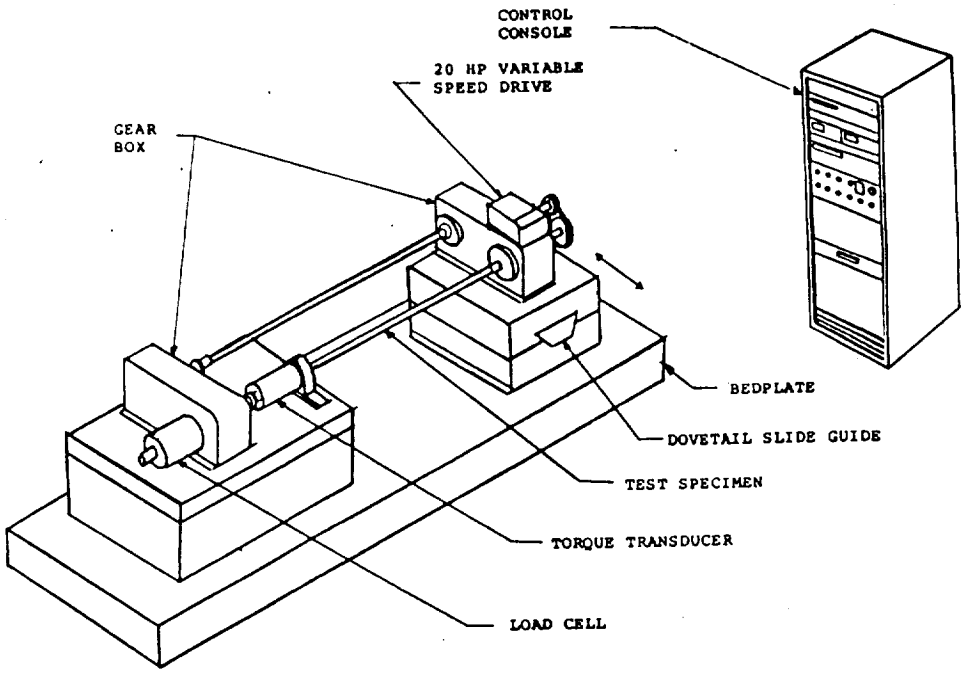

Fig. 3.2(a) Torsional four-square test machine

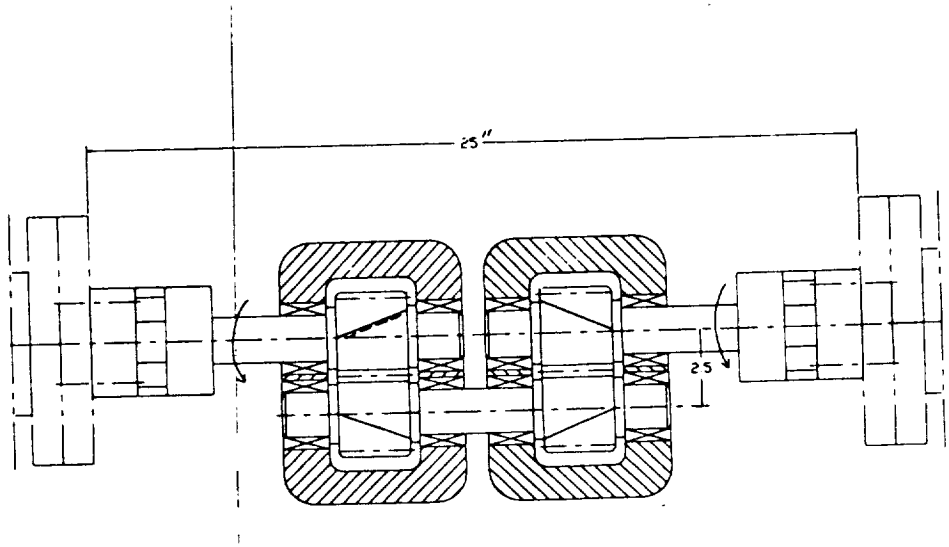

Fig. 3.2(b) Test gear box (1) and motion reversal gear box (2) for schenck pegasus test set-up

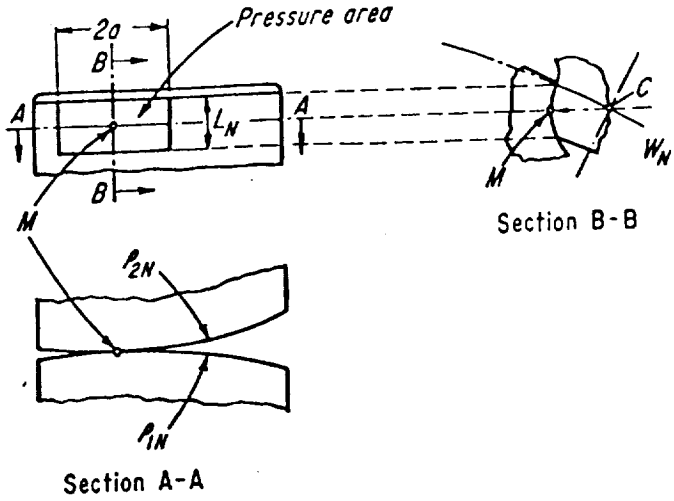

Fig 3.3(a) Radii of curvature

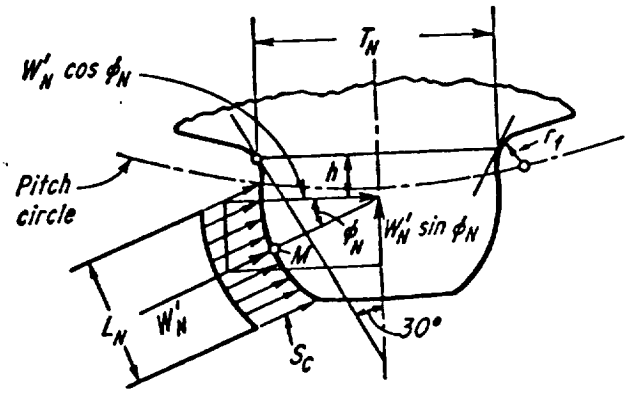

Fig. 3.3(b) Surface-Loading analysis of W/N gears

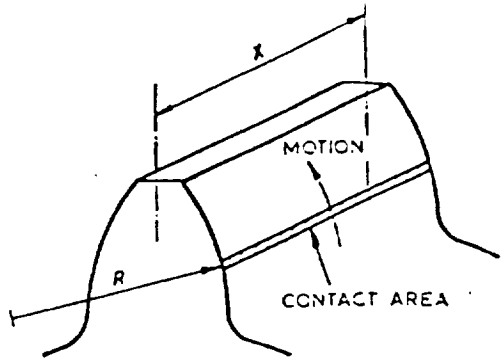

a Involute.

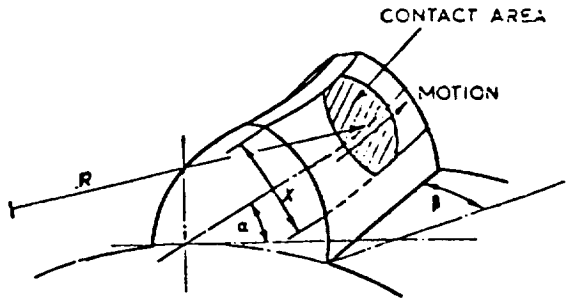

b Novikov.

Fig. 3.4 Compression of approximate contact area and related factors for involute and W/N gears

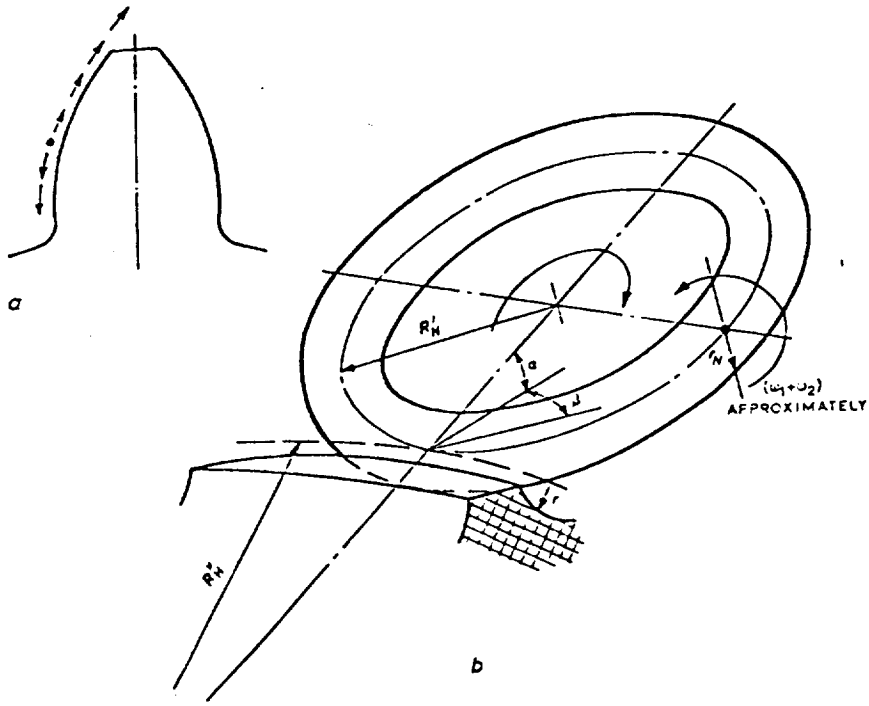

a Involute tooth. *b* Novikov contact.

Fig. 3.5 Sliding and rolling in conformal gear mesh

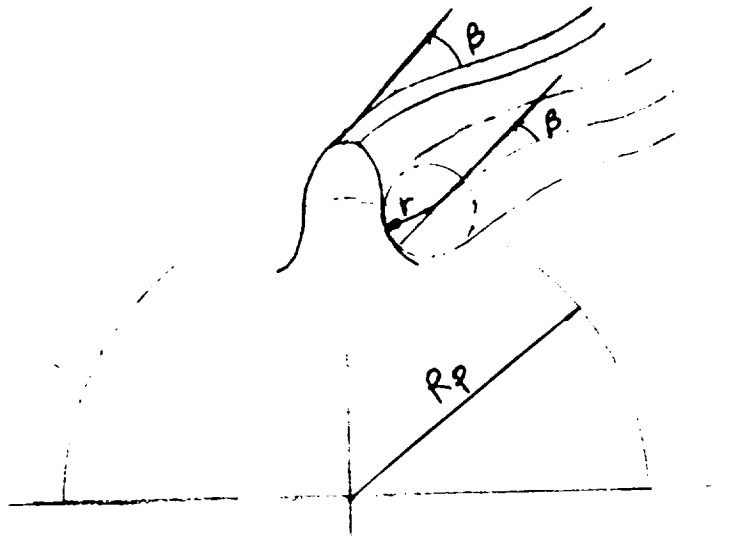

Fig. 3.6 Profile surface of Symmark gear

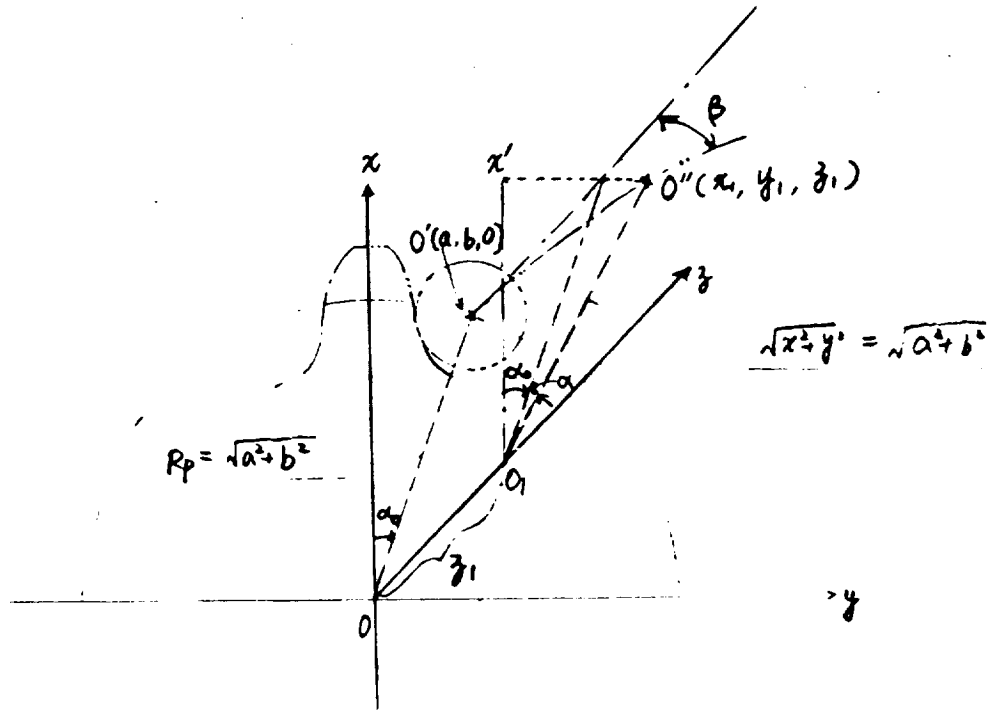

Fig. 3.7 Coordinate frame of hellical cylinder

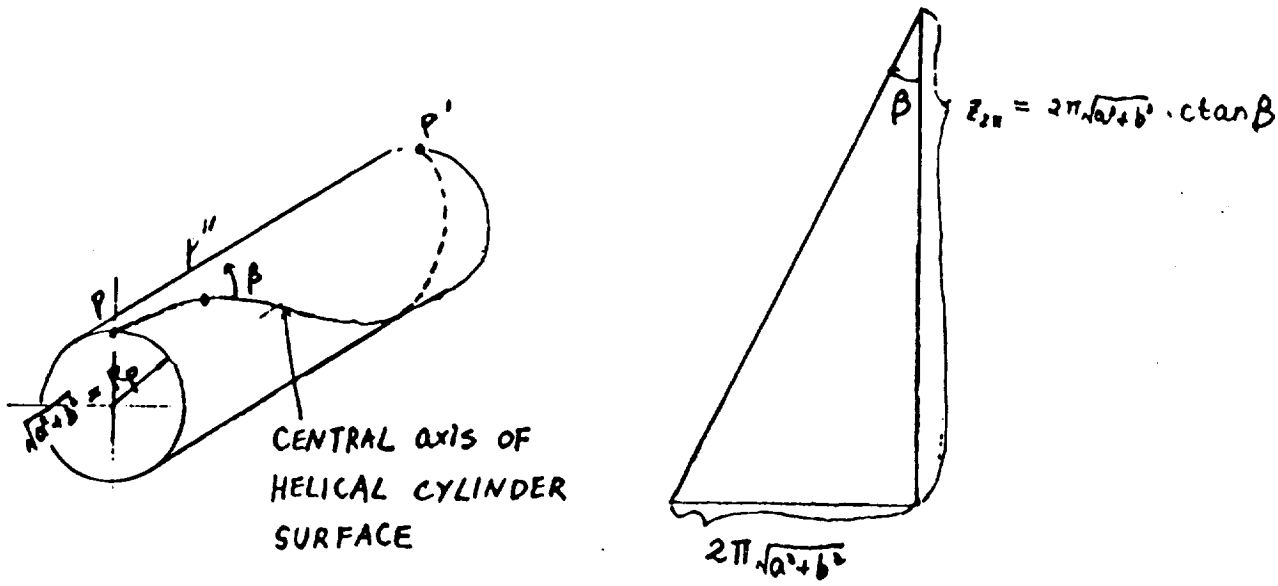

Fig. 3.8 Schematic for determining angle

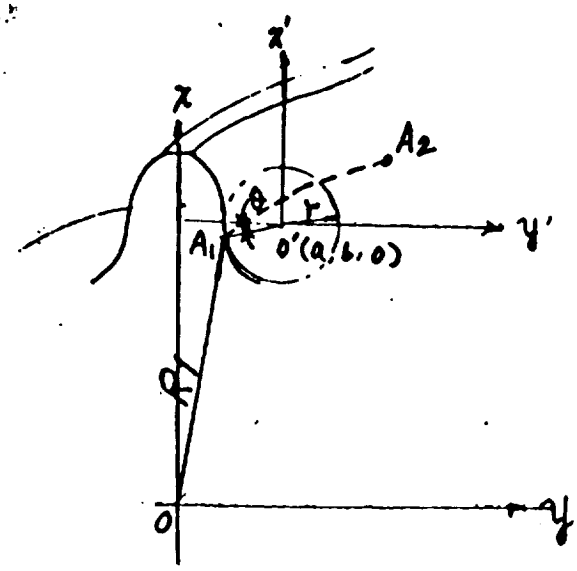

Fig. 3.9 Tooth profile of Symmark gear

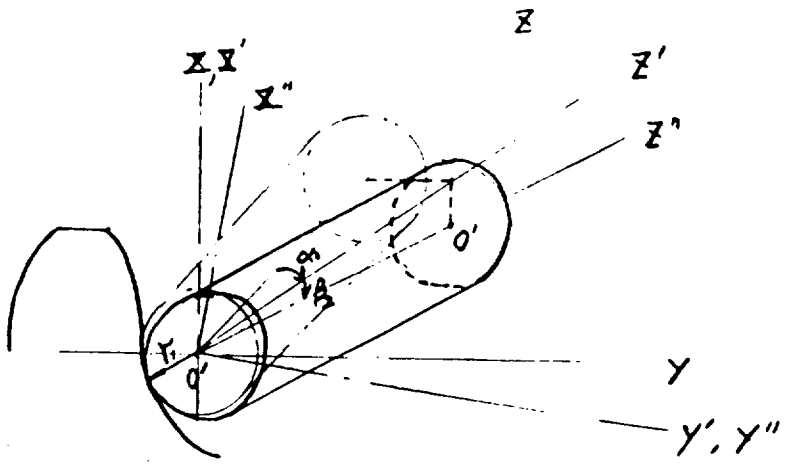

Fig. 3.10 Oblique cylinder double rotating

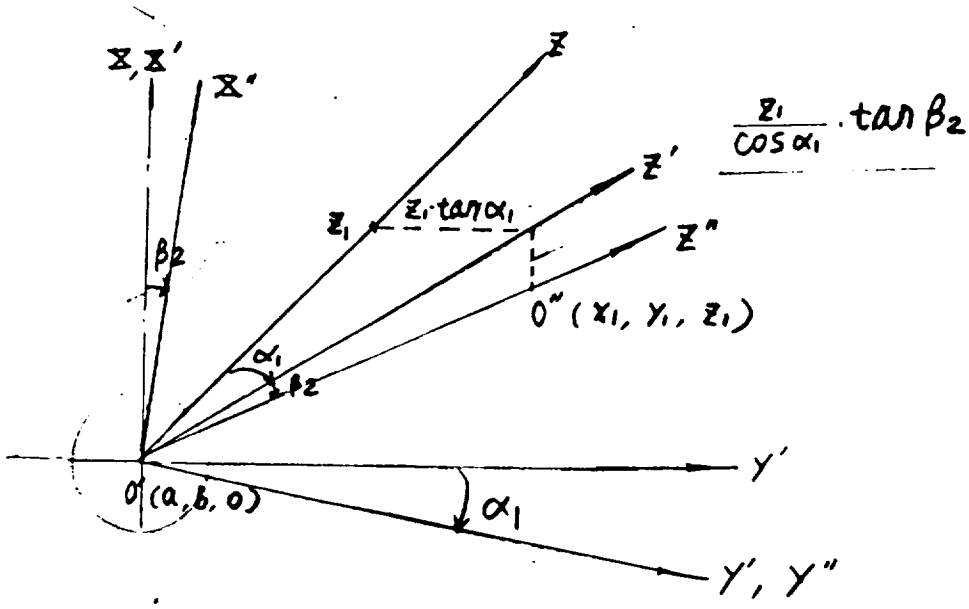

Fig. 3.11 Demonstration of rotation transform

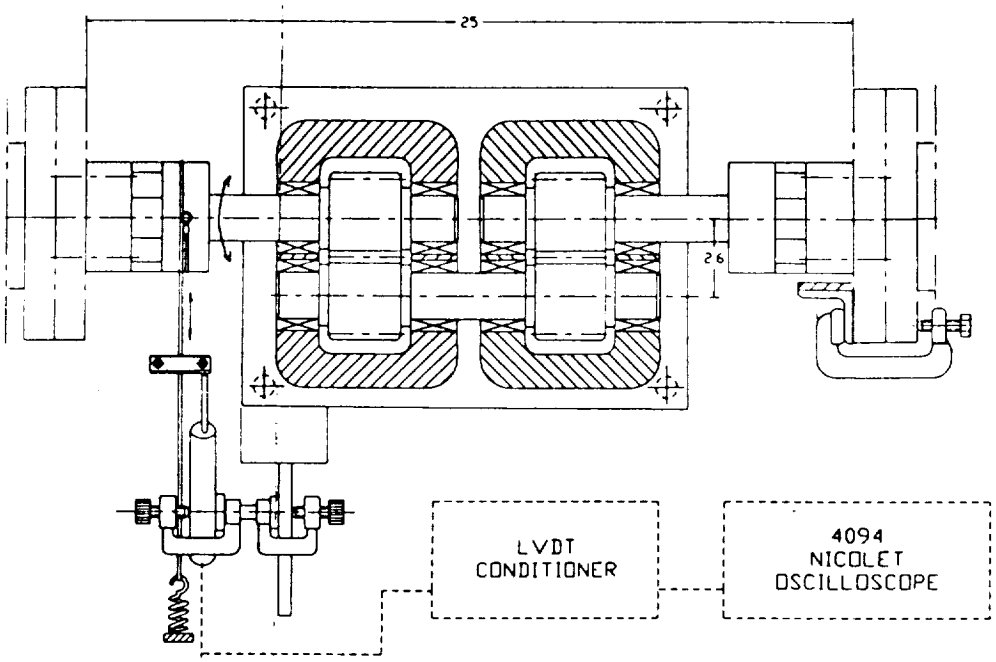

Fig. 3.12 Test set-up for vibration testing of laminate coated gears

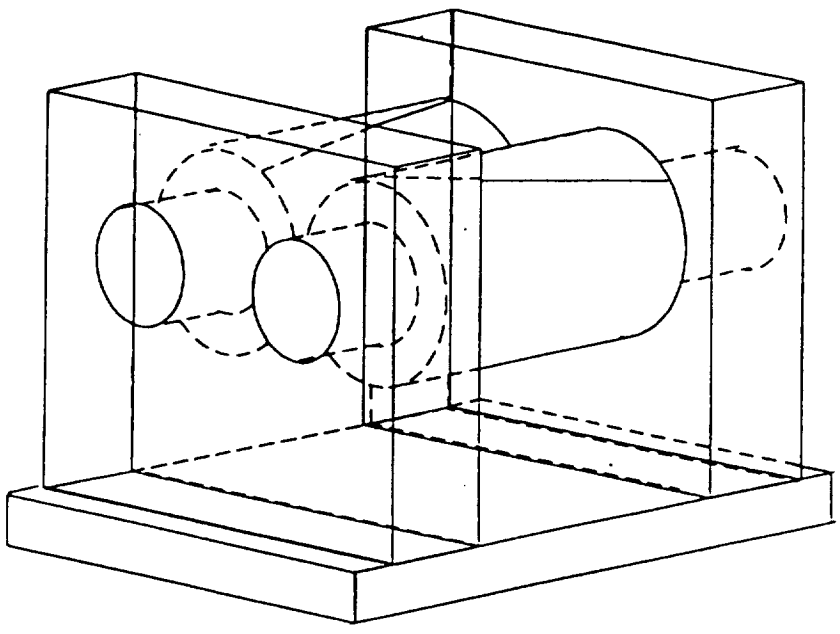

Fig. 3.13 Transparent gear box for study of meshing

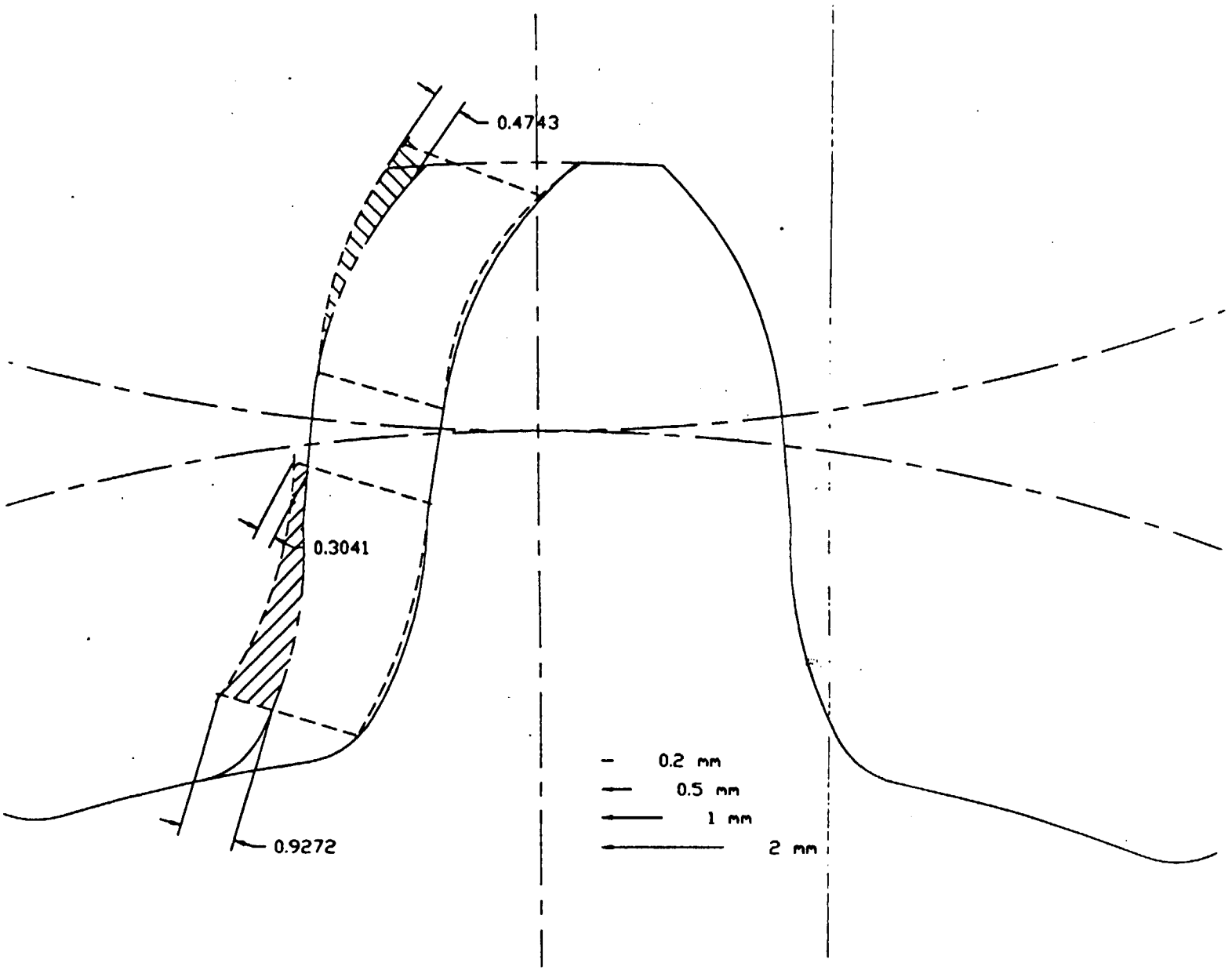

Fig. 3.14 **Computer simulation of meshing of laminate coated symmark gears**

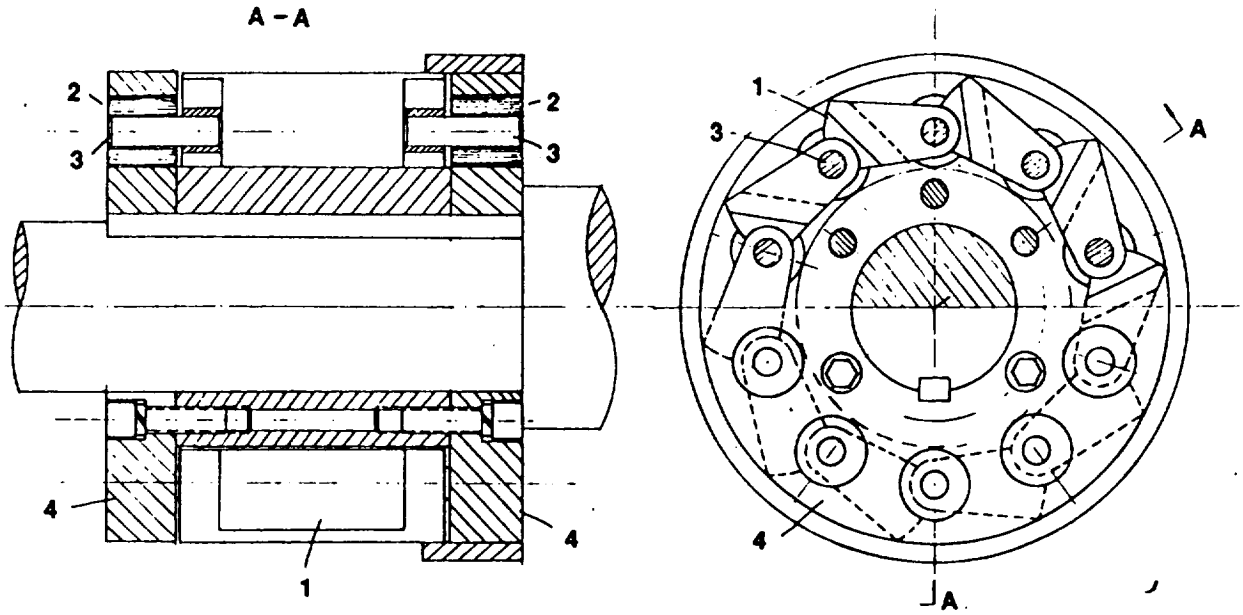

Fig. 4.1 Design of the prototype composite gear

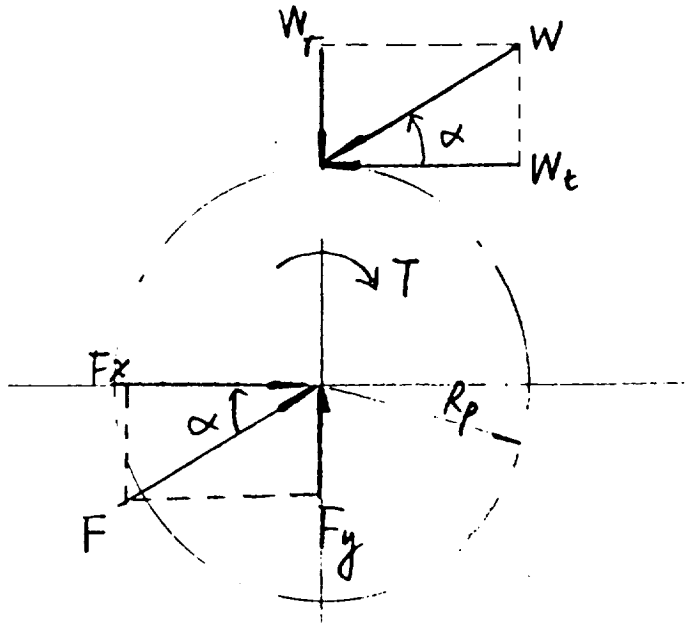

Fig. 4.2 Forces acting on a gear

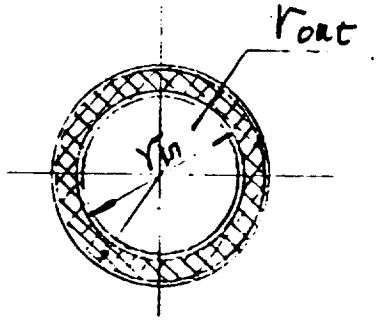

Fig. 4.3 Rubber-metal laminated bushing

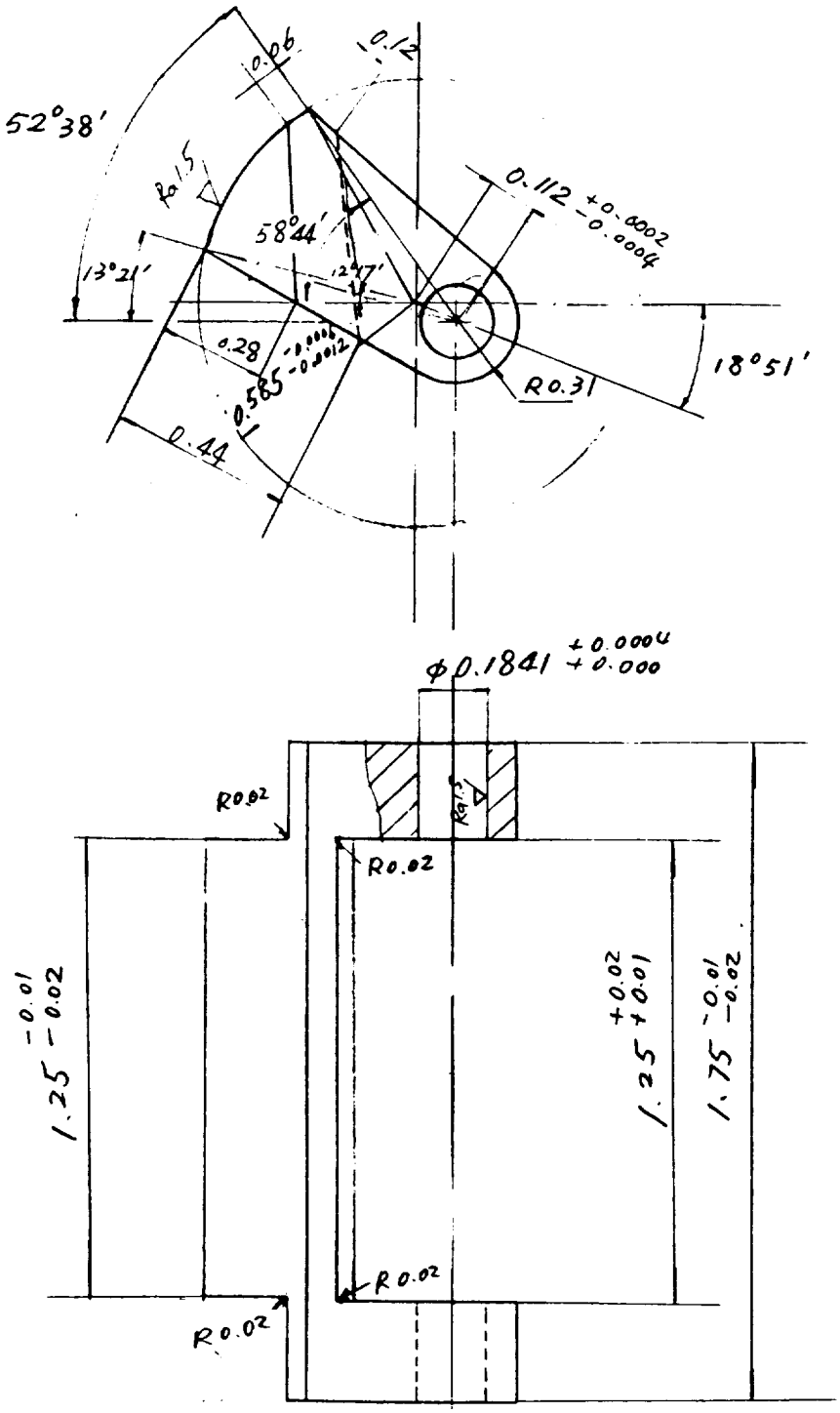

Fig. 4.4 Tooth segment

Note:

Before machining material has to be heat treated to RC 28-31.

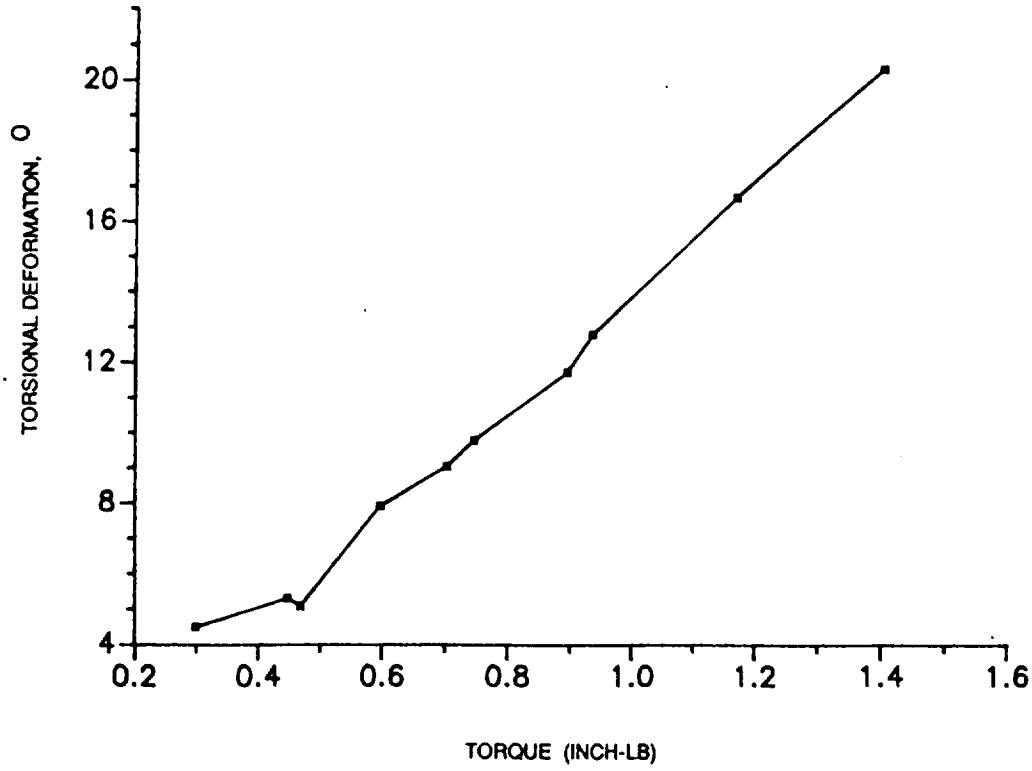

Fig. 4.5 Torque-twist characteristic of laminated bushing

Fig. 4.6 Test set-up for bushing testing

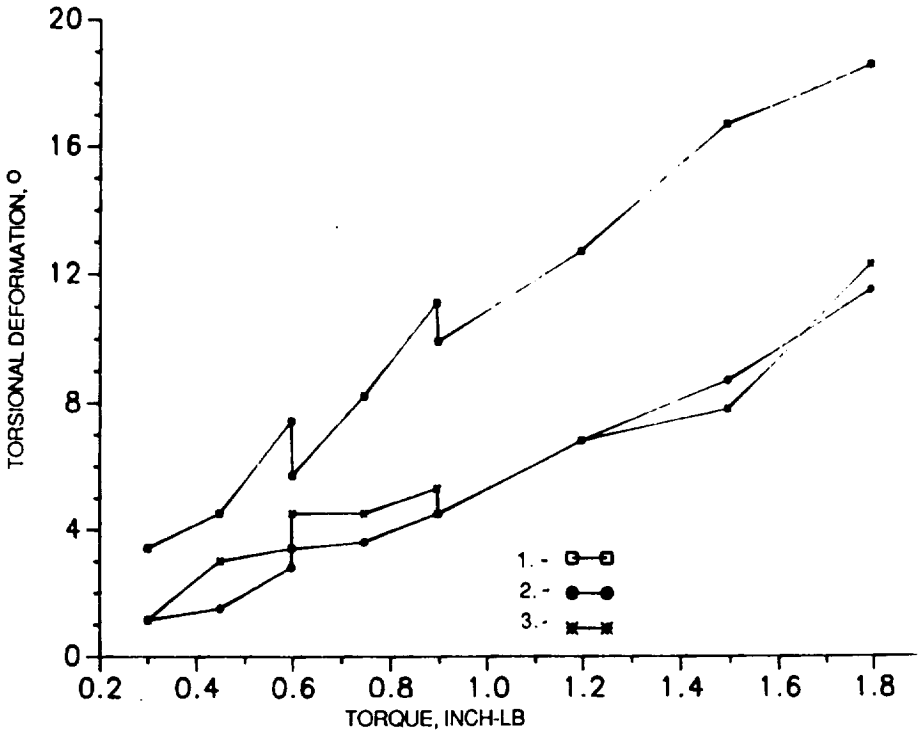

Fig. 4.7 Torque-Twist characteristics of laminated bushings without axial cut 1,2 before fatigue testing; 1-radial preload 5 lb; 2-radial preload 120 lb; 3-after one hour fatigue test (radial preload 120 lb)

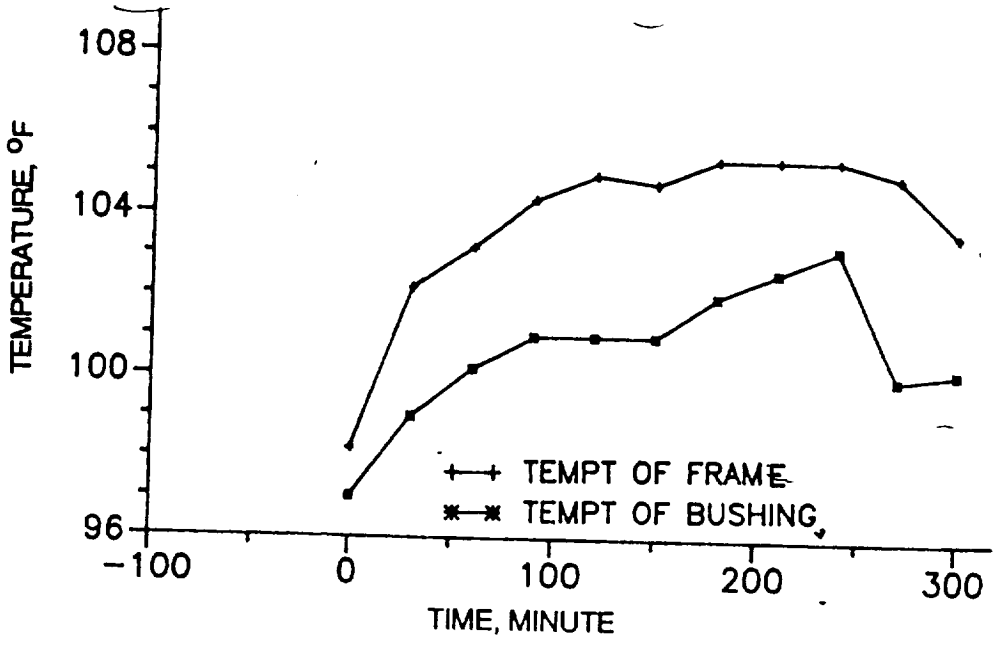

Fig. 4.8 Temperature increase during cyclical testing of laminated bushings (f=5Hz; α=±7.50; radial preload 120 lb; radial deformation 0.015 in)

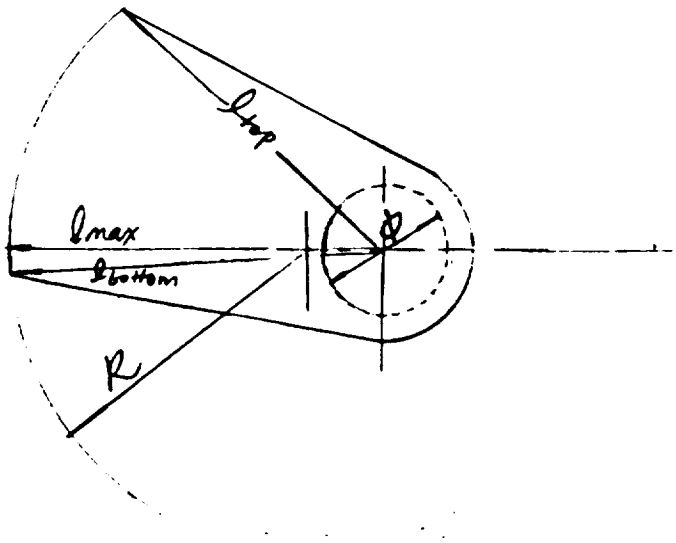

Fig. 4.9

STUDY OF MESHING CONDITION OF A NOVEL GEAR SYSTEM

Bangyi Dong, Graduate Student *

(* Adviser : E. Rivin, Professor)

Department of Mechanical Engineering
Wayne State University, Detroit, MI 48202

Introduction :

While two involute gear are meshing, a combined rolling and sliding action takes place between the tooth profiles. Because sliding velocity has opposite signs on the profiles below and above the pitch circle which causes reversal of the friction force and a possible breakdown of lubrication film, sliding between highly loaded surfaces leads to deterioration of the meshing conditions and results in noise, power loses, increasing working temperature on the profile and developing pits on the tooth surface. As it is indicated in [1] that the allowable stress in case of simultaneous rolling and sliding action between two rollers is only 50% of the allowable stress for pure rolling action under the same 10^6 reference number of stress cycles.

In order to alleviate these disadvantages, a novel concept of gear design [2] was developed which eliminates physical sliding between meshing profiles by means of using internal shear deformation in a special rubber-metal laminate coating on one of the meshing tooth profiles in order to accommodate geometrically-necessary sliding. Test data in [2] shows that the sound pressure level is reduced 10-20dB compared with traditional gears during the meshing process. The largest noise reduction (15-20dB) has been achieved for conformal (Symmark) gears, while a lower amount (10-15dB) was demonstrated for involute gears.

The inferior results for the involute gears are partly explained by varying curvature radius along the involute tooth profile. Since the curvature radius in each point of involute tooth profile is different, the laminate coating undergoes compression deformation in order to accommodate of change curvature during the meshing process. This is in addition to its shear deformation which serves to accommodate the geometrically-necessary sliding between the profile. Due to high compression modulus of laminate which is 2000-3000 times of shear modulus [3], the shear deformation of laminate is obstructed due to the local compression, and thus physical sliding also partly exist.

Thus the change of the profile curvature which is the intrinsic characteristic of involute reduces the advantages of this gear system. Accordingly, there was a need to develop a modified gear system with a less pronounced variation of curvature radii or constant curvature radii during whole mesh cycle in order to reduce or eliminate distortions of laminates along the profile, so that the physical sliding between the two meshing profiles of gears could be eliminated. Such a gear system has recently been developed at the Wayne State University [4].

In this paper, this novel gear system is analyzed. It is a composite gear, which is meshing with a conventional involute gear. Each tooth of the composite gear consists of two component. Its tooth core has cylindrical profile along which a sliding "crescent" is moving. The concave surface of crescent is also a circular cylinder which matches the circular cylindrical surface of the tooth core. Shape of the outer cylinder convex surface of crescent should be of such geometry, that when such a composite gear is meshing with an involute gear, there would be only pure rolling motion between the two meshing profiles and geometry-necessitated sliding between the contacting surfaces is accommodated by the concave surface of the crescent sliding along the cylindrical surface of the tooth core. Thus, there is a kinematic separation of sliding and rolling component of motion in the involute gears. This paper describes a computational method of generating points of the crescent surface to achieve this effect and shows some computational results as well as computer graphics simulation of the meshing plots. It also gives an analysis of effects of some design parameters on the shape of the crescent and on meshing parameters.

1 Computational Algorithm for Generation of Points on the Crescent Profile

Nomenclature (refer to Fig.1)

R_{bi} base radius of the involute gear

R_{pin} pitch radius of the involute gear

Z_i tooth number of the involute gear

R_b	base radius of the composite gear
R_p	pitch radius of the composite gear
Z	tooth number of the composite gear
O	center of the involute gear
O'	center of the composite gear
O"	center of the convex circular arc of cross section of the tooth core of the composite gear
R_t	radius of the convex circular arc of the tooth core of composite gear
R_c	distance from O' to O"
ψ	angle between lines OO' and O'O"
ϕ	pressure angle of the involute gear
θ_i	angle of rotation of the involute gear
θ	angle of rotation of the composite gear
O"B'	curvature radius of the crescent
η	angle of rotation of the crescent about O" when the composite gear is rotating for angle $d\theta$
CC'	length of sliding arc of concave surface of the crescent along the convex surface of the tooth core

We assume that when a composite gear is meshing with an involute gear, there is only a pure rolling between the profiles, while the concave circular surface of the crescent is sliding along the convex circular surface of the tooth core of the composite gear. These two motions replace sliding between the meshing profiles of two gears. Consequently, a computational algorithm for generation of points of the crescent profile should satisfy the following three conditions:

(1) There is a given transmission ratio, thus

$$d\theta_i = d\theta \cdot Z / Z_i$$

(2) Meshing conditions between the composite and involute gears are equivalent to meshing conditions between two involute gears; accordingly, all contact points should be located on the common tangent line to two base circles.

(3) Since the motion between the meshing profiles is pure rolling, the lengths of the curves traveled along two meshing profiles should be equal, AA'= BB'.

We define the computational origin to be the pitch points A for the involute and B for the crescent as shown in Fig.1(a) at these points angles of rotation $d\theta_i$ and $d\theta$ are both zeros and $d\theta_i$ η are considered positive in counterclockwise direction. Conversely, $d\theta$ is negative in the counterclockwise direction. After the composite gear had rotated for $d\theta$, and the involute gear for $d\theta_i$, the new contact point is designated as A' on the involute profile and as B' on the crescent, as shown in Fig.1(b).

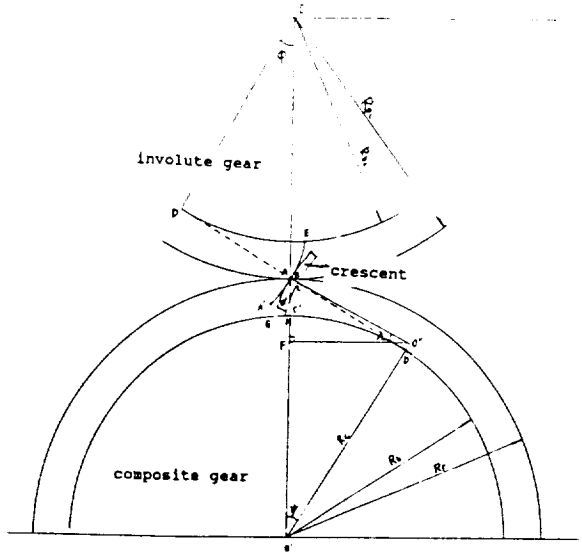

Fig.1(a) Composite Gear Meshes with Involute Gear at Pitch Point

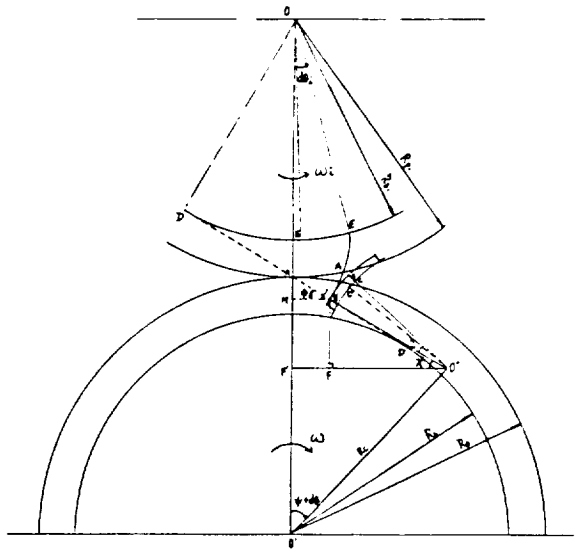

Fig.1(b) Composite Gear Rotates $d\theta$ when Involute Gear Rotates $d\theta_i$

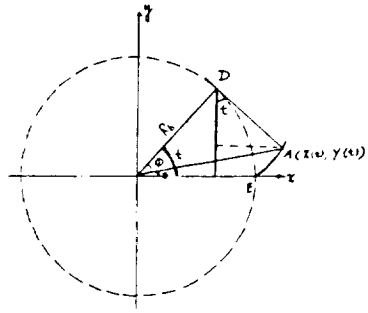

Fig.1(c) Generating Line of Involute Profile

In Fig.1(a) and Fig.1(b), EAA' is the involute profile curve, GB'B is curve describing the convex surface of the crescent, HC'C is the circular arc of the concave surface of the crescent, and straight line DD' is the common tangent line for two base circles of the gears. From Fig.1(a), the following expressions can be written for the right-angled triangles O'O"F and O"FB :

$$O"B = [(R_p - R_c \cdot \cos\psi)^2 + (R_c \cdot \sin\psi)^2]^{\frac{1}{2}} \quad (1)$$

$$\lambda = \tan^{-1}[(R_p - R_c \cdot \cos\psi)/(R_c \cdot \sin\psi)] \quad (2)$$

In the right-angled triangle ODA,

$$DA = R_{pin} \cdot \sin\phi$$

For the involute gear, from Fig.1(c),

$$X(t) = R_b \cdot [\cos(t) + t \cdot \sin(t)]$$

$$Y(t) = R_b \cdot [\sin(t) - t \cdot \cos(t)]$$

$$X'(t) = dX(t)/dt = R_b \cdot t \cdot \cos(t)$$

$$Y'(t) = dY(t)/dt = R_b \cdot t \cdot \sin(t)$$

$$\overset{\frown}{EA} = \int_\beta^\alpha \sqrt{[X'(t)]^2 + [Y'(t)]^2} \cdot dt$$

$$= \int_0^t R_b \cdot t \cdot \sqrt{[\cos(t)]^2 + [\sin(t)]^2} \cdot dt$$

$$= 0.5 \cdot R_b \cdot t^2 \Big|_0^{\theta+\phi}$$

$$= 0.5 \cdot R_b \cdot (\theta + \phi)^2$$

$$\theta = \overset{\frown}{ED}/R_b - \phi$$

$$= DA/R_b - \phi$$

$$\overset{\frown}{EA} = 0.5 \cdot R_b \cdot (DA/R_b - \phi + \phi)^2$$

$$= (DA)^2/(2R_{bi})$$

$$= (R_{pin} \cdot \sin\phi)^2/(2R_{bi}) \quad (3)$$

From Fig.1(b), for the right-angled triangle ODA

$$\overset{\frown}{AA'} = \overset{\frown}{EE'} = R_{bi} \cdot d\theta_i$$

$$DA' = R_{pin} \cdot \sin\phi + R_{bi} \cdot d\theta_i$$

$$\overset{\frown}{EA'} = (DA')^2/(2R_{bi})$$

$$= (R_{pin} \cdot \sin\phi + R_{bi} \cdot d\theta_i)^2/(2R_{bi}) \quad (4)$$

$$\overset{\frown}{AA'} = |\overset{\frown}{EA'} - \overset{\frown}{EA}| \quad (5)$$

$$\overset{\frown}{BB'} = \overset{\frown}{AA'} \quad (6)$$

Substituting equations (3),(4),(5) into (6)

$$\overset{\frown}{BB'} = |(R_{pin} \cdot \sin\phi + R_{bi} \cdot d\theta_i)^2/(2R_{bi}) - (R_{pin} \cdot \sin\phi)^2/(2R_{bi})|$$

$$= |[2R_{pin} \cdot R_{bi} \cdot \sin\phi \cdot d\theta_i + (R_{bi} \cdot d\theta_i)^2]/(2R_{bi})|$$

$$= |R_{pin} \cdot \sin\phi \cdot d\theta_i + 0.5R_{bi} \cdot (d\theta)^2| \quad (7)$$

In the right-angled triangles O'O"F' and AA'M

$$O"F = R_c \cdot \sin(\psi + d\theta) - R_{bi} \cdot d\theta_i \cdot \cos\phi$$

$$B'F = R_p - R_c \cdot \cos(\psi + d\theta) - R_{bi} \cdot d\theta_i \cdot \sin\phi$$

In the right-angled triangle B'FO",

$$\lambda' = \tan^{-1}(B'F/O"F)$$

$$O"B' = (O"F^2 + B'F^2)^{\frac{1}{2}}$$

$$= \{[R_c \cdot \sin(\psi + d\theta) - R_{bi} \cdot d\theta_i \cdot \cos\phi]^2 + [R_p - R_c \cdot \cos(\psi + d\theta) - R_{bi} \cdot d\theta_i \cdot \sin\phi]^2\}^{\frac{1}{2}} \quad (8)$$

In triangle BB'O", since iteration step $d\theta$ is very small, BB' also is very small, so it can be assumed

$$BB' = \overset{\frown}{BB'}$$

$$\eta = \cos^{-1}([O"B'^2 + O"B^2 - BB'^2]/[2 \cdot O"B' \cdot O"B]) \quad (9)$$

$$CC' = R_i \cdot [(\lambda' + \eta) - (\lambda + d\theta)]$$

2 Effect of Various Parameters on Shape of Crescent and on Meshing Process

According to the above equations (1)-(9), we can write CALCOMP program to compute position vectors of the crescent O"B' and the angle η using iteration step $d\theta$ and also to plot the crescent profile. We took the following set of data as input data and obtained meshing plots shown in Fig.2 from which we observed that the crescent curve is smooth and the meshing process is good.

$R_{bi} = 3.0$ in.; $R_{pin} = 3.5$ in.; $R_b = 3.0$ in.;
$R_p = 3.5$ in.; $Z_i = 8$; $Z = 8$;
$R_c = 3.1$ in.; $\psi = 32°$

Effects of the above parameters were studied in three aspects: The smallest teeth number without undercut of the composite gear Z_{min} ; interference during meshing process; shape of the crescent.

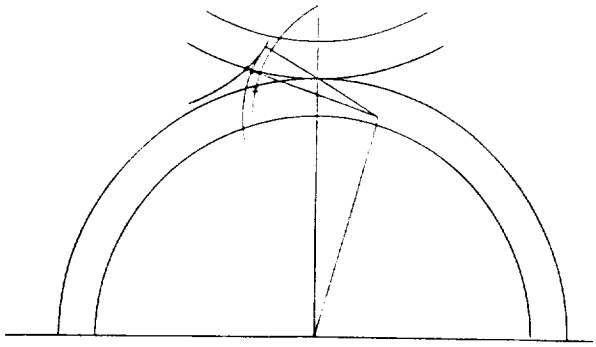

(a) at Addendum Part

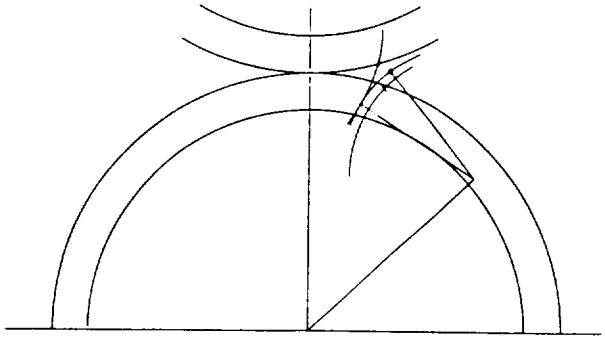

(b) at Dedendum Part

Fig.2 Generating Line of Crescent Surface with $\phi = 32°$ and $R_c = 3.1$ in.

For an involute gear, $(Z_i)_{min}$ is calculated as equation

$$(Z_i)_{min} = (2 \cdot h_a)/(\sin\phi)^2$$

where h_a is addendum coefficient assumed to be $h_a = 1$;

$$\phi = \cos^{-1}(R_{bi}/R_{pin}) = 31°$$

$$(Z_i)_{min} = 7.5$$

We take $Z = Z_i = 8$, thus the largest angle of rotation without undercut for the meshing process of one tooth of involute gear is

$$(2\theta_i)_{max} = 360°/8 = 45°$$

When zero of the angle of rotation is at the pitch point, the largest angle of rotation of the crescent without undercut in counterclockwise direction θ_{max} is defined to be negative and in the clockwise direction θ_{max} is positive. In the following discussion, the crescent profile is divided into two parts: addendum part from the pitch point to addendum; dedendum part from the pitch point to dedendum. Now we shall look for Z_{min} of the composite gear and discuss the effects of changing some parameters on θ_{max} through examples.

The second problem is whether an interference or a separation phenomenon will happen in the range of $2\theta_{max}$ during the meshing process. When two involute gears are meshing, neither interference nor separation would happen in the range of $(2\theta_i)_{max}$ since it is a pair of meshing conjugate curves. However, when a composite gear is meshing with an involute gear, in addition to pure rolling between the profiles, there is also sliding along the circular arc which has some distance from the contact surface, so these can not be considered a pair of conjugate curves in the strict sense. The following examples show that sometimes interference may happen within the range of the largest angle without undercut $2\theta_{max}$ during meshing process of a composite gear and an involute gear. However, no separation does happen.

The third aspect we should discuss is whether the shape of crescent is close to circular. If it is, is this a benefit to the meshing process or not?

2.1 Effects of Values of ψ and R_c

Shape variation of the crescent has an influence over the meshing parameters and the shape of crescent depends largely on ψ and R_c, when the other essential parameters of gears R_{bi}, R_{pin}, R_b, R_p, Z_i, Z are fixed. Since generation of the crescent curve depends on the position vector O"B' and angle η, equation(8), (9) are useful. From equation (7), we get BB' as follows

$$BB' = \left| R_{pin} \cdot \sin\phi \cdot d\theta_i + 0.5 \cdot R_{bi} \cdot (d\theta_i)^2 \right|$$

There are seven variables ψ, R_c, $d\theta$, $d\theta_i$, R_{bi}, ϕ, R_p in the above equation together with (8) and (9). It can also be written that

$$\phi = \cos^{-1}(R_{bi}/R_{pin})$$

$$d\theta_i = d\theta \cdot Z/Z_i$$

Since $d\theta$ is the iteration step which is very small, values of O"B' and η depend mostly on R_c and ψ, as well as on essential parameters of the gears: R_{bi}, R_b, R_{pin}, R_p, Z_i, Z. If R_{bi}, R_b, R_{pin}, R_p, Z_i, Z are fixed, then values of O"B' and η depend on R_c and ψ. In other words, values of R_c and ψ are directly influencing the crescent shape as well as meshing parameters. When the essential parameters of the gear pair are fixed, even a little change of R_c and ψ can noticeably change the largest angle without

undercut or interference in the range of θ_{max} . This conclusion can be proved by the following examples.

2.1.1 Variation of ψ (with other parameters having the same values as above)

2.1.1.1 Relationship Between ψ and Interference within the range of θ_{max}

As it was mentioned above, when ψ is changed, the shape of crescent will also change which results in a change of meshing parameters. From Table 1 and Fig.3 we can see that when ψ is increasing, (1) the θ_{max} of the addendum part is also increasing, but (2) θ_{max} of the dedendum part is decreasing and (3) interference is increasing during addendum part. Accordingly, these three factor should be considered when the value of ψ is selected. Here $\psi = 32°$ is an optimum value at which θ_{max} of both addendum and dedendum parts are 16° . This corresponds to $Z_{min} = 12$ for the composite gear and Z_{ratio} is 70% [$Z_{ratio} = (Z_{min})_{crescent}/(Z_{min})_{involute}$] . In the same time interference is only 0.0006in. Which can be compensated by resilience of the bearing between the crescent and the metal core (rubber-metal laminate hydrostatic, etc.).

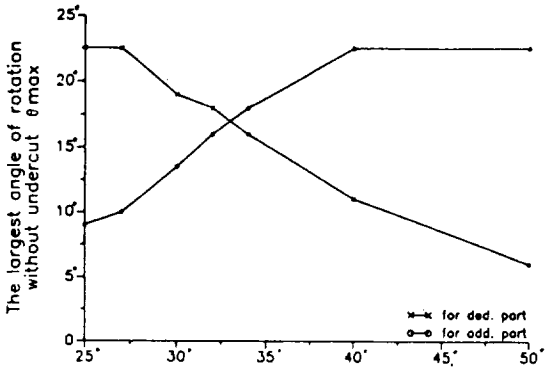

Fig.3(a) θmax vs. ψ

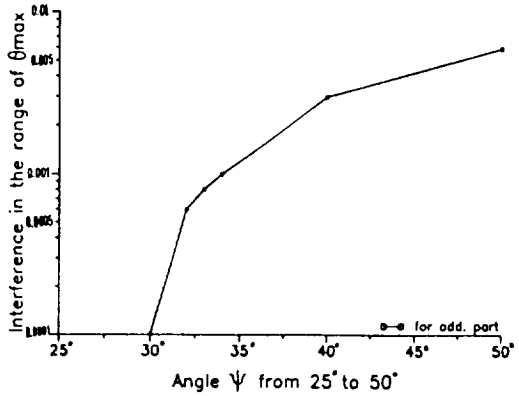

Fig.3(b) Interference (In.) vs. ψ

Table-1 the value of θmax, Zmin, Ratio-z, Interf with the value of ψ varying from 25° to 50° (Φ=3°)

	ψ	25°	27°	30°	32°	33°	34°	40°	50°
add.	θ max	9°	10°	14°	16°	16°	18°	22°	22°
	Z min.	20	18	14	12	12	10	8	8
	Ratio-z	40%	45%	60%	70%	70%	80%	100%	100%
	Interf. in	0.000	0.000	0.0001	0.0006	0.0008	0.001	0.003	0.006
ded.	θ max	22°	22°	19°	18°	17°	16°	11°	6°
	Z min.	8	8	10	10	11	16	16	32
	Ratio-z	100%	100%	85%	80%	76%	70%	50%	26%
	Interf. in	0.000	0.000	0.000	0.000	0.000	0.000	0.000	0.000

Note:
θmax ----- the largest angle of rotating without undercut from pitch point to addendum or from pitch point to dedendum
Zmin ----- the smallest teeth number without undercut
Ratio-z--- (Zmin-crescent / Zmin-involute)%
Interf.--- the interference in the range of θmax

2.1.1.2 Relationship Between Position Vector O"B' and θ_{max} while Varying ψ

Variation of O"B' illustrates the shape variation of the crescent and correlates with meshing parameters, as shown in fig.1(b), due to O" is a fixed point on gear, the generating points of crescent depend on variation of the length of O"B'. Thus, variation of O"B' has a direct correlation with θ_{max} . We define:

Variation of $O"B' = (O"B'_{max} - O"B'_{min})/O"B'_{min}$

If Fig.4 is compared with Fig.3, an interesting phenomenon can be discovered. When the composite gear is rotated clockwise, the contact point moves from the addendum part to the pitch point and from the pitch point to the dedendum part. If magnitude of O"B' increasing gradually, as in Fig.4, then slope of line is positive and the meshing parameters are good, no undercut is present. If O"B' is decreasing gradually, then slope of line is negative, the meshing process deteriorates due to undercut. These clearly show in Fig3.(a) and Fig.4.

In Fig.3(a) and Table 1, when $\psi = 25°$, θ_{max} of the addendum part is 9° and θ_{max} of the dedendum part is 22°, which corresponds to line(1) of $\psi = 25°$ in Fig.4 that shows the slope of line(1) is positive, namely O"B' increases gradually from the addendum part $\theta = -9°$ to the dedendum part $\theta = 22°$.

In Fig.3(a) and Table 1, when $\psi = 32°$, θ_{max} of the addendum part is 16° and θ_{max} of the dedendum part is 18°, which corresponds to line(2) of $\psi = 32°$ in Fig.4, that shows the slope of line(2) is positive from $\theta = -17°$ to $\theta = 16°$.

In Fig.3(a) and Table 1, when $\psi = 40°$, θ_{max} of the addendum part is 22° and θ_{max} of the dedendum part is 11°, which corresponds to line(3) of $\psi = 40°$ in Fig.4 that shows slope of line(3) is positive from $\theta = -22°$ *to* $\theta = 6°$.

From these three examples, it is clear if magnitude of O"B' increasing gradually from the addendum part to the dedendum part of crescent, then the mesh angle is within the range of θ_{max} and no undercut occurs; if O"B' decreasing gradually from the addendum part to the dedendum part, then the mesh angle exceeds the range of θ_{max} and undercut would occur.

In brief, if slope of the variation of O"B' is positive, the meshing process is satisfactory and undercut will not develop; if slope of the variation of O"B' is negative, the meshing process is unsatisfactory and undercut will develop. Therefore, the meshing process can be monitored by observing the change of O"B'.

On other hand, when the variation of O"B' is increased above a certain value, then interference will develop and the larger the variation of O"B', the more interference is developing as shown in Fig.3(b), 4. For example:

In Fig.4, for line(1) to $\psi = 25°$ from $\theta = -9°$ *to* $\theta = 0°$ on addendum part, the variation of O"B' is smaller(0.5%), which corresponds to interference = 0.000 in. In Fig.3(b) and Table 1 for $\psi = 25°$.

In Fig.4, for line(2) to $\psi = 32°$ from $\theta = -17°$ *to* $\theta = 0°$ on addendum part, the variation of O"B' is medium (1.0%), which corresponds to interference = 0.0006 in. In Fig.3(b) and Table 1 for $\psi = 32°$.

In Fig.4, for line(3) to $\psi = 40°$ from $\theta = -22°$ *to* $\theta = 0°$ on addendum part, the variation of O"B' is larger (1.4%), which correspond to interference = 0.003 in. in Fig.5(b) and Table 1 for $\psi = 40°$.

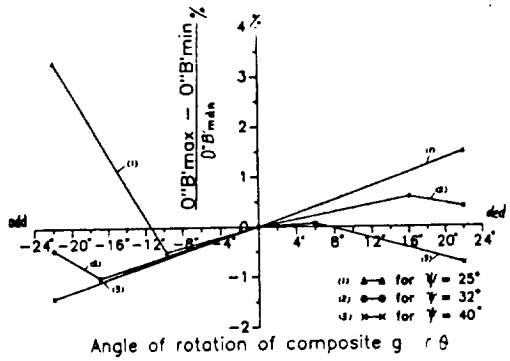

Fig.4 Varying Ratio of O"B' vs. θ
(varying ratio of $O^{\cdot}B^{\cdot} = \frac{O^{\cdot}B^{\cdot}_{max} - O^{\cdot}B^{\cdot}_{min}}{O^{\cdot}B^{\cdot}_{min}}$)

2.1.1.3 Influence of ψ Variation on the Crescent Shape

From Fig.5, 2, 6, we can observe how the crescent shape is changing with variation of ψ :

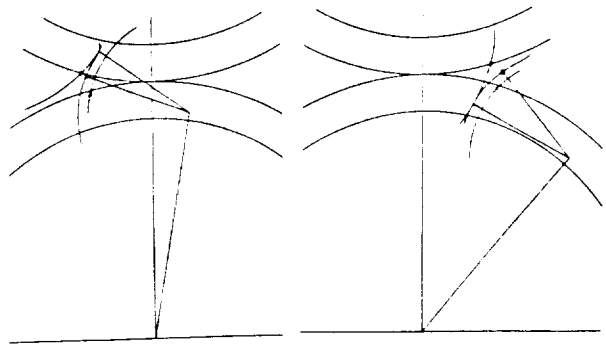

(a) at Addendum Part (b) at Dedendum Part

Fig.5 Generating Line of Crescent Surface with $\psi = 25°$ and $R_c = 3.1$ in.

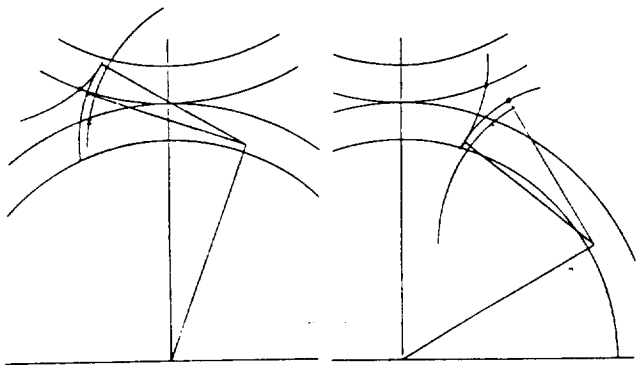

(a) at Addendum Part (b) at Dedendum Part

Fig.6 Generating Line of Crescent Surface with $\psi = 40°$ and $R_c = 3.1$ in.

In Fig.5, ψ is relatively small (25°), profile of the addendum part hold up, undercut of the addendum part is developing and θ_{max} is relatively small. However, profile of the dedendum part is smooth, the meshing process is satisfactory and θ_{max} is the largest (22°) to equal θ_{max} for the genuine involute system, namely $Z_{min} = 8$ same as $(Z_i)_{min}$ of involute gear .

In Fig.2, ψ is optimal (32°), profile of addendum and dedendum parts of are both smooth, the meshing process is satisfactory and θ_{max} value for both parts are larger. However there is a little interference within the range of θ_{max} addendum part.

In Fig.6, ψ is large(40°), profile of the addendum part is smooth and θ_{max} of the addendum part is the largest to equal θ_{max}

for the involute system. However, undercut is developing in the dedendum part.

2.1.2 Influence of R_c

The value of R_c was varied for $\psi = 32°$, while all other parameters were kept same as above.

2.1.2.1 Correlation Between R_c and θ_{max} and Extent of Interference

As it was mentioned in 2.1, a small change of R_c is influencing both crescent shape and meshing process. From Fig.7(a),(b), we can see the following:

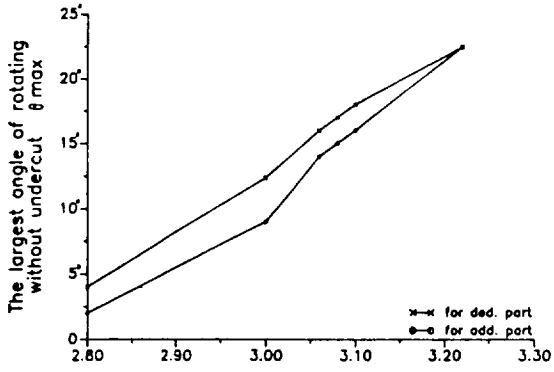

Rc varying from 2.8 to 3.22

Fig.7(a) θmax vs. Rc

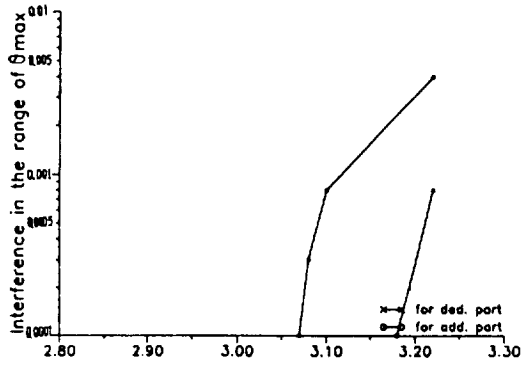

Rc varying from 2.8 to 3.22 (in.)

Fig.7(b) Interference(in) vs. Rc(1n.)

When R_c is increasing from the initial value of 2.8 in., θ_{max} of the addendum part and θ_{max} of the dedendum part are also increasing. However, extent of interference is also increasing starting from $R_c = 3.07$ in. for addendum part and $R_c = 3.19$ in. for dedendum part.

Thus, optimum R_c should be selected in accordance to Fig.7, in order to satisfy design requirement of Z_{min} and to limit interference within an acceptable range.

2.1.2.2 Relationship between O"B' and θ_{max} When R_c Is Varying

Comparing Fig.8 with Fig.7, the same conclusions can be found as ones in Section 2.1.1.2. Namely, from the addendum part to pitch point and from pitch point to the dedendum part, if the slope of the variation of O"B' is positive, then the meshing parameters are satisfactory and no undercut will occur. Conversely, if the slope of variation of O"B' is negative, then meshing parameters are unsatisfactory and an undercut will develop.

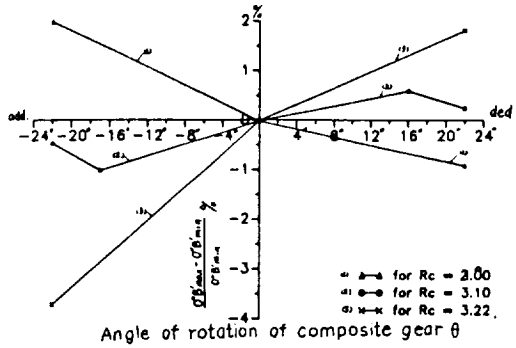

Angle of rotation of composite gear θ

Fig.8 Varying Ratio of O"B' vs. θ

(varying ratio of $O''B'' = \frac{O''B''_{max} - O''B''_{min}}{O''B''_{min}}$)

Table-2 the value of θmax, Zmin, Ratio-z, Interf. with the value of Rc varying from 2.8 to 3.22 ($\phi = 32°$)

	Rc	2.8	3.0	3.06	3.08	3.10	3.22
add.	θ max	2°	9°	14°	16°	16°	22°
	Z min.	80	20	14	13	12	8
	Ratio-z	10%	40%	80%	85%	70%	100%
	Interf.in	0.000	0.000	0.000	0.0003	0.0008	0.004
ded.	θ max	4°	12°	16°	17°	18°	22°
	Z min.	53	15	12	11	10	8
	Ratio-z	15%	55%	70%	75%	80%	100%
	Interf.in	0.000	0.000	0.000	0.000	0.000	0.0008

From Fig.7(a) and Table 2, when $R_c = 2.8$ in., θ_{max} of the addendum part is 2°, and θ_{max} of the dedendum part is 4°, which correspond to line(1) of $R_c = 2.8$ in. in Fig.8 which shows the slope of line(1) is negative from $\theta = -22°$ *to* $\theta = 22°$.

When $R_c = 3.1$ in. θ_{max} of the addendum part is 16° and θ_{max} of the dedendum part is 18°. This corresponds to line(2) for $R_c = 3.1$ in. in Fig.8 that shows the slope of line(2) is positive from $\theta = -17°$ *to* $\theta = 16°$.

For $R_c = 3.22$ in., θ_{max} of the addendum part is 22° and θ_{max} of dedendum part is also 22°, which corresponds to line(3) of $R_c = 3.22$ in. in Fig.8 that shows that the slope of line(3) is positive from $\theta = -22°$ *to* $\theta = 22°$.

These three examples correlated to the above conclusion.

2.1.2.3 Influence of R_c Variation on Shape of the Crescent

It can be observed that shape of the crescent is changing with variation of R_c :

When R_c is relatively small($R_c = 2.8$ in.), profile of the addendum part curling up, and profile of the dedendum part has a larger radius of curvature, so both θ_{max} are small and undercut develops early in both addendum and dedendum parts.

For an intermediate $R_c = 3.1$ in., profile of both addendum and dedendum parts are smooth.

For a large $R_c = 3.22$ in., profile of both addendum and dedendum parts are smooth, but interference is larger than above.

2.2 Effect of Variation of Teeth Number of the Involute Gear

We assume the following parameter values : pressure angle $\phi = 31°$ and diametral pitch $P_d = 1.14$; $R_b = 3.0$ in.; $R_p = 3.5$ in.; $Z = 8$; $R_c = 3.07$ in.; $\psi = 32°$.

With these parameters being kept constant, influence of the essential parameters of the involute gear Z_i, R_{bi}, R_{pin} were studied. The first set of the involute gear parameters is as follows :

$Z_i = 15$; $R_{pin} = Z_i/(2P_d) = R_p \cdot (Z_i/Z) = 6.5625$ in.

$R_{bi} = R_{pin} \cdot \cos\phi = 5.625$ in.

The second set of data of involute gear is in a similar way :

$Z_i = 50$; $R_{bi} = 18.75$ in.; $R_{pin} = 21.875$ in.

From Table 3, it can be seen that when teeth number of involute gear Z_i is changed from $Z_i = 8$ to $Z_i = 15$, θ_{max} of both addendum and dedendum parts do not change and when Z_i is changed from $Z_i = 8$ to $Z_i = 50$, θ_{max} of both addendum and dedendum parts are changing only for 1° from $(\theta_{max})_{add} = 14°$ to 13° or from $(\theta_{max})_{ded} = 16°$ to 15° and Z-ratio is only changing 5% addendum part from 60% to 55% and dedendum part from 70% to 65%. This means that the variation of teeth number of involute gear has a little effect both on crescent shape and on meshing parameters. The same conclusion can be obtained by analyzing equation (7) and (8).

Table-3 the value of θ max, Zmin, Ratio-z, Interf. with the value of Zi varying ($\phi = 31°$)

	Zi	8	16	80
add.	θ max	14°	14°	13°
	Z min.	14	14	16
	Ratio-z	60%	60%	55%
	Interf. in.	0.0003	0.0003	0.0003
ded.	θ max	16°	16°	15°
	Z min.	12	12	13
	Ratio-z	70%	70%	65%
	Interf. in.	in 0.000	0.000	0.000

As it was pointed out before, the crescent shape depends on position vector O"B' and on length of BB' in the triangle O"BB'(Fig.1(b)). Let us see what will happen for O"B' and BB' when Z_i, R_{bi}, R_{pin} are changed while the other parameters are fixed.

From equation (2):

$$BB' = |R_{pin} \cdot \sin\phi \cdot d\theta_i + 0.5 \cdot R_{bi} \cdot d\theta_i|$$

For the original set of parameters

$$R_{bi} = R_b \quad ; \quad R_{pin} = R_p \quad ; \quad d\theta_i = d\theta$$

$$BB' = |R_p \cdot \sin\phi \cdot d\theta + 0.5 \cdot R_p \cdot \cos\phi \cdot (d\theta)^2|$$

For the modified set of parameters (teeth number of involute gear Z_i and R_{pin} having been changed, while P_d not changed)

$$P_d = Z/(2R_p) \quad ; \quad R_{pin} = R_p \cdot Z_i/Z \quad ; \quad d\theta_i = d\theta \cdot Z/Z_i$$

$$newBB' = |R_p \cdot (Z/Z_i) \cdot \sin\phi \cdot d\theta \cdot (Z/Z_i) + 0.5 \cdot R_p \cdot (Z_i/Z) \cdot \cos\phi \cdot [d\theta \cdot (Z/Z_i)]^2|$$

$$= |R_p \cdot \sin\phi \cdot d\theta + 0.5 \cdot R_p \cdot \cos\phi \cdot (d\theta)^2 \cdot (Z/Z_i)|$$

Expression BB' for the new and original differ only by a factor (Z/Z_i) in the second term. Since $d\theta$ is very small, the second order term can be neglected, thus the new BB' is almost equal to BB'.

From equation (8):

$$O"B' = \{[R_c \cdot \sin(\psi + d\theta) - R_{bi} \cdot d\theta \cdot \cos\phi]^2 + [R_p - R_c \cdot \cos(\psi + d\theta) - R_{bi} \cdot d\theta \cdot \sin\phi]^2\}^{\frac{1}{2}}$$

There are five terms in the equation(8). Since R_c and ψ are is fixed, values of the first, third and fourth terms do not change and values of second and fifth terms has only little influence on the O"B' value since $d\theta$ is very small. Therefore, the new O"B' is very close to O"B'.

This analysis confirms the above given conclusion of the simulation, when teeth number of the involute gear is changed (with the same diametral pitch) position vectors O"B' and BB' change only a little. Accordingly, there is only a small effect on the crescent shape and meshing parameters.

2.3 Effect of Variation of Pressure Angle ϕ

We assume the following parameters : $R_{bi} = 3.0$ in.(same as above examples); pressure angle $\phi = 20°$ (changed from 31° to 20°) , so we can get :

$$R_{pin} = R_{bi}/\cos\phi = 3.1925 \text{ in.}$$

$$(Z_i)_{min} = 2 \cdot h_a/(\sin\phi)^2 = 17°$$

$$2\theta_{max} = 360°/17 = 21°$$

At first, we took the $\psi = 32°$ and $R_c = 3.1$ in. Which are about the same as in the above examples ($\phi = 31°$). However, the computational result showed poor meshing parameters. This means that since when ϕ is changed, R_{pin} also is changing, then the center distance of two gears is changed which significantly effects the shape of crescent and the meshing parameters. This conclusion can also be obtained from equation (8)

$$O"B' = \{[R_c \cdot \sin(\psi + d\theta) - R_{bi} \cdot d\theta_i \cdot \cos\phi]^2 + [R_p - R_c \cdot \cos(\psi + d\theta) - R_{bi} \cdot d\theta \cdot \sin\phi]^2\}^{\frac{1}{2}}$$

in which the first term of first bracket and the first, second terms of the second bracket determine the value of O"B'. The largest influence on O"B' is the first term R_p of the second bracket.

Then adjustments of values of ψ and R_c were simulated. Finally, from Table 4 the same conclusion as before can be made ($\phi = 31°$). Increase of ψ is favorable for the meshing process on the addendum part, (θ_{max} is increasing), but unfavorable for the dedendum part, (θ_{max} is decrease).

Table-4 the value of θ max, Zmin, Ratio-z, Interf. with the value of ψ varying from 21° to 25° (ϕ = 20°)

	ψ	21°	22°	25°
add.	θ max	7°	8°	10°
	Z min.	33	31	25
	Ratio-z	65%	70%	85%
	Interf. in.	0.000	0.000	0.000
ded.	θ max	7°	7°	5°
	Z min.	33	33	43
	Ratio-z	65%	65%	60%
	Interf. in.	0.000	0.000	0.000

On the other hand, we found that there is no interference developing when ϕ is reduced ($\phi = 20°$). Thus for $\psi = 21°$ and R_c = 3.0 in., very good meshing plots have been obtained.

3 Conclusion

(1) Conjugate meshing engagement between an involute gear and a proposed composite gear is feasible. During the engagement process, the rolling only contact develops between the meshing profiles, while the sliding only contact develops between the internal surface of the slider (crescent) and external circular cylindrical surface of the tooth core. If we select suitable teeth number and the most optimum R_c and ψ , the uniform crescent shape and good meshing parameters can be obtained. Thus meshing conditions are improving greatly, optimal materials can be used for the engaging part and the core, thus strength and acoustics of the gears can be significantly improved.

(2) To eliminate undercut and interference, magnitude of position vector from axis of the composite gear to axis of external circular cylindrical surface of the tooth core should be close to the base radius of the composite gear and angular distance of the position vector from the axial plane of the engaging gears should be close to the pressure angle .

Magnitude of the position vector should be close to the base radius of the composite gear and value of the angular distance should be close to the pressure angle .

(3) If the optimum values of both position vector and its angular distance are selected, then the variation of ratio of radius of curvature of external surface of the crescent is less than 1.2%, thus it is close to circular.

(4) Variation of the teeth number of the involute gear (with both diametral pitch and pressure angle fixed) has only a very little effect on shape of the crescent.

(5) There are some shortcomings of the composite gear:

a) While a small number of teeth is usually beneficial for the pinion, the smallest number of teeth of composite gear without undercut according to the performed analysis, is 1.3-1.4 larger than the minimum teeth number for an involute gear with the same pressure angle.

b) The meshing motion of crescent and involute profiles can be considered as the meshing motion of a pair of conjugate curves only approximately. A small interference is

always developing. Variation of pressure angle or center distance of two gears is slightly influencing meshing parameters. However, these factors are not expected to be a limitation of the suggested gear system since a small influence would be compensated by compliance in the joint between the crescent and the tooth core.

(6) The proposed and investigated gear system is promising for plastic gears since a unit crescent-elastic connection-tooth core can be extruded. Load-carrying capacity of plastic gears would be substantially enhanced if a pure rolling develops between the meshing profiles.

Reference

1. R. E. Denning and S.L.Rice, " Surface Fatigue Research with the Geared Roller Test Machine " SAE Automotive Engineering Congress Jan.14-16 1963.

2. E.I.Rivin and Rui-Ning Wu, "A Novel Concept of Power Transmission Gear Design ", SAE Technical Paper Series 871646, SAE 1987.

3. E.I.Rivin, "Properties and Prospective Applications of Ultra Thin Layered Rubber-Metal Laminates for Limited Travel Bearings", Tribology International, Volume 16 Number 1 February 1983.

4. E.I.Rivin, " Conjugate Gear System ", U.S. Patent Application.